Mechanisms controlling the cell envelope remodeling activities of the *Escherichia coli* cytokinetic ring

A dissertation presented

by

Mary-Jane Tsang Mui Ching

to

The Division of Medical Sciences

in partial fulfillment of the requirements

for the degree of

Doctor of Philosophy

in the subject of

Biological and Biomedical Sciences

Harvard University

Cambridge, Massachusetts

April 2016

Dissertation Advisor: Professor Thomas G. Bernhardt Mary-Jane Tsang Mui Ching

Mechanisms controlling the cell envelope remodeling activities of the *Escherichia coli* cytokinetic ring

Abstract

In *Escherichia coli*, cytokinesis requires the constriction of all the cell envelope layers: the inner membrane, the peptidoglycan (PG) cell wall and the outer membrane (OM). Such dramatic cell envelope remodeling requires tight coordination of the different activities of the division complex or cytokinetic ring in order to avoid potentially lethal breaches in cell envelope integrity. However, the mechanisms coordinating these cell wall and membrane remodeling events remain poorly defined.

To better understand the constriction process, I studied an allele of the essential division gene *ftsL* with an unusual lytic phenotype and showed that it accelerated the division process by prematurely initiating cytokinesis. Additionally, this mutant bypassed the requirement for other essential division proteins. These results suggest a role for FtsL as part of a mechanism that senses the assembly status of the cytokinetic apparatus and triggers constriction when assembly is complete.

Cell wall remodeling during cytokinesis requires the hydrolytic enzymes called amidases and their activators. One of the activators is the OM lipoprotein NlpD, but how amidase activation by NlpD is controlled is unknown. To gain insight into its activity and regulation, I performed a structure-function analysis. Sub-domains required for

recruitment to the division site or proper regulation of PG hydrolysis were identified. Interestingly, I found that aberrant amidase activation by a subset of NlpD truncations disrupted cytokinetic ring assembly and inhibited cell division. These findings support a model in which cell wall processing is communicated to cytoskeletal polymers in the cytoplasm to ensure continued cell constriction at the chosen division site.

Next, I investigated the regulation of NlpD using a flow cytometry-based enrichment strategy to isolate mutants with a cell chaining phenotype similar to that of NlpD-defective cells. I identified the Tol-Pal system, which has been implicated in OM constriction during cytokinesis, and an OM lipoprotein of unknown function called YraP as possible control factors for NlpD. My genetic analysis suggests a possible coupling between PG processing and OM constriction during cell division. Overall, these studies reveal a central role for cell wall remodeling in the coordinated constriction of the cell envelope layers.

Table of Contents

Acknowledgements

Throughout the course of my graduate studies, many individuals have supported and guided me in numerous ways and deserve immense thanks. First and foremost, I want to express my heartfelt gratitude to my advisor, Thomas Bernhardt, for all his advice and support in all aspects of my PhD. Tom is a talented scientist who has inspired my love and appreciation for bacterial genetics. In addition, he taught me how to think critically about science and how to communicate my work effectively. My time in his lab has allowed me to grow tremendously as a scientist.

I would therefore like to acknowledge all members of the Bernhardt Lab (past and present) who contributed to my scientific growth and the progress of my work. The lab has grown in recent years but it has been fun working in such a collaborative and stimulating environment. I especially want to thank Hongbaek Cho for all the helpful discussions and technical assistance that were instrumental in building up both my scientific abilities and confidence. I will always consider Hongbaek a role model for his wealth of knowledge, his creativity, and his scientific rigor. In addition, I am grateful to Desiree Yang, Monica Markovski, and Nick Peters who welcomed me when I first joined and taught me the ins and outs of the lab. Rachel Yunck and Ghee Chuan Lai are fellow students and have inspired me through their creativity and their hard work. I also want to acknowledge Chris Sham, my biochemistry guru. Finally, thanks to Hongbaek Cho, Assya Yakhnina, Patty Rohs, Chris Sham, and Jackson Buss for critical reading of this dissertation.

I am very grateful to the members of my dissertation advisory committee, Simon Dove, Marcia Goldberg, and David Rudner. Their critical evaluation of my data and constant advice were extremely valuable throughout my PhD. I also want to thank Marcia Goldberg, Piet de Boer, Karine Gibbs, and Suzanne Walker, for agreeing to be on my defense committee and taking the time to read my thesis. It is a great privilege to have them evaluate my work and discuss it with me.

Lastly, I must thank my family and friends who were an invaluable support all throughout graduate school. My parents have supported me in all my endeavors and although they are physically miles away, they are always an unwavering source of encouragement, advice, and love. Over the past few years, I am particularly grateful to my brother, Jean Marc, and my sister, Sarah Jane. I have enjoyed living with them over the past few years and their presence have kept me grounded and sane when things were not working in lab.

List of Figures

List of Tables

Chapter 1: Introduction to cell division in gram-negative bacteria

Chapter 1: Introduction to cell division in gram-negative bacteria

Sections of this chapter have been published [1]; adapted and reprinted with permission from Elsevier Publishing and the journal *Current Opinion in Microbiology*.

Section 1.1: The gram-negative bacterial cell envelope

Gram-negative bacteria, such as *Escherichia coli* (*E. coli*), are surrounded by a multi-layered cell envelope [2] (**Figure 1.1**). The inner or cytoplasmic membrane is a symmetrical phospholipid bilayer that surrounds the cytoplasmic space. The outer membrane is an asymmetric bilayer consisting of phospholipids in the inner leaflet and glycolipids, primarily lipopolysaccharide (LPS) in the outer leaflet. Finally, the space sandwiched between the two membranes is known as the periplasm and it contains the peptidoglycan (PG) cell wall layer. PG is a macromolecular structure composed of strands of alternating N-acetyl-glucosamine (GlcNAc) and N-acetyl-muramic acid (MurNAc) sugars linked to each other by β-1,4-glycosidic bonds. These glycan strands are further crosslinked via short stem peptides, which are covalently attached to the MurNAc sugar. In *E. coli*, the primary sequence of the attached peptide of newly synthesized glycan strands is (L-alanine)—(D-glutamate)-(γ)-(*meso*-diaminopimelic acid or m-DAP)—(D-alanine)—(D-alanine), with the terminal D-Ala being subsequently removed. Most peptide cross-bridges link D-Ala at position 4 of one stem peptide to the free amino group of m-DAP at position 3 on another stem peptide (**Figure 1.1**). Therefore, the PG cell wall layer is a continuous meshwork that acts as a force-bearing

structure that allows the cell to withstand its internal osmotic pressure, thus maintaining cell integrity and providing cell shape [3].

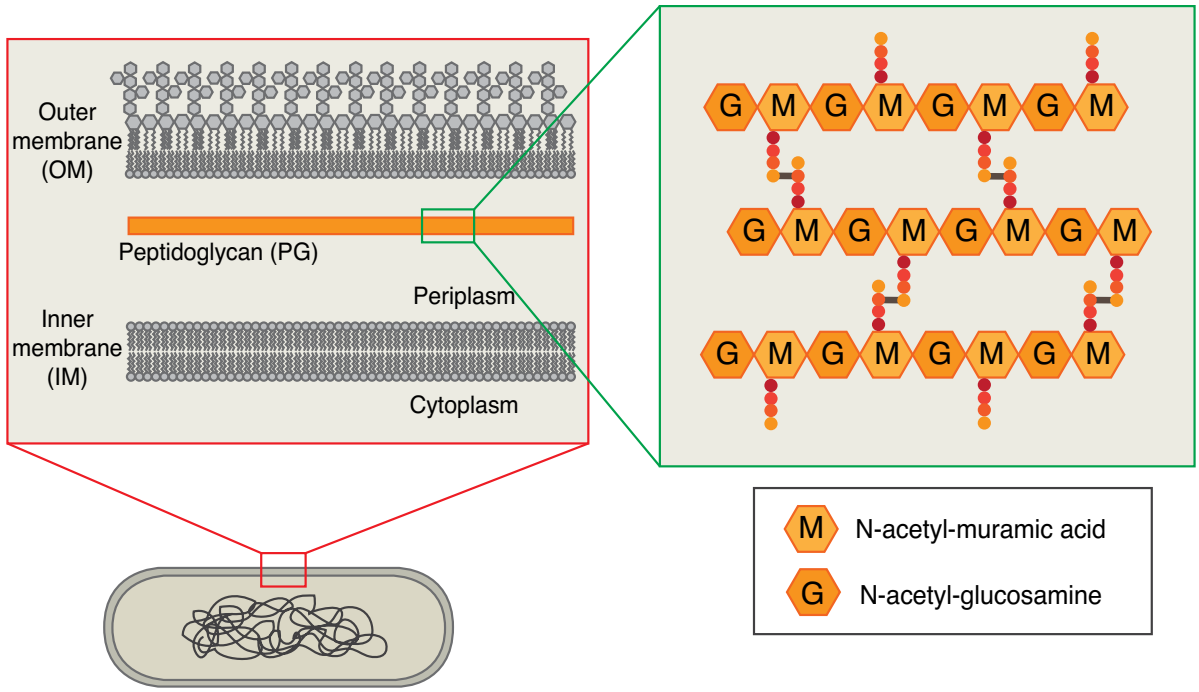

Figure 1.1. Gram-negative bacterial cell envelope. Diagram of a rod-shaped bacterium with three distinct envelope layers. The red box on the left contains a close-up representation of the IM, inner membrane; OM, outer membrane; and PG, peptidoglycan cell wall layer within the periplasmic space between the two membranes. Within the green box on the right is a schematic of the PG chemical structure composed of alternating units of N-acetyl-glucosamine (G) and N-acetyl-muramic acid (M). Colored dots represent the attached peptides, with peptide cross bridges indicated as bars between the amino acids at position 4 and 3 respectively of two neighboring peptides.

Section 1.2: Growth of the cell wall structure

Growth of the bacterial cell requires the concurrent growth of the cell wall structure. This essential process requires two opposing enzymatic activities: (1) PG synthesis, which involves glycan polymerization by transglycosylation and crosslinking of these strands to the existing meshwork through transpeptidation, and (2) PG hydrolysis, which breaks existing bonds within the meshwork to allow for its expansion [3] (**Figure 1.2**).

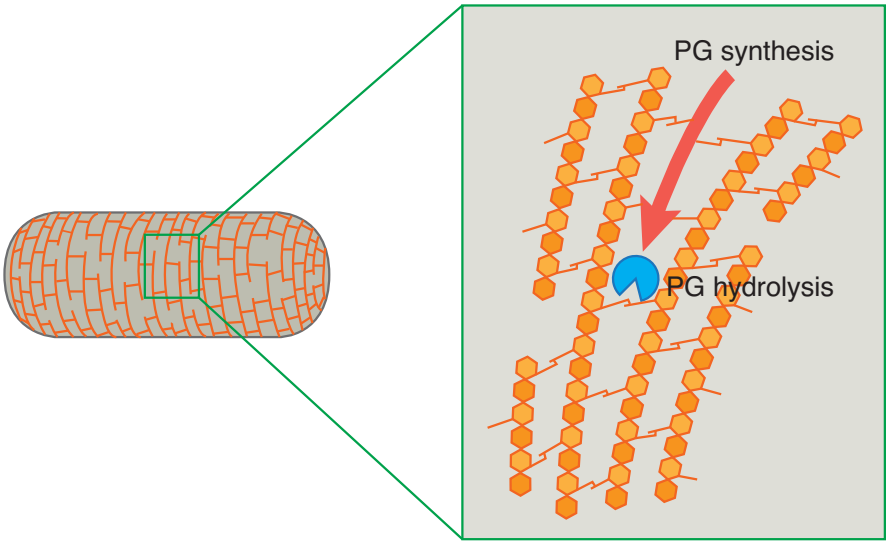

Figure 1.2. Growth of the peptidoglycan (PG) structure. The PG cell wall layer is a continuous meshwork that encases the cytoplasmic membrane and needs to be expanded to allow cell growth. The box contains a diagram highlighting the need for both PG synthesis and hydrolysis for the expansion of the cell wall. PG hydrolases are required to make space within the cell wall structure to allow the incorporation of new glycan strands (indicated by the red arrow) that are produced by the PG synthases.

The major class of PG synthetic enzymes is comprised of the so-called penicillin-binding proteins (PBPs). These enzymes are either mono-functional, with only transpeptidase activity, or bifunctional, with both glycosyltransferase and transpeptidase activities [4]. On the other hand, PG hydrolytic enzymes are diverse, with a wide range of cleavage site specificities (**Figure 1.3**). N-acetylmuramyl-L-alanine amidases cleave the amide bond between N-acetyl-muramic acid and L-alanine, thus separating the stem peptide from the glycan strand. On the other hand, endopeptidases and carboxypeptidases cleave the various peptide bonds within the stem peptide. Finally, there are three types of glycan strand-cleaving enzymes: N-acetylglucosaminidases, lysozymes and lytic transglycosylases. Although PG hydrolytic enzymes play an essential role in cell wall expansion, the exact function of each enzyme or class of enzymes is difficult to assign because many bacteria possess a large number of hydrolases, with redundant functions. Consequently, much is still unclear about the contribution and regulation of cell wall hydrolytic enzymes during bacterial cell growth. The most clearly defined function for cell wall hydrolases is during cell division to allow the separation of the two daughter cells. In *E. coli*, the periplasmic LytC-type amidases are the PG hydrolytic enzymes required for cell separation and will be discussed in further detail later on [5, 6].

.

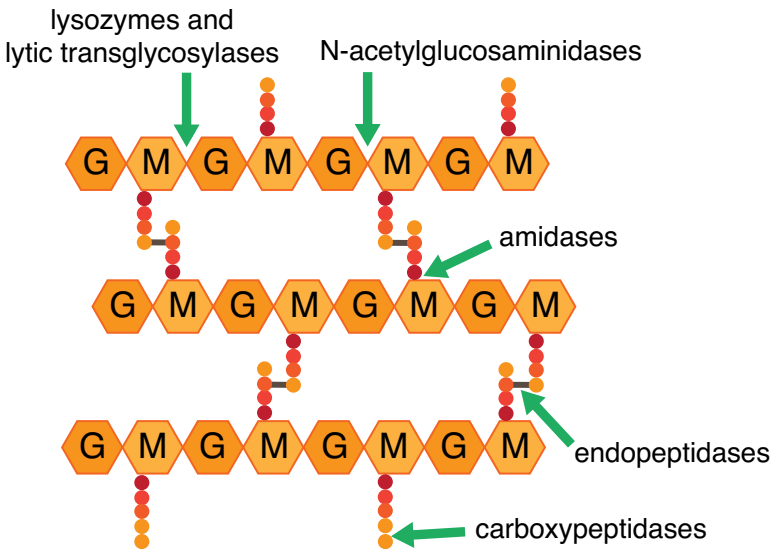

Figure 1.3. Diverse cleavage site specificities of PG hydrolases. Some sites of bond hydrolysis in the PG structure are indicated by the green arrows. Each class of hydrolytic enzymes consists of multiple members with potentially redundant function(s) in cell wall expansion. G, N-acetyl-glucosamine; M, N-acetyl-muramic acid. Colored dots represent the attached peptides.

Section 1.3: Cell division, an essential and multi-stage process

As said by the famous French biologist Francois Jacob, “The dream of every cell is to become two cells”. Cell division is an essential and complex process, even in the simplest of organisms. In gram-negative bacteria, it involves the coordinated constriction of both the inner and outer cell membranes as well as the synthesis and remodeling of the PG cell wall layer located between them, ultimately leading to the formation of the new daughter cell poles. This delicate, yet critical, endeavor can be broken down into four phases: (1) assembly of the division machinery, (2) constriction initiation, (3) active constriction, and (4) septal closure/pole completion. Many of the

players implicated in the various stages of cell division have been identified; however, their exact role and regulation during cytokinesis are poorly understood [7].

Cell division is a significant molecular construction project carried out by a ring-shaped, multi-protein machine called the divisome or septal ring. Over the years, dozens of proteins, both essential and non-essential, have been localized to this apparatus. In fact, based on studies from many laboratories using several different model organisms, most, if not all, of the core proteins required for divisome activity have likely been identified [8-10]. Additionally, interaction studies suggest that all these factors are linked to one another via a complex web of connections that span the cell envelope. However, despite this progress, major questions remain unanswered. The current challenge is to determine the molecular function of these factors and uncover functional connections between divisome components responsible for coordinating the many activities of this complex machine.

Section 1.4: Divisome assembly: defining the division site

The first step of cytokinesis is the most well-understood and is a two-part process: first, the formation of the Z-ring, followed by the assembly of the divisome machinery. The process initiates with the polymerization of the tubulin-like FtsZ protein into a ring structure (the Z-ring) at the midcell position just underneath the cytoplasmic membrane [11]. Though it shows limited sequence homology to eukaryotic tubulins, FtsZ is a GTPase that shares both structural homology and functional properties with tubulin [12, 13]. The crystal structure of FtsZ revealed that the main body of the protein

has a similar fold and nucleotide-binding motif as tubulin [14, 15]. Additionally, both proteins assemble into similar protofilaments in the presence of GTP *in vitro* [16-19]. However, FtsZ also possesses a conserved C-terminal tail that is absent in tubulin [20]. Ultimately, analogously to tubulin, FtsZ is a cytoskeletal element whose dynamic properties play a critical role in cell division *in vivo* [12, 13]. Once the Z-ring is assembled, numerous essential and non-essential division proteins are recruited to the midcell to form the mature divisome or septal ring. The completed machine is then capable of initiating cell constriction to shape the new daughter cell poles.

Mechanisms regulating Z-ring placement

In *E. coli*, the Z-ring assembles at the midcell position with remarkable accuracy. This spatial and temporal regulation of Z-ring placement is mediated by two partially redundant negative regulatory systems: the Min system and nucleoid occlusion [21-26] (**Figure 1.4**). The Min system inhibits Z-ring formation at the cell poles and, in *E. coli*, it is composed of the proteins MinC, MinD and MinE [21]. This system has been extensively characterized, both cytologically and biochemically. MinC is the division inhibitor that blocks Z-ring formation *in vivo* and, under normal conditions, requires the MinD protein for its activity [27, 28]. MinD is an ATPase that associates with the cytoplasmic membrane in its ATP-bound state [29-31]. MinC activation by MinD is mediated by the membrane attachment of the MinCD complex and allows MinC to bind FtsZ, disrupt FtsZ filaments, and ultimately inhibit Z-ring formation [32, 33]. The topological specificity of the division inhibitor is provided by the MinE protein, which

suppresses the MinCD-mediated division block specifically at midcell [34]. MinE dynamically antagonizes membrane binding of the MinCD complex by stimulating the ATPase activity of MinD, thus resulting in the formation of rapid wavelike oscillations of the membrane-associated complex from one cell pole to the other [30, 31, 33, 35-38]. Consequently, the time-averaged concentration of MinCD is the highest at the cell poles and the lowest at the midcell position where Z-ring formation becomes favored.

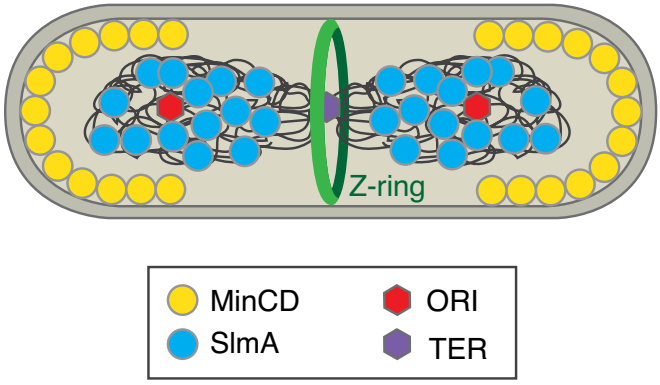

Figure 1.4. Mechanisms regulating Z-ring placement in *E. coli*. The Min system consists of the division inhibitor complex MinCD and directs Z-ring formation away from the cell poles, towards the midcell. Nucleoid occlusion, mediated by the DNA-binding protein SlmA, ensures that cell division occurs only in nucleoid-free regions at the midcell or at the poles. Together, these two partially redundant negative regulatory systems ensure that the Z-ring assembles at midcell. Adapted from [1].

The second system regulating Z-ring placement is nucleoid occlusion. It was first proposed by Woldringh and co-workers based on the cytological observation that cell division was inhibited in regions of the cell occupied by the nucleoid [23, 24]. In *E coli*,

the division inhibitor that associates with the nucleoid to mediate nucleoid occlusion is SlmA, a DNA-binding protein of the TetR family [39]. Although conflicting reports exist concerning the mechanism of SlmA action, recent genetic and biochemical results support the idea that it functions to antagonize FtsZ polymerization in a manner similar to MinC [40-44]. The antagonistic activity of SlmA is significantly enhanced by binding to specific DNA sequences that are broadly distributed in the origin-proximal region of the chromosome, but absent from the replication terminus (Ter) region [40, 41]. This asymmetric binding site distribution is thought to be one of the possible mechanisms for properly coordinating chromosome replication and segregation with cell division.

Formation of the Z-ring and assembly of the divisome

In addition to FtsZ, several FtsZ-binding proteins appear to play important roles in the formation of the Z-ring at the inner face of the cytoplasmic membrane [10] (**Figure 1.5**). Although FtsZ is the first protein to assemble at the prospective division site, it has no intrinsic affinity for phospholipid membranes. Consequently, in *E. coli*, the assembly of the Z-ring at the membrane requires the presence of either FtsA or ZipA, which are essential membrane-associated proteins that bind FtsZ directly through its conserved C-terminal tail [20, 45-49]. FtsA belongs to the actin family of proteins and is a structural homolog of eukaryotic actin, although its fold deviates from the canonical actin fold [50]. However, similar to actin, FtsA forms protofilaments *in vitro* on lipid monolayers and *in vivo* when overexpressed [51]. As FtsA lacks a transmembrane domain, its membrane association is mediated through a conserved C-terminal amphipathic helix [52]. On the

other hand, ZipA is a bitopic integral inner-membrane protein with an N-terminal transmembrane domain and a cytoplasmic C-terminal FtsZ-binding domain [45, 46]. Although FtsA and ZipA are dispensable for nucleation of the Z-ring, at least one of them is required for the formation and stability of the Z-ring structure [53].

Once its assembly is complete, the Z-ring serves as a scaffold for the recruitment of the remaining division proteins, both essential and auxiliary, to the division site at midcell (**Figure 1.5**). Importantly, besides tethering the Z-ring to the membrane, both FtsA and ZipA are also required for the subsequent assembly of a constriction-competent division machine. In *E. coli*, the recruitment of all the essential divisome components has been shown to follow a mostly linear dependency pathway, starting with FtsZ and ending with FtsN (FtsZ --> FtsA/ZipA --> FtsK --> FtsQLB --> FtsW --> FtsI --> FtsN) [8, 47, 54-59]. In this pathway, the localization of each divisome component to the septal ring is dependent on the prior localization of all the upstream components.

It is important to note, however, that this simple hierarchical arrangement of the recruitment order conceals a more complex network of interactions that includes connections between divisome proteins that are not neighbors in the dependency pathway [60-65]. Suppressor analyses and overexpression studies also support this model of cooperative protein-protein interactions or functional redundancy in the divisome since the requirement for individual divisome proteins can be partially suppressed by mutations within or overexpression of another divisome component [66-72].

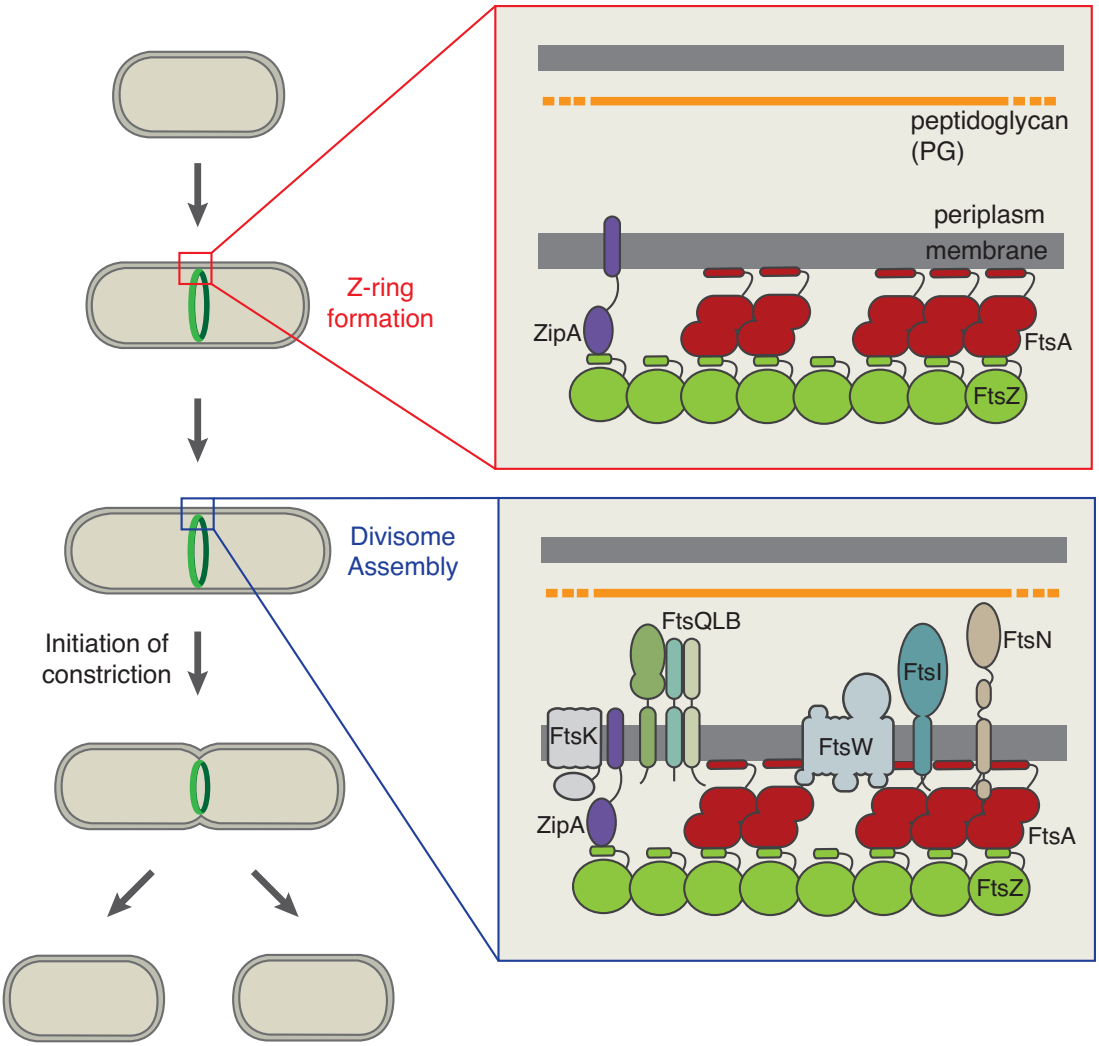

Figure 1.5. Cell division in *E. coli* is a multi-stage process. The first step is the formation of the Z-ring structure at the potential site of division. This structure consists of the tubulin-homologue FtsZ, anchored to the cytoplasmic membrane through direct interaction with the division proteins FtsA and ZipA (red box on top). The Z-ring then recruits the remaining division proteins to form the division machine known as the divisome or septal ring. The blue box on the bottom contains a diagram of the essential divisome proteins in *E. coli*. Once the divisome is assembled and in position, cell constriction is initiated and ultimately culminates in the formation of two daughter cells.

Moreover, studies of the temporal sequence of protein recruitment to the divisome have shown that the assembly is likely to be a two-step process. In *E. coli*, the components of the Z-ring assemble early and persist for about 20% of the cell cycle prior to the near simultaneous localization of the remaining “late” divisome components at about the time when the first signs of cell constriction become apparent [73].

Very little is known about the function and regulation of the “late” divisome proteins, especially with respect to their essential role during cell division. FtsK is a multi-pass membrane protein with an N-terminal domain essential for cell division and a C-terminal ATPase domain that allows ATP-dependent DNA translocation [67, 74-77]. Although not essential for cell viability and division, the C-terminal domain of FtsK has been implicated in segregation of the terminus regions of sister chromosomes as well as chromosome dimer resolution during septation [78, 79].

FtsQ, FtsL, and FtsB are bitopic inner membrane proteins that form a subcomplex prior to assembly in the divisome [80]. Although these proteins are essential and well-conserved among bacterial species, little is known about their physiological role [81]. Due to the many protein interactions reported for this subcomplex, it has been suggested that it functions solely as a scaffold for divisome assembly [62, 81].

FtsW is part of the SEDS family of proteins, which consists of multi-pass membrane proteins involved in shape, elongation, division and sporulation [82, 83]. FtsW is proposed to function as a Lipid II flippase, which transports the lipid-linked

precursors of peptidoglycan across the inner membrane in order to make them available to the PG synthases in the periplasmic space. However, this function is controversial due to conflicting reports [84-86]. FtsI (PBP3) is the monofunctional penicillin-binding protein (PBP) essential for PG synthesis during cell division [87, 88].

Finally, FtsN is the last essential protein in the localization dependency pathway. It is another bitopic membrane protein and was first identified as a multicopy suppressor of a temperature-sensitive mutant of *ftsA* [66]. Since then, overexpression of *ftsN* has been shown to suppress thermosensitive mutants of many other essential division proteins [66, 67, 69, 71]. All the "late" divisome proteins have been extensively studied, yet in many cases, their precise function remains to be determined. Moreover, of the proteins with defined functions, much is still unclear about how their activities are regulated within the division machine.

Section 1.5: Regulation of constriction initiation

Once the divisome is assembled and in position, cell constriction can begin. Since missteps in the envelope remodeling process can have catastrophic consequences, the conversion of the divisome from a state of assembly to one of active constriction likely involves a number of regulatory inputs. The triggering event that initiates the constriction process remains largely unclear, but it may involve a mechanism that "senses" the proper completion of divisome assembly before any major remodeling of the cell envelope is allowed to proceed.

Given that it is the last essential protein recruited to the divisome in the dependency pathway, the bitopic membrane protein FtsN has long been thought to play a role in the initiation of constriction in *E. coli* [61, 89]. This idea was reinforced with the demonstration that FtsN is recruited to the divisome in a self-enhancing process involving its small, membrane-proximal essential domain (^{E}FtsN) and its C-terminal, PG-binding SPOR domain (^{S}FtsN) [90, 91]. Based on this observation, it was proposed that cell constriction is driven by a positive feedback loop in which ^{E}FtsN stimulates the synthesis and remodeling of cell wall material at the division site to create the recruitment signal for ^{S}FtsN, which brings more ^{E}FtsN to the division site to stimulate more cell wall synthesis, and so on [90] (**Figure 1.6**).

FtsA was demonstrated to interact directly with the cytoplasmic N-terminal region of FtsN (^{N}FtsN) [65]. This interaction was shown to be important for the initial localization of FtsN to the divisome [92], suggesting that the FtsA-^{N}FtsN interaction may be responsible for initiating the proposed positive feedback loop that promotes constriction (**Figure 1.6**). This interaction involves the 1c domain of FtsA, which is important for FtsA self-interaction [61, 65, 93]. In fact, based on a structural analysis of FtsA polymers, the FtsA-^{N}FtsN interaction is likely to interfere with FtsA-FtsA interactions [51]. These observations point to a competition between FtsA-FtsA and FtsA-^{N}FtsN complexes as a possible mechanism for controlling constriction initiation. Clues as to how this interplay between FtsA and FtsN may provide a signal for the initiation of cell constriction have come from the isolation and analysis of *E. coli ftsA* mutants that bypass the normal requirements for other essential division proteins,

especially ZipA [68-70, 72, 94]. Many of these FtsA variants possess reduced self-interaction ability and promote early cell division, suggesting that a reduction in FtsA-FtsA interactions may stimulate division [94, 95].

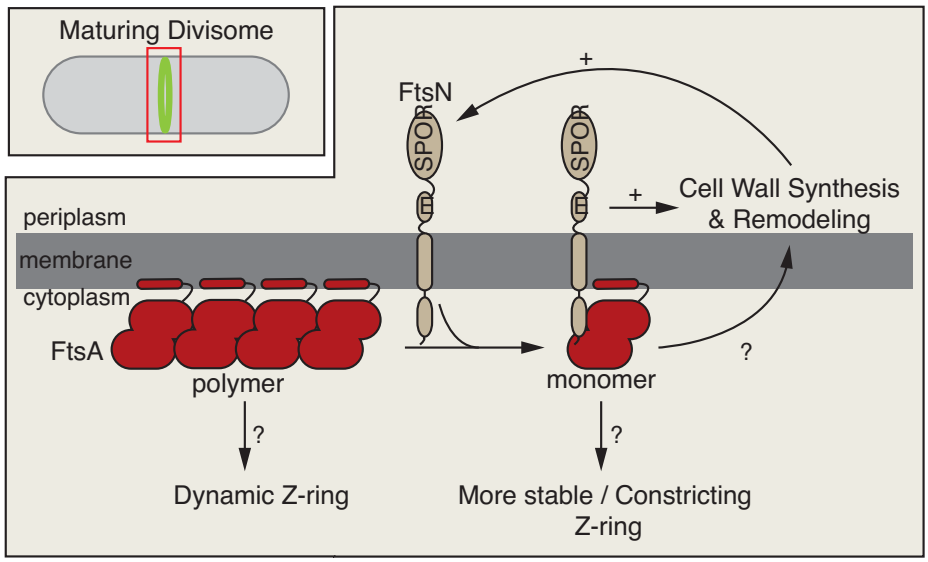

Figure 1.6. Potential role of FtsA-FtsN interactions in triggering cell constriction. Shown is a diagram depicting a model of events occurring at a maturing divisome, focusing on the FtsA-FtsN interaction. Studies indicate that FtsA and FtsN interact directly at the divisome and that this interaction is antagonistic with FtsA-FtsA interactions. These findings suggest the attractive possibility that FtsA serves as a "sensor" of divisome assembly. As late components of the divisome, like FtsN, are recruited to the structure, they reduce the polymerization state of FtsA. Once a threshold level of this altered FtsA form accumulates at midcell, it may trigger changes in FtsZ polymer dynamics to initiate contraction of the ring and coordinate cytoplasmic events with cell wall remodeling processes on the other side of the membrane. Adapted from [1].

One previously suggested scenario is that the disruption of FtsA-FtsA interactions at the Z-ring, possibly by ZipA, is responsible for generating free FtsA interfaces for the recruitment of downstream divisome proteins like FtsN and the eventual onset of constriction [10, 94, 96]. Alternatively, rather than strictly serving as a recruitment factor for other division proteins, the polymeric status of FtsA may also serve as a sensor used to monitor the status of the divisome assembly and promote constriction only after the machinery is deemed stable enough to successfully complete division (**Figure 1.6**). In this case, FtsA may be progressively converted to a reduced polymeric form via the recruitment of FtsN and other divisome components. This conversion of FtsA would proceed during the assembly process until a threshold level of monomers or small oligomers is achieved, which would then somehow trigger a change in the Z-ring and/or other components of the machinery to stimulate cell constriction. More work is needed to uncover the mechanistic details of this potential sensing and triggering event, including the protein-protein interactions or conformational changes involved.

Section 1.6: Active cell constriction

Once constriction is initiated, all layers of the cell envelope are actively constricted. In gram-negative bacteria, during active constriction, the divisome or septal ring needs to accomplish specific tasks in a coordinated manner to avoid possible catastrophic damage to the cell envelope as it undergoes remodeling at the division site

[7]. These include (1) invagination of the cytoplasmic/inner membrane, (2) synthesis of the new septal PG layer that is initially shared by the developing daughter cells, (3) hydrolysis and splitting of the septal PG to allow cell separation, and (4) outer membrane invagination. In fact, thin-section electron micrographs of dividing *E. coli* cells reveal a tight coordination of the invagination of all three envelope layers, with each layer closely following the other [11, 97, 98].

Coordination of septal PG synthesis and hydrolysis during constriction

An important function of the divisome is to synthesize the new PG cell wall layer that will ultimately form the daughter cell poles. As previously mentioned, this so-called septal PG layer is initially shared by the developing daughter cells and must be split by hydrolytic enzymes to allow cell separation. Thus, proper cell division requires the coordinated action of PG synthases to build the cell wall material and PG hydrolases to remodel it (**Figure 1.7**). Since the PG layer is crucial for maintaining cell shape and integrity, the balance between these opposing enzymatic functions of the divisome must be carefully maintained to avoid potentially lethal breaches in the cell wall structure. Importantly, this balance is disrupted by penicillin and related β-lactams antibiotics, which inhibit PG synthesis while allowing continued hydrolysis to generate lesions in the PG layer, thus inducing cell lysis [99, 100].

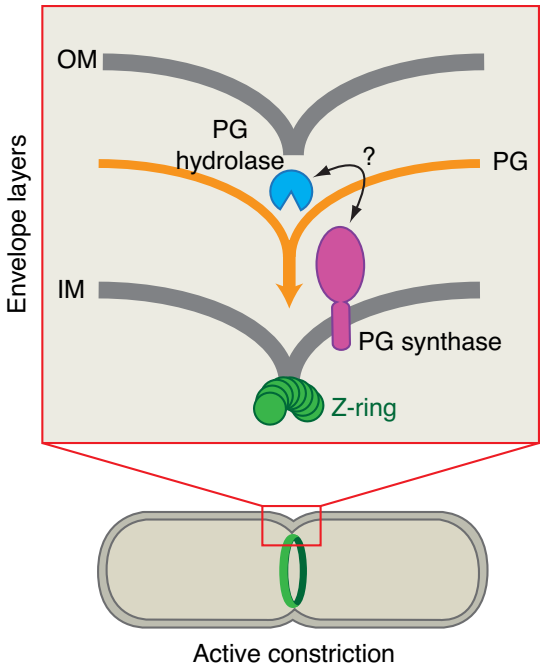

Figure 1.7. Coordination in peptidoglycan (PG) remodeling during cell constriction. Active cell constriction involves highly localized synthesis and hydrolysis of the so-called septal PG layer. The box contains a close-up diagram of the division site; the black arrow indicates potential coordination between PG synthesis and hydrolysis, in order to avoid potentially lethal breaches in the cell wall structure. OM, outer membrane; PG, peptidoglycan; IM, inner membrane.

Cell constriction is characterized by highly localized synthesis of septal PG at the division site [101, 102]. This process requires the transpeptidase activity of FtsI/PBP3 and the glycosyltransferase activity of another PG synthase, possibly one of the bifunctional PBPs. In *E. coli*, the resulting septal PG is processed by the periplasmic LytC-type N-acetylmuramyl-L-alanine amidases (AmiA, AmiB, and AmiC) in order to shape the new polar caps and allow formation of two separate daughter cells [103, 104]. Consequently, *E. coli* mutants lacking all three amidases are able to complete the

constriction of the inner membrane, but fail to split the septal PG layer. These mutants therefore form long chains of cells connected by the shared septal PG layer and a partially constricted outer membrane layer. Of the three amidases, AmiB and AmiC localize to the septal ring during cell division via their amidase N-terminal (AMIN) targeting domain [105-107]. Interestingly, in the absence of septal PG synthesis, these PG hydrolases fail to localize to the division machinery, suggesting a mechanism to ensure that PG synthesis precedes the PG hydrolytic activity that is likely to accompany amidase localization [107]. This failsafe mechanism may play a role in the coordination of PG synthesis and hydrolysis during cell division

Regulation of the PG amidases

Targeting to the division site likely plays a role in the spatiotemporal regulation of the amidases. However, a strain lacking both AmiB and AmiC exhibits only mild growth or separation defect, indicating that AmiA alone is sufficient for normal septal PG hydrolysis [103, 108]. Given that AmiA is not specifically recruited to the septal ring, this suggests that other regulatory mechanisms exist to ensure that the amidases are active only at the right time and place. In fact, the amidases were found to possess an autoregulatory alpha helix that occludes their active site [109]. Therefore, amidase activity might be inhibited in predivisional cells or in regions of the cells away from the septal ring. Upon assembly of the division machinery and initiation of constriction, this autoinhibition is relieved and septal PG is hydrolyzed (**Figure 1.8**).

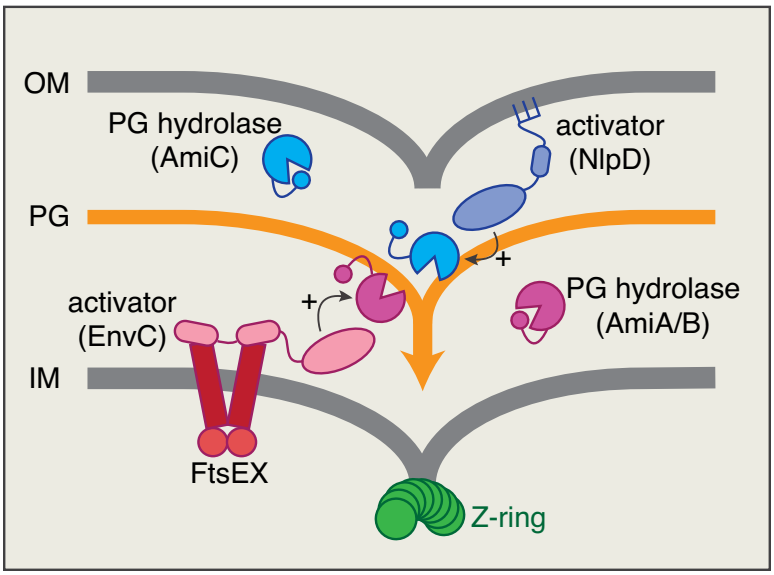

Figure 1.8. Regulation of two redundant PG-splitting systems in *E. coli*. Shown is a close-up of the division site, summarizing what is currently known about the regulation of the septal PG-splitting systems in *E. coli*. The PG amidases (AmiA/B/C) are the hydrolytic enzymes responsible for cleaving septal PG to allow cell separation. The divisome-associated LytM-containing factors EnvC and NlpD specifically activate AmiA/B and AmiC respectively. The current model is that, at the division site, PG amidase activity is controlled by a conformational switch involving the LytM-stimulated release of an autoregulatory helix from the amidase active site. Additionally, EnvC is further regulated *in vivo* by direct interaction with FtsEX that potentially modulates EnvC activity through conformational changes induced by ATP hydrolysis.

Relief of the amidase autoinhibition requires another set of periplasmic factors critical for cell separation, the divisome-associated LytM factors, EnvC and NlpD [98, 110, 111]. These proteins possess a degenerate active site (dLytM domain) that lacks

the critical residues necessary for PG hydrolytic activity. Therefore, they are not PG hydrolases themselves, but instead function as specific activators of the PG amidases, with EnvC activating AmiA/B and NlpD activating AmiC [110, 111]. Accordingly, loss of both EnvC and NlpD results in a similar cell chaining phenotype as that observed upon deletion of the genes encoding all three amidases. These LytM factors are thought to stimulate the activity of their target amidase(s) by promoting the release of the autoregulatory alpha helix from the amidase active site, either by directly binding the helix or by inducing a conformational change in the amidases [111].

Interestingly, the LytM factors themselves are subject to further regulation *in vivo*, potentially to ensure that PG hydrolytic activity is ultimately coordinated with the many other activities of the divisome. Specifically, EnvC is regulated by an ATP-binding cassette (ABC) transporter-like complex composed of the ATPase FtsE and the integral membrane subunit FtsX [112]. FtsEX directly recruits EnvC to the division site and anchors it to the inner membrane. Additionally, although the mechanistic details are still unclear, FtsEX may modulate EnvC activity and amidase activation in the periplasm through conformational changes induced by ATP hydrolysis in the cytoplasm.

Much less is known about the regulation of NlpD. Additionally, it is also unclear why *E. coli* possesses two redundant septal PG-splitting systems. Given that EnvC is anchored to the outer face of the inner membrane through FtsEX and NlpD is an outer membrane lipoprotein, an attractive hypothesis is that these two PG-splitting systems ensure proper coordination between septal PG hydrolysis and the invagination of the membranes in which they localize.

Is outer membrane invagination a passive or facilitated process?

In gram-negative bacteria such as *E. coli*, cell division requires the invagination of the outer membrane (OM). For a long time, the outer membrane was thought to passively follow the constriction of the other layers of the cell envelope through protein linkages between the OM and the PG [7, 113]. The tethering of the OM to the PG layer would cause the OM to follow the septal PG as it is split into the new daughter cell poles during the constriction process. One of the main players in this passive process is the major lipoprotein Lpp, also known as Braun's lipoprotein. Lpp is an abundant PG-bound OM lipoprotein that physically tethers the OM to the PG layer, thus allowing contacts between the OM and PG around the cell periphery and also at the division site. Accordingly, cells lacking Lpp exhibit general OM integrity defects, but also OM invagination defects, such as OM blebs at the division site and cell poles [114-116]. However, Lpp is uniformly distributed throughout the cell and is not believed to be specifically associated with the division machinery [117].

Recently, it has been proposed that efficient OM invagination requires the action of a conserved trans-envelope complex known as the Tol-Pal system [118], which has been implicated in the maintenance of OM integrity [119, 120]. The phenotypes of *tol-pal* mutants are consistent with a role for the Tol-Pal system in OM invagination and cell separation: these mutants chain in rich medium with either low or high osmolarity, display increased periplasmic volume at the constriction site and shed OM vesicles primarily from the division sites and cell poles [118, 121]. Additionally, members of the

Tol-Pal complex localize to the septal ring, suggesting that they may play a specific role in the division process [118].

The Tol-Pal system consists of five main members: TolQ, TolR and TolA are IM proteins, TolB is a periplasmic protein, and Pal is an abundant OM lipoprotein that binds PG through non-covalent interactions [122, 123]. TolQ, TolR, and TolA associate within the IM through their transmembrane helices to form a complex, which may use the proton motive force to induce conformational changes in TolA [124-128]. TolB and Pal interact at the OM [129-133]. This interaction has been proposed to promote the OFF state of the system by blocking both TolA-TolB interaction and Pal-PG interaction [130-136] (**Figure 1.9**). In the ON state, TolB and Pal dissociate, allowing TolA to interact with TolB and Pal to interact with PG. Additionally, although still controversial, the 'energized' TolA has been reported to interact with Pal, thereby bridging the IM and OM [127, 133, 134] (**Figure 1.9**). How the Tol-Pal system promotes OM invagination is still unclear, but one model is that the interplay of mutually exclusive interactions within the complex establishes transient trans-envelope connections that pull in the OM specifically at the division site where the Tol-Pal system localizes [118].

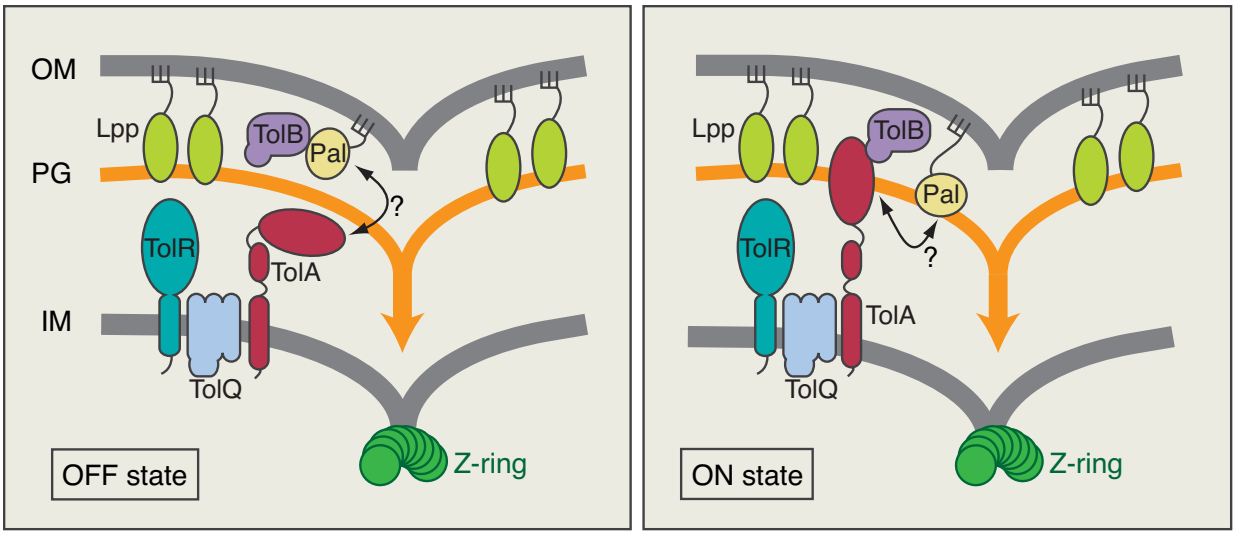

Figure 1.9. The Tol-Pal system in *E. coli*. Shown are diagrams depicting the interactions within the Tol-Pal system when the system is in the OFF state (left) or ON state (right). The interaction between TolB and Pal at the OM has been proposed to promote the OFF state of the system by blocking both TolA-TolB interaction and Pal-PG interaction. In the ON state, TolB and Pal dissociate, allowing TolA to interact with TolB and Pal to interact with PG. TolA, TolQ, and TolR associate within the IM to form a complex that may use the proton motive force to induce conformational changes in TolA. This 'energized' TolA may then interact with Pal (as indicated with the black arrow and question mark), although the existence of this interaction is still controversial. Finally, the abundant PG-bound OM lipoprotein, Lpp, physically tethers the OM to the PG layer. OM, outer membrane; PG, peptidoglycan; IM, inner membrane.

Section 1.7: Dissertation overview

Most of the relatively straightforward aspects of divisome assembly, such as which proteins localize to the divisome and when they arrive there, have been extensively characterized over the last two decades. However, surprisingly little is known about the mechanism of cell constriction by the divisome or the control of

constriction initiation. A major constraint limiting our understanding of divisome regulation has been the limited phenotypic range of division mutants, which mostly display filamentous morphology resulting from a failure in divisome assembly. I was therefore interested in mutants with phenotypes indicative of defects occurring post-initiation of constriction. I specifically focused on a previously reported mutant of *ftsL*, *ftsL**, that results in an accelerated division phenotype, possibly through the premature initiation of constriction. Further genetic analyses revealed a link between FtsL and two division proteins previously implicated in constriction initiation, FtsA and FtsN, suggesting that all three proteins function in a sensing mechanism that governs divisome activation and constriction initiation (see Chapter 2) [137].

Once constriction has been initiated, coordination of septal PG synthesis and hydrolysis is critical to ensure cell integrity during cytokinesis. Septal PG hydrolysis is achieved via two largely redundant septal PG-splitting systems, EnvC/AmiA/AmiB and NlpD/AmiC. Recent studies have uncovered details about the regulation of the EnvC protein [111, 112], however very little is known about NlpD function and regulation. In order to gain molecular insight into the activity of NlpD, I performed a structure-function analysis, which is summarized in Chapter 3. NlpD is an OM lipoprotein with two main protein domains: a LysM domain which is thought to possess PG-binding activity, and the dLytM domain, which is responsible for amidase activation. While only the full-length protein was functional for cell separation, the LysM domain was both necessary and sufficient for NlpD localization to division sites. Interestingly, expression of a truncated version of NlpD containing only the dLytM domain resulted in increased cell lysis,

potentially due to unregulated and mislocalized activation of the amidases throughout the cell. Interestingly, this mislocalized amidase activity inhibited cell division in the absence of the other amidase activator EnvC, possibly through destabilization of the Z-ring. These findings support a model in which the denuded glycan strands produced in the periplasm upon amidase activity influence Z-ring stability in the cytoplasm.

Chapter 4 describes my efforts towards identifying the regulatory mechanism(s) governing the ability of NlpD to activate its cognate amidase AmiC. I first determined that the subcellular localization of NlpD to the OM is important for proper NlpD function and PG hydrolysis during cell division. Using a flow cytometry-based cell sorting approach, I identified genes that may be required for proper NlpD activity as a means of searching for a critical activator. This screen was based on the hypothesis that the inactivation of these genes would phenocopy the loss of NlpD. Interestingly, the Tol-Pal system is required for NlpD function in a manner dependent on the growth medium. Given the role of the Tol-Pal system in OM invagination, these results suggest a possible coupling between PG hydrolysis mediated by NlpD/AmiC and OM invagination. Another potential regulator of NlpD identified in the screen is YraP, an OM lipoprotein that localizes to the septal ring. Loss of YraP phenocopies the loss of NlpD independent of the growth medium, suggesting a more direct regulatory effect on NlpD. Therefore, NlpD activation may involve two regulatory mechanisms: coupling with OM invagination and a possible direct activation by YraP.

In Chapter 5, I summarize the findings discussed in this thesis as we are gaining new insights in the mechanisms that ensure the coordination of the many activities of

the division machine in *E. coli*. In addition, I discuss the implications that these results have on our current understanding of the cell division process. Lastly, I identify and address some of the important questions that are raised by our work and others that remain unanswered in the field.

Section 1.8: References

1. Tsang, M.-J., and Bernhardt, T. G. (2015). Guiding divisome assembly and controlling its activity. Curr Opin Microbiol *24*, 60–65.

2. Silhavy, T. J., Kahne, D., and Walker, S. (2010). The bacterial cell envelope. Cold Spring Harb Perspect Biol *2*, a000414.

3. Höltje, J. V. (1998). Growth of the stress-bearing and shape-maintaining murein sacculus of Escherichia coli. Microbiol Mol Biol Rev *62*, 181–203.

4. Sauvage, E., Kerff, F., Terrak, M., Ayala, J. A., and Charlier, P. (2008). The penicillin-binding proteins: structure and role in peptidoglycan biosynthesis. FEMS Microbiol Rev *32*, 234–258.

5. Vollmer, W., Joris, B., Charlier, P., and Foster, S. (2008). Bacterial peptidoglycan (murein) hydrolases. FEMS Microbiol Rev *32*, 259–286.

6. van Heijenoort, J. (2011). Peptidoglycan hydrolases of Escherichia coli. Microbiol Mol Biol Rev *75*, 636–663.

7. de Boer, P. A. (2010). Advances in understanding E. coli cell fission. Current Opin Microbiol *13*, 730–737.

8. Goehring, N. W., and Beckwith, J. (2005). Diverse paths to midcell: assembly of the bacterial cell division machinery. Curr Biol *15*, R514–26.

9. Typas, A., Banzhaf, M., Gross, C. A., and Vollmer, W. (2012). From the regulation of peptidoglycan synthesis to bacterial growth and morphology. Nat Rev Microbiol *10*, 123–136.

10. Lutkenhaus, J., Pichoff, S., and Du, S. (2012). Bacterial cytokinesis: From Z ring to divisome. Cytoskeleton *69*, 778–790.

11. Bi, E. F., and Lutkenhaus, J. (1991). FtsZ ring structure associated with division in Escherichia coli. Nature *354*, 161–164.

12. de Boer, P., Crossley, R., and Rothfield, L. (1992). The essential bacterial cell-division protein FtsZ is a GTPase. Nature *359*, 254–256.

13. Mukherjee, A., Dai, K., and Lutkenhaus, J. (1993). Escherichia coli cell division protein FtsZ is a guanine nucleotide binding protein. Proc Natl Acad Sci USA *90*, 1053–1057.

14. Löwe, J., and Amos, L. A. (1998). Crystal structure of the bacterial cell-division protein FtsZ. Nature *391*, 203–206.

15. Nogales, E., Downing, K. H., Amos, L. A., and Löwe, J. (1998). Tubulin and FtsZ form a distinct family of GTPases. Nat Struct Biol *5*, 451–458.

16. Bramhill, D., and Thompson, C. M. (1994). GTP-dependent polymerization of Escherichia coli FtsZ protein to form tubules. Proc Natl Acad Sci USA *91*, 5813–5817.

17. Mukherjee, A., and Lutkenhaus, J. (1998). Dynamic assembly of FtsZ regulated by GTP hydrolysis. EMBO J *17*, 462–469.

18. Löwe, J., and Amos, L. A. (1999). Tubulin-like protofilaments in Ca2+-induced FtsZ sheets. EMBO J *18*, 2364–2371.

19. Oliva, M. A., Cordell, S. C., and Löwe, J. (2004). Structural insights into FtsZ protofilament formation. Nat Struct Mol Biol *11*, 1243–1250.

20. Wang, X., Huang, J., Mukherjee, A., Cao, C., and Lutkenhaus, J. (1997). Analysis of the interaction of FtsZ with itself, GTP, and FtsA. J Bacteriol *179*, 5551–5559.

21. de Boer, P. A., Crossley, R. E., and Rothfield, L. I. (1989). A division inhibitor and a topological specificity factor coded for by the minicell locus determine proper placement of the division septum in E. coli. Cell *56*, 641–649.

22. Mulder, E., and Woldringh, C. L. (1989). Actively replicating nucleoids influence positioning of division sites in Escherichia coli filaments forming cells lacking DNA. J Bacteriol *171*, 4303–4314.

23. Woldringh, C. L., Mulder, E., Valkenburg, J. A. C., Wientjes, F. B., Zaritsky, A., and Nanninga, N. (1990). Role of the nucleoid in the toporegulation of division. Res Microbiol *141*, 39–49.

24. Woldringh, C. L., Mulder, E., Huls, P. G., and Vischer, N. (1991). Toporegulation of bacterial division according to the nucleoid occlusion model. Res Microbiol *142*, 309–320.

25. Bi, E., and Lutkenhaus, J. (1993). Cell division inhibitors SulA and MinCD prevent formation of the FtsZ ring. J Bacteriol *175*, 1118–1125.

26. Yu, X. C., and Margolin, W. (1999). FtsZ ring clusters in min and partition mutants: role of both the Min system and the nucleoid in regulating FtsZ ring localization. Mol Microbiol *32*, 315–326.

27. de Boer, P. A., Crossley, R. E., and Rothfield, L. I. (1990). Central role for the Escherichia coli minC gene product in two different cell division-inhibition systems. Proc Natl Acad Sci USA *87*, 1129–1133.

28. de Boer, P. A., Crossley, R. E., and Rothfield, L. I. (1992). Roles of MinC and MinD in the site-specific septation block mediated by the MinCDE system of Escherichia coli. J Bacteriol *174*, 63–70.

29. de Boer, P. A., Crossley, R. E., Hand, A. R., and Rothfield, L. I. (1991). The MinD protein is a membrane ATPase required for the correct placement of the Escherichia coli division site. EMBO J *10*, 4371–4380.

30. Hu, Z., Gogol, E. P., and Lutkenhaus, J. (2002). Dynamic assembly of MinD on phospholipid vesicles regulated by ATP and MinE. Proc Natl Acad Sci USA *99*, 6761–6766.

31. Lackner, L. L., Raskin, D. M., and de Boer, P. A. J. (2003). ATP-dependent interactions between Escherichia coli Min proteins and the phospholipid membrane in vitro. J Bacteriol *185*, 735–749.

32. Hu, Z., Mukherjee, A., Pichoff, S., and Lutkenhaus, J. (1999). The MinC component of the division site selection system in Escherichia coli interacts with FtsZ to prevent polymerization. Proc Natl Acad Sci USA *96*, 14819–14824.

33. Hu, Z., Saez, C., and Lutkenhaus, J. (2003). Recruitment of MinC, an inhibitor of Z-ring formation, to the membrane in Escherichia coli: role of MinD and MinE. J Bacteriol *185*, 196–203.

34. Raskin, D. M., and de Boer, P. A. (1997). The MinE ring: an FtsZ-independent cell structure required for selection of the correct division site in E. coli. Cell *91*, 685–694.

35. Raskin, D. M., and de Boer, P. A. (1999). Rapid pole-to-pole oscillation of a protein required for directing division to the middle of Escherichia coli. Proc Natl Acad Sci USA *96*, 4971–4976.

36. Hu, Z., and Lutkenhaus, J. (1999). Topological regulation of cell division in Escherichia coli involves rapid pole to pole oscillation of the division inhibitor MinC under the control of MinD and MinE. Mol Microbiol *34*, 82–90.

37. Hu, Z., and Lutkenhaus, J. (2001). Topological regulation of cell division in E. coli. spatiotemporal oscillation of MinD requires stimulation of its ATPase by MinE and phospholipid. Mol Cell *7*, 1337–1343.

38. Loose, M., Fischer-Friedrich, E., Ries, J., Kruse, K., and Schwille, P. (2008). Spatial regulators for bacterial cell division self-organize into surface waves in vitro. Science *320*, 789–792.

39. Bernhardt, T. G., and de Boer, P. A. J. (2005). SlmA, a nucleoid-associated, FtsZ binding protein required for blocking septal ring assembly over Chromosomes in E. coli. Mol Cell *18*, 555–564.

40. Tonthat, N. K., Arold, S. T., Pickering, B. F., Van Dyke, M. W., Liang, S., Lu, Y., Beuria, T. K., Margolin, W., and Schumacher, M. A. (2011). Molecular mechanism by which the nucleoid occlusion factor, SlmA, keeps cytokinesis in check. EMBO J *30*, 154–164.

41. Cho, H., McManus, H. R., Dove, S. L., and Bernhardt, T. G. (2011). Nucleoid occlusion factor SlmA is a DNA-activated FtsZ polymerization antagonist. Proc Natl Acad Sci USA *108*, 3773–3778.

42. Tonthat, N. K., Milam, S. L., Chinnam, N., Whitfill, T., Margolin, W., and Schumacher, M. A. (2013). SlmA forms a higher-order structure on DNA that inhibits cytokinetic Z-ring formation over the nucleoid. Proc Natl Acad Sci USA *110*, 10586–10591.

43. Cho, H., and Bernhardt, T. G. (2013). Identification of the SlmA Active Site Responsible for Blocking Bacterial Cytokinetic Ring Assembly over the Chromosome. PLoS Genet *9*, e1003304.

44. Du, S., and Lutkenhaus, J. (2014). SlmA Antagonism of FtsZ Assembly Employs a Two-pronged Mechanism like MinCD. PLoS Genet *10*, e1004460.

45. Hale, C. A., and de Boer, P. A. (1997). Direct binding of FtsZ to ZipA, an essential component of the septal ring structure that mediates cell division in E. coli. Cell *88*, 175–185.

46. Liu, Z., Mukherjee, A., and Lutkenhaus, J. (1999). Recruitment of ZipA to the division site by interaction with FtsZ. Mol Microbiol *31*, 1853–1861.

47. Hale, C. A., and de Boer, P. A. (1999). Recruitment of ZipA to the septal ring of Escherichia coli is dependent on FtsZ and independent of FtsA. J Bacteriol *181*, 167–176.

48. Ma, X., and Margolin, W. (1999). Genetic and functional analyses of the conserved C-terminal core domain of Escherichia coli FtsZ. J Bacteriol *181*, 7531–7544.

49. Haney, S. A., Glasfeld, E., Hale, C., Keeney, D., He, Z., and de Boer, P. (2001). Genetic analysis of the Escherichia coli FtsZ.ZipA interaction in the yeast two-hybrid system. Characterization of FtsZ residues essential for the interactions with ZipA and with FtsA. J Biol Chem *276*, 11980–11987.

50. van den Ent, F., and Löwe, J. (2000). Crystal structure of the cell division protein FtsA from Thermotoga maritima. EMBO J *19*, 5300–5307.

51. Szwedziak, P., Wang, Q., Freund, S. M., and Löwe, J. (2012). FtsA forms actin-like protofilaments. EMBO J *31*, 2249–2260.

52. Pichoff, S., and Lutkenhaus, J. (2005). Tethering the Z ring to the membrane through a conserved membrane targeting sequence in FtsA. Mol Microbiol *55*, 1722–1734.

53. Pichoff, S., and Lutkenhaus, J. (2002). Unique and overlapping roles for ZipA and FtsA in septal ring assembly in Escherichia coli. EMBO J *21*, 685–693.

54. Wang, L., Khattar, M. K., Donachie, W. D., and Lutkenhaus, J. (1998). FtsI and FtsW are localized to the septum in Escherichia coli. J Bacteriol *180*, 2810–2816.

55. Weiss, D. S., Chen, J. C., Ghigo, J. M., Boyd, D., and Beckwith, J. (1999). Localization of FtsI (PBP3) to the septal ring requires its membrane anchor, the Z ring, FtsA, FtsQ, and FtsL. J Bacteriol *181*, 508–520.

56. Chen, J. C., and Beckwith, J. (2001). FtsQ, FtsL and FtsI require FtsK, but not FtsN, for co-localization with FtsZ during Escherichia coli cell division. Mol Microbiol *42*, 395–413.

57. Buddelmeijer, N., Judson, N., Boyd, D., Mekalanos, J. J., and Beckwith, J. (2002). YgbQ, a cell division protein in Escherichia coli and Vibrio cholerae, localizes in codependent fashion with FtsL to the division site. Proc Natl Acad Sci USA *99*, 6316–6321.

58. Mercer, K. L. N., and Weiss, D. S. (2002). The Escherichia coli cell division protein FtsW is required to recruit its cognate transpeptidase, FtsI (PBP3), to the division site. J Bacteriol *184*, 904–912.

59. Hale, C. A., and de Boer, P. A. J. (2002). ZipA is required for recruitment of FtsK, FtsQ, FtsL, and FtsN to the septal ring in Escherichia coli. J Bacteriol *184*, 2552–2556.

60. Di Lallo, G., Fagioli, M., Barionovi, D., Ghelardini, P., and Paolozzi, L. (2003). Use of a two-hybrid assay to study the assembly of a complex multicomponent protein machinery: bacterial septosome differentiation. Microbiology (Reading, Engl) *149*, 3353–3359.

61. Corbin, B. D., Geissler, B., Sadasivam, M., and Margolin, W. (2004). Z-ring-independent interaction between a subdomain of FtsA and late septation proteins as revealed by a polar recruitment assay. J Bacteriol *186*, 7736–7744.

62. Karimova, G., Dautin, N., and Ladant, D. (2005). Interaction network among Escherichia coli membrane proteins involved in cell division as revealed by bacterial two-hybrid analysis. J Bacteriol *187*, 2233–2243.

63. Goehring, N. W., Gueiros-Filho, F., and Beckwith, J. (2005). Premature targeting of a cell division protein to midcell allows dissection of divisome assembly in Escherichia coli. Genes Dev *19*, 127–137.

64. Alexeeva, S., Gadella, T. W. J., Verheul, J., Verhoeven, G. S., and Blaauwen, den, T. (2010). Direct interactions of early and late assembling division proteins in Escherichia coli cells resolved by FRET. Mol Microbiol *77*, 384–398.

65. Busiek, K. K., Eraso, J. M., Wang, Y., and Margolin, W. (2012). The Early Divisome Protein FtsA Interacts Directly through Its 1c Subdomain with the Cytoplasmic Domain of the Late Divisome Protein FtsN. J Bacteriol *194*, 1989–2000.

66. Dai, K., Xu, Y., and Lutkenhaus, J. (1993). Cloning and characterization of ftsN, an essential cell division gene in Escherichia coli isolated as a multicopy suppressor of ftsA12(Ts). J Bacteriol *175*, 3790–3797.

67. Draper, G. C., McLennan, N., Begg, K., Masters, M., and Donachie, W. D. (1998). Only the N-terminal domain of FtsK functions in cell division. J Bacteriol *180*, 4621–4627.

68. Geissler, B., Elraheb, D., and Margolin, W. (2003). A gain-of-function mutation in ftsA bypasses the requirement for the essential cell division gene zipA in Escherichia coli. Proc Natl Acad Sci USA *100*, 4197–4202.

69. Geissler, B., and Margolin, W. (2005). Evidence for functional overlap among multiple bacterial cell division proteins: compensating for the loss of FtsK. Mol Microbiol *58*, 596–612.

70. Bernard, C. S., Sadasivam, M., Shiomi, D., and Margolin, W. (2007). An altered FtsA can compensate for the loss of essential cell division protein FtsN in Escherichia coli. Mol Microbiol *64*, 1289–1305.

71. Goehring, N. W., Robichon, C., and Beckwith, J. (2007). Role for the nonessential N terminus of FtsN in divisome assembly. J Bacteriol *189*, 646–649.

72. Goehring, N. W., Petrovska, I., Boyd, D., and Beckwith, J. (2007). Mutants, suppressors, and wrinkled colonies: mutant alleles of the cell division gene ftsQ point to functional domains in FtsQ and a role for domain 1C of FtsA in divisome assembly. J Bacteriol *189*, 633–645.

73. Aarsman, M. E. G., Piette, A., Fraipont, C., Vinkenvleugel, T. M. F., Nguyen-Distèche, M., and Blaauwen, den, T. (2005). Maturation of the Escherichia coli divisome occurs in two steps. Mol Microbiol *55*, 1631–1645.

74. Yu, X. C., Tran, A. H., Sun, Q., and Margolin, W. (1998). Localization of cell division protein FtsK to the Escherichia coli septum and identification of a potential N-terminal targeting domain. J Bacteriol *180*, 1296–1304.

75. Wang, L., and Lutkenhaus, J. (1998). FtsK is an essential cell division protein that is localized to the septum and induced as part of the SOS response. Mol Microbiol *29*, 731–740.

76. Pease, P. J., Levy, O., Cost, G. J., Gore, J., Ptacin, J. L., Sherratt, D., Bustamante, C., and Cozzarelli, N. R. (2005). Sequence-directed DNA translocation by purified FtsK. Science *307*, 586–590.

77. Saleh, O. A., Pérals, C., Barre, F.-X., and Allemand, J.-F. (2004). Fast, DNA-sequence independent translocation by FtsK in a single-molecule experiment. EMBO J *23*, 2430–2439.

78. Yu, X. C., Weihe, E. K., and Margolin, W. (1998). Role of the C terminus of FtsK in Escherichia coli chromosome segregation. J Bacteriol *180*, 6424–6428.

79. Steiner, W., Liu, G., Donachie, W. D., and Kuempel, P. (1999). The cytoplasmic domain of FtsK protein is required for resolution of chromosome dimers. Mol Microbiol *31*, 579–583.

80. Buddelmeijer, N., and Beckwith, J. (2004). A complex of the Escherichia coli cell division proteins FtsL, FtsB and FtsQ forms independently of its localization to the septal region. Mol Microbiol *52*, 1315–1327.

81. Gonzalez, M. D., Akbay, E. A., Boyd, D., and Beckwith, J. (2010). Multiple interaction domains in FtsL, a protein component of the widely conserved bacterial FtsLBQ cell division complex. J Bacteriol *192*, 2757–2768.

82. Ikeda, M., Sato, T., Wachi, M., Jung, H. K., Ishino, F., Kobayashi, Y., and Matsuhashi, M. (1989). Structural similarity among Escherichia coli FtsW and

RodA proteins and Bacillus subtilis SpoVE protein, which function in cell division, cell elongation, and spore formation, respectively. J Bacteriol *171*, 6375–6378.

83. Henriques, A. O., Glaser, P., Piggot, P. J., and Moran, C. P. (1998). Control of cell shape and elongation by the rodA gene in Bacillus subtilis. Mol Microbiol *28*, 235–247.

84. Mohammadi, T., van Dam, V., Sijbrandi, R., Vernet, T., Zapun, A., Bouhss, A., Diepeveen-de Bruin, M., Nguyen-Distèche, M., de Kruijff, B., and Breukink, E. (2011). Identification of FtsW as a transporter of lipid-linked cell wall precursors across the membrane. EMBO J *30*, 1425–1432.

85. Ruiz, N. (2008). Bioinformatics identification of MurJ (MviN) as the peptidoglycan lipid II flippase in Escherichia coli. Proc Natl Acad Sci USA *105*, 15553–15557.

86. Sham, L.-T., Butler, E. K., Lebar, M. D., Kahne, D., Bernhardt, T. G., and Ruiz, N. (2014). Bacterial cell wall. MurJ is the flippase of lipid-linked precursors for peptidoglycan biogenesis. Science *345*, 220–222.

87. Spratt, B. G. (1975). Distinct penicillin binding proteins involved in the division, elongation, and shape of Escherichia coli K12. Proc Natl Acad Sci USA *72*, 2999–3003.

88. Wientjes, F. B., and Nanninga, N. (1991). On the role of the high molecular weight penicillin-binding proteins in the cell cycle of Escherichia coli. Res Microbiol *142*, 333–344.

89. Addinall, S. G., Cao, C., and Lutkenhaus, J. (1997). FtsN, a late recruit to the septum in Escherichia coli. Mol Microbiol *25*, 303–309.

90. Gerding, M. A., Liu, B., Bendezú, F. O., Hale, C. A., Bernhardt, T. G., and de Boer, P. A. J. (2009). Self-enhanced accumulation of FtsN at Division Sites and Roles for Other Proteins with a SPOR domain (DamX, DedD, and RlpA) in Escherichia coli cell constriction. J Bacteriol *191*, 7383–7401.

91. Lutkenhaus, J. (2009). FtsN--trigger for septation. J Bacteriol *191*, 7381–7382.

92. Busiek, K. K., and Margolin, W. (2014). A role for FtsA in SPOR-independent localization of the essential Escherichia coli cell division protein FtsN. Mol Microbiol *92*, 1212–1226.

93. Rico, A. I., García-Ovalle, M., Mingorance, J., and Vicente, M. (2004). Role of two essential domains of Escherichia coli FtsA in localization and progression of the division ring. Mol Microbiol *53*, 1359–1371.

94. Pichoff, S., Shen, B., Sullivan, B., and Lutkenhaus, J. (2012). FtsA mutants impaired for self-interaction bypass ZipA suggesting a model in which FtsA's self-interaction competes with its ability to recruit downstream division proteins. Mol Microbiol *83*, 151–167.

95. Geissler, B., Shiomi, D., and Margolin, W. (2007). The ftsA* gain-of-function allele of Escherichia coli and its effects on the stability and dynamics of the Z ring. Microbiology (Reading, Engl) *153*, 814–825.

96. Pichoff, S., Du, S., and Lutkenhaus, J. (2015). The bypass of ZipA by overexpression of FtsN requires a previously unknown conserved FtsN motif essential for FtsA-FtsN interaction supporting a model in which FtsA monomers recruit late cell division proteins to the Z ring. Mol Microbiol *95*, 971–987.

97. Lutkenhaus, J. (1993). FtsZ ring in bacterial cytokinesis. Mol Microbiol *9*, 403–409.

98. Uehara, T., Dinh, T., and Bernhardt, T. G. (2009). LytM-domain factors are required for daughter cell separation and rapid ampicillin-induced lysis in Escherichia coli. J Bacteriol *191*, 5094–5107.

99. Höltje, J. V. (1995). From growth to autolysis: the murein hydrolases in Escherichia coli. Arch Microbiol *164*, 243–254.

100. Uehara, T., and Bernhardt, T. G. (2011). More than just lysins: peptidoglycan hydrolases tailor the cell wall. Curr Opin Microbiol *14*, 698–703.

101. Woldringh, C. L., Huls, P., Pas, E., Brakenhoff, G. J., and Nanninga, N. (1987). Topography of peptidoglycan synthesis during elongation and polar cap formation in a cell division mutant of Escherichia coli MC4100. Microbiology *133*, 575–586.

102. Wientjes, F. B., and Nanninga, N. (1989). Rate and topography of peptidoglycan synthesis during cell division in Escherichia coli: concept of a leading edge. J Bacteriol *171*, 3412–3419.

103. Heidrich, C., Templin, M. F., Ursinus, A., Merdanovic, M., Berger, J., Schwarz, H., de Pedro, M. A., and Höltje, J. V. (2001). Involvement of N-acetylmuramyl-L-alanine amidases in cell separation and antibiotic-induced autolysis of Escherichia coli. Mol Microbiol *41*, 167–178.

104. Priyadarshini, R., de Pedro, M. A., and Young, K. D. (2007). Role of peptidoglycan amidases in the development and morphology of the division septum in Escherichia coli. J Bacteriol *189*, 5334–5347.

105. Bernhardt, T. G., and de Boer, P. A. J. (2003). The Escherichia coli amidase AmiC is a periplasmic septal ring component exported via the twin-arginine transport pathway. Mol Microbiol *48*, 1171–1182.

106. de Souza, R. F., Anantharaman, V., de Souza, S. J., Aravind, L., and Gueiros-Filho, F. J. (2008). AMIN domains have a predicted role in localization of diverse periplasmic protein complexes. Bioinformatics *24*, 2423–2426.

107. Peters, N. T., Dinh, T., and Bernhardt, T. G. (2011). A fail-safe mechanism in the septal ring assembly pathway generated by the sequential recruitment of cell separation amidases and their activators. J Bacteriol *193*, 4973–4983.

108. Chung, H. S., Yao, Z., Goehring, N. W., Kishony, R., Beckwith, J., and Kahne, D. (2009). Rapid β-lactam-induced lysis requires successful assembly of the cell division machinery. Proc Natl Acad Sci USA *106*, 21872–21877.

109. Yang, D. C., Tan, K., Joachimiak, A., and Bernhardt, T. G. (2012). A conformational switch controls cell wall-remodelling enzymes required for bacterial cell division. Mol Microbiol *85*, 768–781.

110. Uehara, T., Parzych, K. R., Dinh, T., and Bernhardt, T. G. (2010). Daughter cell separation is controlled by cytokinetic ring-activated cell wall hydrolysis. EMBO J *29*, 1412–1422.

111. Peters, N. T., Morlot, C., Yang, D. C., Uehara, T., Vernet, T., and Bernhardt, T. G. (2013). Structure-function analysis of the LytM domain of EnvC, an activator of cell wall remodelling at the Escherichia coli division site. Mol Microbiol *89*, 690–701.

112. Yang, D. C., Peters, N. T., Parzych, K. R., Uehara, T., Markovski, M., and Bernhardt, T. G. (2011). An ATP-binding cassette transporter-like complex governs cell-wall hydrolysis at the bacterial cytokinetic ring. Proc Natl Acad Sci USA *108*, E1052–60.

113. Rothfield, L. I., and Justice, S. S. (1997). Bacterial cell division: the cycle of the ring. Cell *88*, 581–584.

114. Fung, J., MacAlister, T. J., and Rothfield, L. I. (1978). Role of murein lipoprotein in morphogenesis of the bacterial division septum: phenotypic similarity of lkyD and lpo mutants. J Bacteriol *133*, 1467–1471.

115. Suzuki, H., Nishimura, Y., Yasuda, S., Nishimura, A., Yamada, M., and Hirota, Y. (1978). Murein-lipoprotein of Escherichia coli: a protein involved in the stabilization of bacterial cell envelope. Mol Gen Genet *167*, 1–9.

116. Yem, D. W., and Wu, H. C. (1978). Physiological characterization of an Escherichia coli mutant altered in the structure of murein lipoprotein. J Bacteriol *133*, 1419–1426.

117. Hiemstra, H., Nanninga, N., Woldringh, C. L., Inouye, M., and Witholt, B. (1987). Distribution of newly synthesized lipoprotein over the outer membrane and the peptidoglycan sacculus of an Escherichia coli lac-lpp strain. J Bacteriol *169*, 5434–5444.

118. Gerding, M. A., Ogata, Y., Pecora, N. D., Niki, H., and de Boer, P. A. J. (2007). The trans-envelope Tol-Pal complex is part of the cell division machinery and required for proper outer-membrane invagination during cell constriction in E. coli. Mol Microbiol *63*, 1008–1025.

119. Webster, R. E. (1991). The tol gene products and the import of macromolecules into Escherichia coli. Mol Microbiol *5*, 1005–1011.

120. Lazzaroni, J. C., Germon, P., Ray, M. C., and Vianney, A. (1999). The Tol proteins of Escherichia coli and their involvement in the uptake of biomolecules and outer membrane stability. FEMS Microbiol Lett *177*, 191–197.

121. Meury, J., and Devilliers, G. (1999). Impairment of cell division in tolA mutants of Escherichia coli at low and high medium osmolarities. Biol. Cell *91*, 67–75.

122. Lloubès, R., Cascales, E., Walburger, A., Bouveret, E., Lazdunski, C., Bernadac, A., and Journet, L. (2001). The Tol-Pal proteins of the Escherichia coli cell envelope: an energized system required for outer membrane integrity? Res Microbiol *152*, 523–529.

123. Lazzaroni, J.-C., Dubuisson, J.-F., and Vianney, A. (2002). The Tol proteins of Escherichia coli and their involvement in the translocation of group A colicins. Biochimie *84*, 391–397.

124. Derouiche, R., Bénédetti, H., Lazzaroni, J. C., Lazdunski, C., and Lloubès, R. (1995). Protein complex within Escherichia coli inner membrane. TolA N-terminal domain interacts with TolQ and TolR proteins. J Biol Chem *270*, 11078–11084.

125. Lazzaroni, J. C., Vianney, A., Popot, J. L., Bénédetti, H., Samatey, F., Lazdunski, C., Portalier, R., and Géli, V. (1995). Transmembrane alpha-helix interactions are required for the functional assembly of the Escherichia coli Tol complex. J Mol Biol *246*, 1–7.

126. Germon, P., Clavel, T., Vianney, A., Portalier, R., and Lazzaroni, J. C. (1998). Mutational analysis of the Escherichia coli K-12 TolA N-terminal region and characterization of its TolQ-interacting domain by genetic suppression. J Bacteriol *180*, 6433–6439.

127. Cascales, E., Gavioli, M., Sturgis, J. N., and Lloubès, R. (2000). Proton motive force drives the interaction of the inner membrane TolA and outer membrane pal proteins in Escherichia coli. Mol Microbiol *38*, 904–915.

128. Germon, P., Ray, M. C., Vianney, A., and Lazzaroni, J. C. (2001). Energy-dependent conformational change in the TolA protein of Escherichia coli involves its N-terminal domain, TolQ, and TolR. J Bacteriol *183*, 4110–4114.

129. Bouveret, E., Derouiche, R., Rigal, A., Lloubès, R., Lazdunski, C., and Bénédetti, H. (1995). Peptidoglycan-associated lipoprotein-TolB interaction. A possible key to explaining the formation of contact sites between the inner and outer membranes of Escherichia coli. J Biol Chem *270*, 11071–11077.

130. Clavel, T., Germon, P., Vianney, A., Portalier, R., and Lazzaroni, J. C. (1998). TolB protein of Escherichia coli K-12 interacts with the outer membrane peptidoglycan-associated proteins Pal, Lpp and OmpA. Mol Microbiol *29*, 359–367.

131. Bouveret, E., Bénédetti, H., Rigal, A., Loret, E., and Lazdunski, C. (1999). In vitro characterization of peptidoglycan-associated lipoprotein (PAL)-peptidoglycan and PAL-TolB interactions. J Bacteriol *181*, 6306–6311.

132. Ray, M. C., Germon, P., Vianney, A., Portalier, R., and Lazzaroni, J. C. (2000). Identification by Genetic Suppression of Escherichia coli TolB Residues Important for TolB-Pal Interaction. J Bacteriol *182*, 821–824.

133. Cascales, E., and Lloubes, R. (2004). Deletion analyses of the peptidoglycan-associated lipoprotein Pal reveals three independent binding sequences including a TolA box. Mol Microbiol *51*, 873–885.

134. Bonsor, D. A., Hecht, O., Vankemmelbeke, M., Sharma, A., Krachler, A. M., Housden, N. G., Lilly, K. J., James, R., Moore, G. R., and Kleanthous, C. (2009). Allosteric beta-propeller signalling in TolB and its manipulation by translocating colicins. EMBO J *28*, 2846–2857.

135. Dubuisson, J. F., Vianney, A., and Lazzaroni, J. C. (2002). Mutational Analysis of the TolA C-Terminal Domain of Escherichia coli and Genetic Evidence for an Interaction between TolA and TolB. J Bacteriol *184*, 4620–4625.

136. Walburger, A., Lazdunski, C., and Corda, Y. (2002). The Tol/Pal system function requires an interaction between the C-terminal domain of TolA and the N-terminal domain of TolB. Mol Microbiol *44*, 695–708.

137. Tsang, M.-J., and Bernhardt, T. G. (2015). A role for the FtsQLB complex in cytokinetic ring activation revealed by an ftsL allele that accelerates division. Mol Microbiol *95*, 925–944.

Chapter 2: A role for the FtsQLB complex in cytokinetic ring activation revealed by an *ftsL* allele that accelerates division

Attributions

I designed and performed all the experiments presented in this chapter and generated the subsequent figures and tables. I wrote the published manuscript together with Thomas Bernhardt.

Chapter 2: A role for the FtsQLB complex in cytokinetic ring activation revealed by an *ftsL* allele that accelerates division

Mary-Jane Tsang[1] and Thomas G. Bernhardt[1*]

[1]Department of Microbiology and Immunobiology, Harvard Medical School, Boston, MA 02115

Previously published [1]; reprinted and adapted with permission from *Molecular Microbiology.*

Section 2.1: Summary

The cytokinetic apparatus of bacteria is initially formed by the polymerization of the tubulin-like FtsZ protein into a ring structure at midcell. This so-called Z-ring facilitates the recruitment of many additional proteins to the division site to form the mature divisome machine. Although the assembly pathway leading to divisome formation has been well characterized, the mechanisms that trigger cell constriction remain unclear.

In this report, we study a "forgotten" allele of *ftsL* from *Escherichia coli,* which encodes a conserved division gene of unknown function. We discovered that this allele promotes the premature initiation of cell division. Further analysis also revealed that the mutant bypasses the requirement for the essential division proteins ZipA, FtsK, and FtsN and partially bypasses the need for FtsA. These findings suggest that rather than

serving simply as a protein scaffold within the divisome, FtsL may play a more active role in the activation of the machine. Our results support a model in which FtsL, along with its partners FtsB and FtsQ, functions as part of a sensing mechanism that promotes the onset of cell wall remodeling processes needed for the initiation of cell constriction once assembly of the divisome complex is deemed complete.

Section 2.2: Introduction

Bacterial cell division or septation is an essential process in which new polar caps for the developing daughter cells are formed. In gram-negative organisms, this involves the coordinated constriction of both the inner and outer cell membranes as well as the synthesis and remodeling of the peptidoglycan (PG) cell wall layer located between them. This molecular construction project is carried out by a ring-shaped, multi-protein machine called the divisome or septal ring [2]. Over the years, dozens of proteins have been localized to this apparatus and interaction studies suggest that they are linked to one another via a complex web of connections that span the cell envelope [2]. Although many of these factors are known to be essential for cytokinesis, few of them have clearly defined functions.

Cell division can be broken down into four phases: divisome assembly, constriction initiation, active constriction, and septal closure/pole completion. The first step of the process is the most well understood [2]. In *Escherichia coli,* it begins with the assembly of polymers of the tubulin-like FtsZ protein along with its partners FtsA, ZipA, and other FtsZ-binding proteins into a cytoskeletal structure called the Z-ring [3].

Formation of the Z-ring at the inner face of the cytoplasmic membrane is then thought to promote the localization of the remaining septal ring components to the division site. Recruitment of the essential divisome components of *E. coli* to midcell has been shown to follow a mostly linear dependency pathway starting with FtsZ and ending with FtsN (FtsZ --> FtsA/ZipA --> FtsK --> FtsQ/FtsL/FtsB --> FtsW --> FtsI --> FtsN) [4-12]. In this pathway, the localization of each divisome component to the septal ring is dependent on the prior localization of all upstream proteins. It is important to note, however, that the simple hierarchical arrangement of the recruitment order belies a much more complicated interaction network that involves connections between components extending beyond nearest neighbors in the dependency scheme [13-18]. Moreover, studies of the temporal sequence of protein recruitment to the divisome indicate that its assembly is likely to be a two-step process, with components of the Z-ring assembling early and persisting for about 20% of the cell cycle followed by the near simultaneous localization of the remaining “late” proteins at about the time the first signs of cell constriction become apparent [19].

Because missteps in cell envelope remodeling processes can have catastrophic consequences, the conversion of the divisome from a state of assembly to one of active constriction likely involves a number of regulatory inputs. Similarly, the active phase of constriction is likely to be closely monitored so that the development of potentially dangerous imbalances can be corrected. For example, cells must prevent the hydrolytic enzymes that remodel the cell wall from being activated out of sequence with the initiation of septal PG synthesis as constriction is triggered [20-23]. The division

machinery also needs to prevent the two processes from becoming uncoupled as the new poles are formed. Otherwise, miscoordination of PG synthesis and hydrolysis is likely to induce the formation of substantial breaches in the PG matrix and cause cell lysis.

Surprisingly little is known about the mechanism of cell constriction by the divisome or the controls that govern its initiation, especially considering the extreme changes in cell envelope architecture that are ultimately elicited by the process. One of the major constraints limiting our understanding of divisome regulation has been the limited phenotypic range displayed by commonly studied division mutants. By and large, these mutants simply fail to constrict under non-permissive conditions and form smooth filaments [24-29]. Such a phenotype indicates that the altered factor in question is important for division in general, but yields little information on what it is actually doing during the process. We have therefore been interested in studying mutants with phenotypes indicative of failures occurring after constriction is initiated. One such mutant is an allele of the *ftsL* gene encoding FtsL(E88K) isolated many years ago by Ishino and co-workers [30, 31]. This mutation was reported to result in cell lysis under non-permissive conditions, but outside of its initial identification, it was not studied further. We reasoned that revisiting the properties of this mutant allele, which we will refer to as *ftsL**, would allow us to better understand the role of FtsL during cell division.

FtsL is a bitopic membrane protein of only 121 amino acids, with a short cytoplasmic N-terminal region (residues 1-37), a transmembrane segment (residues 38-57), and a periplasmic domain (residues 58-121) that is predicted to consist mainly

of a coiled-coil structure with a leucine zipper motif [32]. It is known to form a subcomplex with two other essential division proteins, FtsB and FtsQ, independently of their localization to the divisome [33]. The transmembrane segment and leucine zipper motif of FtsL have been shown to be required for optimal interaction with FtsB [34, 35]. Interestingly, homologs of *ftsL*, *ftsB* and *ftsQ* are well conserved among bacterial species [36]. Although they form a core component of the divisome, the physiological role of FtsL and its partners is still unknown. Bacterial two-hybrid experiments have detected interactions between FtsL and several other divisome components in *E. coli* [14]. Due to its involvement in many different protein-protein interactions, it has been suggested that the main role of FtsL may be as a structural or scaffolding protein important for divisome assembly and/or stability [36].

Here, we show that the *ftsL** mutation leads to a divisome malfunction that accelerates the division process, likely through the premature initiation of constriction. Mutant cells harboring this allele divide at a lower than normal cell volume, thus forming smaller daughter cells. This accelerated division phenotype is responsible for the growth defect and cell lysis observed when cells are shifted to non-permissive conditions. Consistent with this interpretation, mutations inactivating division proteins implicated in divisome function and/or stability were found to rescue the *ftsL** growth defect. Furthermore, our suppressor analysis also revealed that the *ftsL** allele can fully bypass the essential functions of the divisome proteins FtsK, FtsN, and ZipA, and partially bypass the need for FtsA activity. Given that FtsA and FtsN have both been previously implicated in the initiation of constriction [13, 16, 37-42], our results support a model in

which FtsL, as part of the FtsQLB subcomplex, also plays an important role in modulating divisome activation rather than merely serving as a scaffolding protein within the apparatus as has been proposed previously [36]. An accompanying study by Liu and co-workers in the de Boer laboratory also reports results supporting a role for the FtsQLB complex in the control of cell constriction stimulated by FtsN [43].

Section 2.3: Results

Phenotypic analysis of *ftsL** mutants

A mutant harboring the mutation *ftsL*(E88K), which we will refer to as *ftsL**, was isolated several years ago by Ishino and co-workers [30, 31]. Rather than inducing a division block, this particular allele was reported to induce cell lysis at the non-permissive temperature of 42°C when cells were grown in LB medium with no added NaCl. Besides the initial description of its isolation, further characterization of the *ftsL** mutant has not been reported. Given the unique phenotype induced by this allele, we thought a reinvestigation of its properties was warranted because it might yield new insight into the function of FtsL.

Allelic replacement was therefore used to introduce *ftsL** into a wild-type MG1655 strain background. When grown in standard LB medium (0.5% NaCl), the resulting strain MT10 [*ftsL**] displayed a growth rate similar to wild-type at both 30°C and 42°C (**Figure 2.1A**). However, the mutant cells were approximately 15-20% shorter and slightly wider than wild-type at both temperatures (**Figure 2.1B-E, Table 2.1**). Mean cell volume was also significantly reduced in *ftsL** cells relative to wild-type at 30°C

(**Table 2.1**). In half-strength LB medium with no added NaCl (0.5xLB-0N), MT10 [*ftsL**] grew at approximately the same rate as wild-type at 30°C, but displayed a severe reduction in growth rate at 42°C (**Figure 2.1F**). Cell length and volume were reduced even further in *ftsL** cells relative to wild-type in this medium (**Figure 2.1G-J, Table 2.1**). The growth defect for strain MT10 [*ftsL**] was accompanied by a higher frequency of lysed ghost cells in the culture and a striking change in morphology with the mutant cells becoming much shorter and approaching a spherical morphology (**Figure 2.1J**). MT10 [*ftsL**] plated with normal efficiency on standard LB agar at both 30°C and 42°C as well as on 0.5xLB-0N agar at 30°C, but displayed a severe plating defect on this medium at 42°C (**Figure 2.1K**). Using RpoC-mCherry as a marker for the nucleoid, we investigated whether the lysis phenotype of the *ftsL** mutant was due to improper chromosome segregation. However, obvious chromosome guillotining events were not observed, nor were anucleate cells, which would be indicative of chromosome segregation defects (data not shown).

Our results thus confirm the original findings of Ishino and coworkers [30] that the *ftsL** allele results in a temperature-sensitive lethal phenotype distinct from typical cell filamentation. However, we did not observe dramatic lysis of liquid cultures upon shifting the mutant to the non-permissive temperature in 0.5xLB-0N medium. Instead, the primary effect of the mutation appeared to be a reduction in cell length that was observable at all temperatures, but was exacerbated at 42°C in 0.5xLB-0N where some cell lysis was also observed. We suspect that the lysis phenotype is much more severe on solid 0.5xLB-0N media at 42°C such that viability is significantly compromised.

Table 2.1. Mean cell length and mean cell volume of WT and *ftsL mutant under different conditions**

	LB (0.5% NaCl)				0.5X LB (No NaCl)			
	30°C		42°C		30°C		42°C	
genotype	Mean L (µm) [% WT length][a]	Mean Vol. (µm^3) [% WT volume][a]	Mean L (µm) [% WT length]	Mean Vol. (µm^3) [% WT volume]	Mean L (µm) [% WT length]	Mean Vol. (µm^3) [% WT volume]	Mean L (µm) [% WT length]	Mean Vol. (µm^3) [% WT volume]
WT	4.37 ± 0.06 [100%]	3.93 ± 0.06 [100%]	3.81 ± 0.09 [100%]	3.65 ± 0.09 [100%]	4.92 ± 0.04 [100%]	3.98 ± 0.12 [100%]	3.89 ± 0.03 [100%]	3.54 ± 0.04 [100%]
*ftsL**	3.63 ± 0.01 [83.1%] **	3.51 ± 0.02 [89.3%] **	3.22 ± 0.05 [84.5%] **	3.70 ± 0.08 [101.4%] NS	3.26 ± 0.06 [66.3%] ***	3.26 ± 0.06 [81.9%] *	2.76 ± 0.00 [71.0%] ***	3.23 ± 0.07 [91.2%] *

Overnight cultures of TB28 [*WT*] and MT10 [*ftsL**] were diluted in the indicated liquid broth and grown to midlog at 30°C. The cultures were then backdiluted to an OD_{600} ~ 0.02 in fresh medium and grown at 30°C or shifted to 42°C until an OD_{600} ~ 0.3 - 0.5. The cells were then imaged using phase contrast microscopy and analyzed using MicrobeTracker to determine cell length and cell volume. 600 cells were analyzed for each condition, n = 3. Shown are the average mean cell length or average mean cell volume ± standard error of the mean (SEM). Statistical significance was determined using two-tailed student's t-test.

[a] % = (Mean cell length (or cell volume) of *ftsL** mutant / Mean cell length (or cell volume) of *WT*) * 100%

* difference significant at $p < 0.05$

** difference significant at $p < 0.01$

*** difference significant at $p < 0.001$

NS, difference not statistically significant

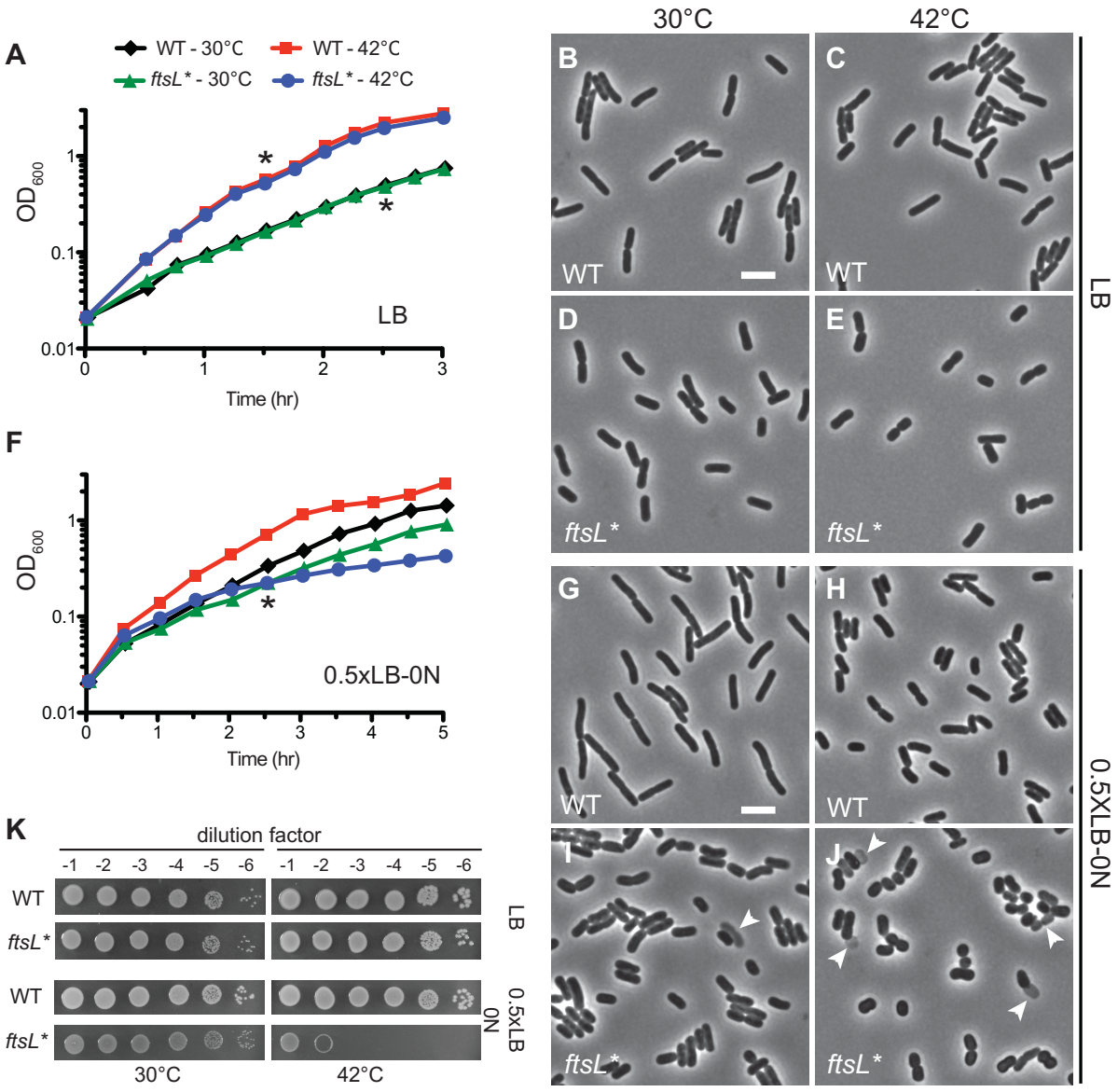

Figure 2.1. Shape and growth defect of the *ftsL mutant.** (**A**) Overnight cultures of TB28 [WT] or MT10 [*ftsL**] cells were diluted in fresh LB broth and grown at 30°C until mid-log. At time t = 0, each strain was diluted into fresh LB and grown at 30°C or shifted to 42°C. (**B-E**) Cells were removed from the TB28 (**B, C**) and MT10 (**D, E**) cultures at the time point indicated by the asterisks, fixed and examined by phase contrast microscopy. Bar = 4µm. (**F**) Growth of TB28 and MT10 was monitored as described in (A) except that growth medium was half-strength LB with no added NaCl (0.5xLB-0N).

Figure 2.1 (Continued). (**G-J**) Cells from the cultures in (F) were removed at the time point indicated by the asterisks, fixed and examined by phase contrast microscopy. Bar = 4μm. Arrows point to lysed cells. (**K**) Cells of TB28 and MT10 were grown overnight in LB broth at 30°C. Following normalization for cell density (OD_{600} = 2), the resulting cultures were serially diluted (10^{-1} to 10^{-6}), and 5 μl of each dilution was spotted on the indicated medium. Plates were incubated overnight at the indicated temperature and photographed.

FtsL* promotes an accelerated division cycle

We reasoned that the dramatic effect of FtsL* on cell morphology could either be due to: (i) a change in the steady-state concentration of FtsL protein, (ii) a mis-localization of the variant protein that adversely affects cell elongation and rod-shape maintenance, or (iii) an alteration of divisome activity by FtsL*. In order to begin distinguishing between these possibilities, we determined the levels of the FtsL protein in both wild-type or *ftsL** mutant cells. As shown by immunoblotting, the level of the FtsL* variant was only 2-fold higher than that of wild-type (**Figure 2.2A**). In addition, expression of wild-type *ftsL* from a multicopy plasmid in a wild-type background does not induce the reduced cell length phenotype observed for the *ftsL** mutant under non-permissive conditions (data not shown). Finally, the growth defect of the *ftsL** mutant was rescued by the overproduction of wild-type FtsL, but not FtsL* (**Figure 2.2B**). Thus, the FtsL* phenotype is unlikely to be caused by a change in FtsL concentration.

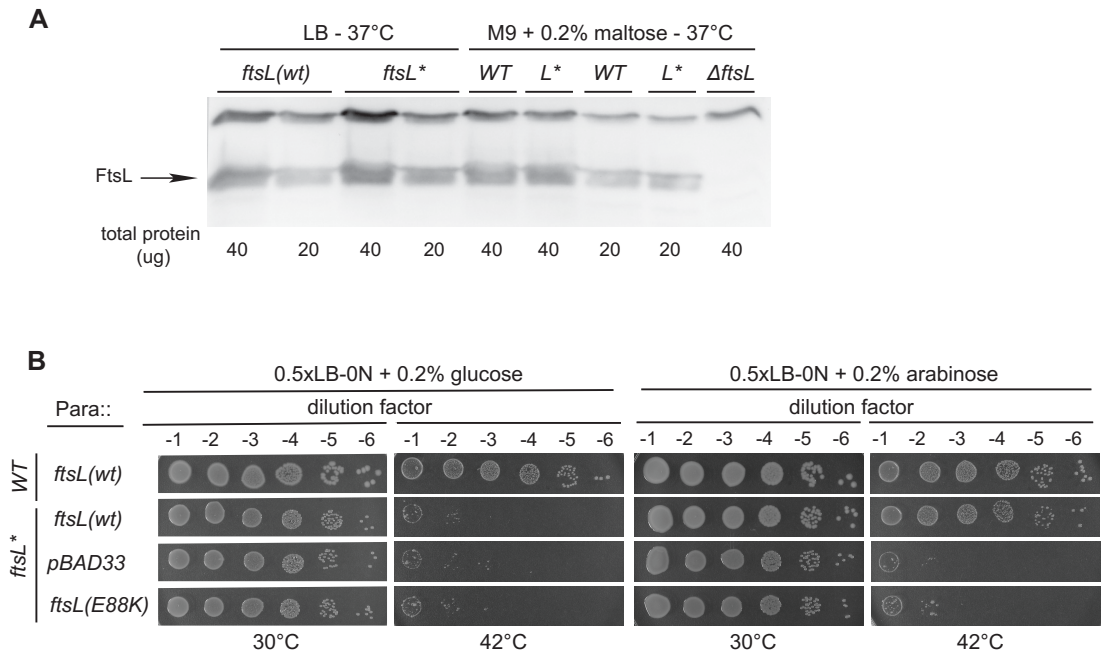

Figure 2.2. FtsL* phenotype not due to protein stabilization. (A) Overnight cultures of TB28 [*WT*] or MT10 [*ftsL**] cells were diluted in fresh LB or M9 maltose medium and grown at 37°C until OD_{600} ~ 0.5 - 0.7 when the cells were harvested for whole-cell extract preparation. Proteins in the resulting extracts were separated by SDS-PAGE, transferred to PVDF, and FtsL was detected with anti-FtsL antisera. **(B**) TB28 or MT10 cells expressing either the empty vector (pBAD33), FtsL(WT) (pMT27) or FtsL(E88K) (pMT28) were grown overnight in LB broth at 30°C. Following normalization for cell density (OD_{600} = 2), the resulting cultures were serially diluted (10^{-1} to 10^{-6}), and 5 µl of each dilution was spotted on the indicated medium. Plates were incubated overnight at the indicated temperature and photographed.

Next, we examined the subcellular localization of the mutant protein relative to wild-type FtsL and estimated the timing of its recruitment to the divisome by measuring the frequency with which the FtsL proteins co-localized with the early divisome recruit ZapA. To do so, we produced GFP-FtsL or GFP-FtsL* from a single-copy expression

construct integrated at the *att*HK022 locus in either a wild-type or an *ftsL** background respectively. The strains also encoded ZapA-mCherry expressed from the native *zapA* locus. When grown in minimal medium at 30°C, both FtsL variants displayed bright fluorescent bands at mid-cell (**Figure 2.3**), indicating that the growth and morphological defects caused by the FtsL* variant are not likely to be due to the mis-localization of the protein.

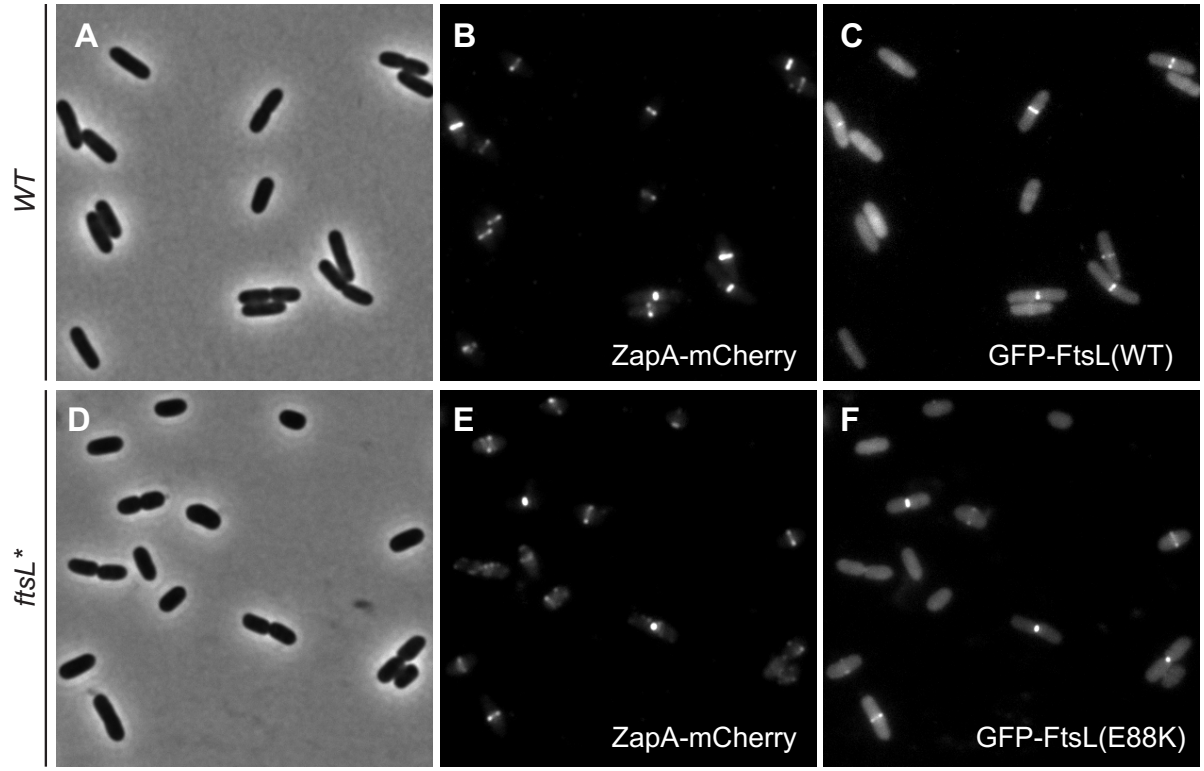

Figure 2.3. Co-localization of ZapA-mCherry and GFP-FtsL*. Overnight cultures of TU211(attHKMT35) [*WT zapA-mCherry (P_{lac}::gfp-ftsL)*] (**A-C**) and MT102(attHKMT36) [*ftsL* zapA-gfp (P_{lac}::gfp-ftsL*)*] (**D-F**) were diluted in minimal M9 medium supplemented with 0.2% maltose and 25 µM IPTG and grown at 30°C until an OD_{600} ~ 0.25 - 0.35. The cells were visualized on 2% agarose pads with phase contrast (**A,D**), mCherry (**B,E**) and GFP (**C,F**) optics. Bar = 4µm.

Consistent with this idea, proper mid-cell localization of the GFP-FtsL* variant was also observed under non-permissive conditions (42°C in 0.5xLB-0N) (**Figure 2.4**). Strikingly, in minimal medium at 30°C, ZapA-mCherry rings were found to co-localize with a ring of GFP-FtsL* at a much higher percentage (76%) than with the wild-type GFP-FtsL fusion (57%) (**Table 2.2**). The fraction of cells with a ZapA-mCherry ring was found to be lower in *ftsL** cells, suggesting that Z-rings form later in the cell cycle in the mutant relative to wild-type. This apparent delay in Z-ring formation likely reflects the fact that the mutant cells are born much shorter than normal cells and therefore take longer to achieve a cell length permissive for Z-ring assembly. Despite the delay in Z-ring formation, the increased co-localization of ZapA-mCherry and GFP-FtsL* suggests that the time between Z-ring assembly and the recruitment of the late component FtsL to the divisome is reduced in the *ftsL** mutant.

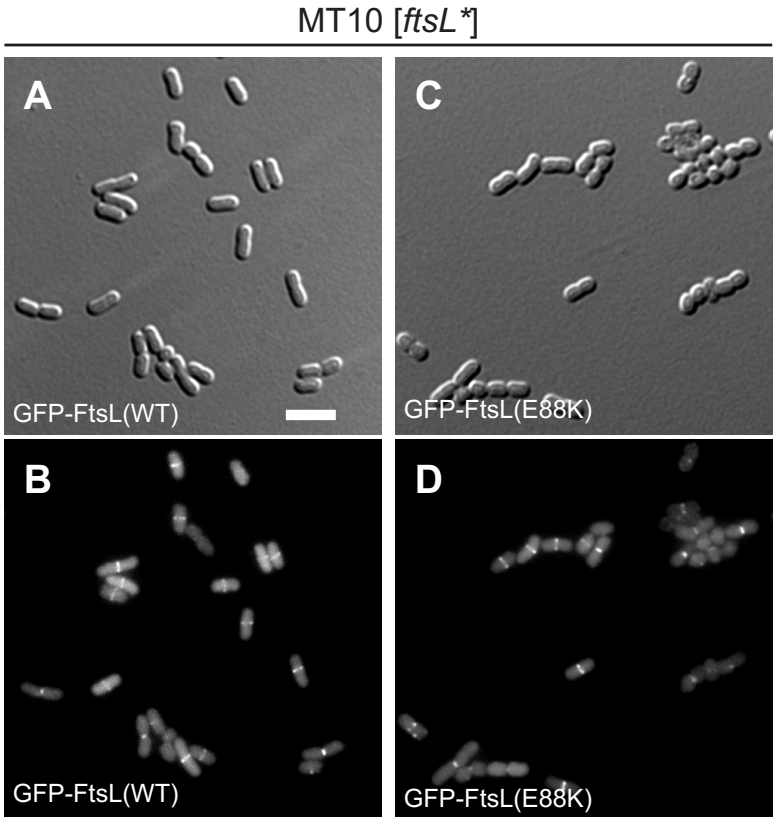

Figure 2.4. Localization of GFP-FtsL* under non-permissive conditions. Overnight cultures of MT10 [*ftsL**] containing the integrated GFP fusion constructs (**A, B**) *att*HKMT35 [P_{lac}*::gfp-ftsL(wt)*] or (**C, D**) *att*HKMT36 [P_{lac}*::gfp-ftsL**] were diluted in 0.5xLB-0N broth and grown to mid-log at 30°C. They were then diluted to a starting OD_{600} of ~ 0.02 in fresh 0.5xLB-0N supplemented with 25 µM IPTG and grown at 42°C to an OD_{600} of 0.3 - 0.5 before they were visualized on 2% agarose pads with DIC (**A, C**) and GFP (**B, D**) optics. Bar = 4µm.

Table 2.2. Co-localization of FtsL or FtsL* with ZapA at the division site.

genotype	% of total cells:		
	with stable ZapA-mCherry ring at the division site	with GFP-FtsL ring at the division site	with colocalized proteins
WT zapA-mCherry (P_{lac}::gfp-ftsL)	64.9 ± 1.1	38.1 ± 4.1	37.3 ± 4.4
ftsL zapA-mCherry (P_{lac}::gfp-ftsL*)*	54.3 ± 1.4	41.8 ± 2.7	41.3 ± 2.5

Overnight cultures of TU211(attHKMT35) [*WT zapA-mCherry (P_{lac}::gfp-ftsL)*] and MT102(attHKMT36) [*ftsL* zapA-gfp (P_{lac}::gfp-ftsL*)*] were diluted in minimal M9 medium supplemented with 0.2% maltose and 25uM IPTG and grown at 30°C until an OD_{600} of ~ 0.25 - 0.35. The cells were imaged using phase contrast, mCherry and GFP optics and analyzed using the imaging software NIS-Elements (Nikon) to determine the number of cells with a ZapA-mCherry ring or a GFP-FtsL(wt or L*) ring or both at the division site. 1200 cells were analyzed for each condition, n = 3. Shown are the average values ± standard deviation.

To examine the effect of FtsL* on the cell cycle further, we monitored the division process of wild-type and mutant cells (140 of each) using time-lapse microscopy. For this analysis, we used ZapA-GFP produced from the endogenous chromosomal locus as a proxy for cellular FtsZ dynamics. The division time was defined as the time between the formation of a stable Z-ring through the end of cell constriction and completion of daughter cell separation (**Figure 2.5A**) (See Experimental Procedures for details). Using MicrobeTracker and SpotFinderZ [44] to quantify the relevant parameters, we determined that, when grown on minimal medium agarose pads at

30°C, the mean division time in the *ftsL** mutant was significantly (ca. 25%) shorter than in wild-type (**Figure 2.5B-C, Table 2.3**). In wild-type cells, the division process made up 63% of the total cell cycle time, while in the mutant, only 52% of the cell cycle was dedicated to division. Thus, cell division proceeded faster in the *ftsL** mutant relative to wild-type cells.

Table 2.3. Measured division times of WT and *ftsL cells**

genotype	Mean cell cycle time (min)	Mean division time (min)	Mean division time as % of total cell cycle[a]
WT zapA-gfp	87.5 ± 2.9	54.6 ± 0.8	62.5 ± 1.6
ftsL zapA-gfp*	79.0 ± 3.0	41.3 ± 1.3	52.3 ± 1.1
	NS	**	**

Overnight cultures of HC261 [*WT zapA-gfp*] and MT90 [*ftsL* zapA-gfp*] were diluted in minimal M9 medium supplemented with 0.2% maltose and grown at 30°C until an OD_{600} of ~ 0.15 - 0.3. The cells were spotted on two separate halves of a 2% agarose pad containing 1X M9 salts and 0.2% maltose, the coverslip was sealed and a timelapse of both strains grown at 30°C was obtained using phase contrast and GFP optics, with frames taken every 1.5 min. The timelapse was analyzed using MicrobeTracker and SpotFinderZ to determine the total cell cycle time, as well as the division time. Division time is defined as the time between the formation of a stable Z-ring (using ZapA-GFP as a proxy for FtsZ) and the end of constriction. 140 cells were analyzed for each strain, n = 3. Shown are the average mean cell cycle time (in min), average mean division time (in min) and average mean division time (as % of total cell cycle time) ± standard error of the mean (SEM). Statistical significance was determined by two-tailed student's t-test.

[a] % = (mean division time / mean cell cycle time) * 100%

** difference significant at $p < 0.01$

NS, difference not statistically significant

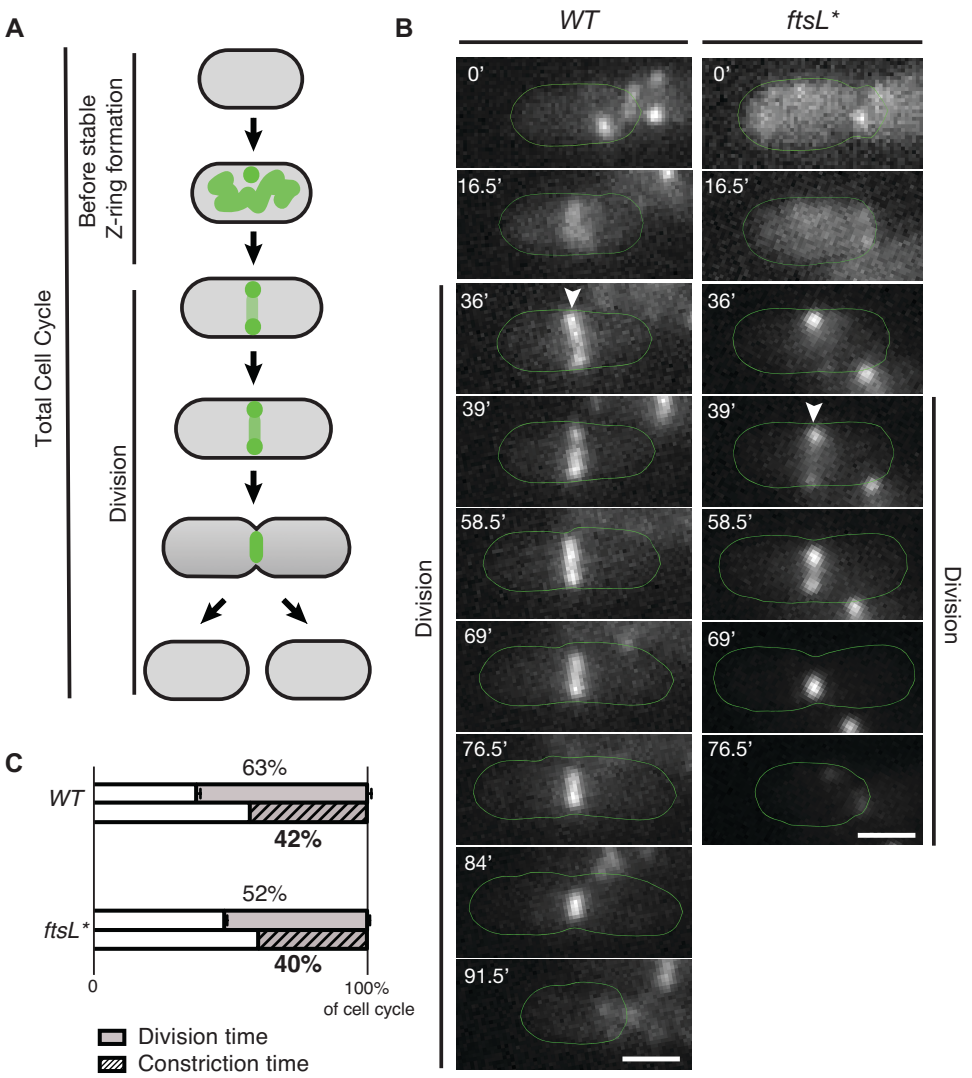

Figure 2.5. Division time is shorter in the *ftsL mutant compared to wild-type.** (**A**) For the purposes of the analysis, total cell cycle time was broken down into time prior to stable Z-ring formation and division time (the time from stable Z-ring formation to the completion of cell constriction). (**B**) Overnight cultures of HC261 [*zapA-gfp*] and MT90 [*ftsL* zapA-gfp*] were diluted in minimal M9 medium supplemented with 0.2% maltose and grown at 30°C until an OD_{600} of ~ 0.15 - 0.3. The cells were spotted on separate sides of a 2% agarose pad that was cut in half and contained 1X M9 salts, 0.02% casamino acids and 0.2% maltose, the coverslip was sealed and a timelapse of both strains grown at 30°C was obtained using phase contrast and GFP optics, with frames

Figure 2.5 (Continued). taken every 1.5 min. Shown are representative time-lapse images for WT and *ftsL** mutant cells. Bar = 1μm. Arrowheads mark the first time point where a stable FtsZ ring was formed. (**C**) Comparison of the division time and constriction time for WT and *ftsL** mutant cells as a percentage of the total cell cycle. To determine division time, the timelapse movies described in (B) were analyzed using MicrobeTracker and SpotFinderZ [44] to determine the total cell cycle time, as well as the division time. 140 cells were analyzed for each strain, n = 3. Error bars indicate the standard error of the mean (SEM) (see data in Table 3). To determine constriction time, TB28 [WT] or MT10 [*ftsL**] cells were grown to steady state in minimal M9 medium supplemented with 0.2% maltose at 30°C until an OD_{600} of ~ 0.1. The cells were visualized on 2% agarose pads with DIC optics and the presence of a constriction was determined manually. The constriction time shown is the average of two independent replicates, with 800 cells total for each strain (see data in Table 2.4).

The accelerated division of *ftsL** cells may either result from the premature initiation of constriction, an enhanced rate of constriction, or a combination of the two. In order to distinguish between these possibilities, we compared the average cell constriction time for wild-type and the *ftsL** mutant. Cells of each strain were grown to steady state in minimal medium at 30°C and the fraction of cells with a visible constriction was determined from DIC images (**Table 2.4**). Given steady-state growth, the constriction time as a percentage of the cell cycle was calculated as in a previous study [19]. Under these conditions, both strains grew with similar doubling times but the mean cell length of *ftsL** was less than that of wild-type as expected from the results described above. Interestingly, the constriction time of *ftsL** was only slightly shorter than wild-type (**Figure 2.5C, Table 2.4**), suggesting that the faster division of the *ftsL** mutant is primarily due to the premature initiation of constriction. Because we also

observed a shorter delay between the stabilization of the Z-ring and the recruitment of FtsL* to the divisome, we infer that the reduced cell length and cell volume of the *ftsL** mutant likely result from the premature maturation of the divisome and the subsequent initiation of cell constriction at a lower than normal cell volume.

Table 2.4. Constriction time of WT and *ftsL cells**

genotype	Mean cell length (*μ*m)[a]	Cell cycle analysis[b]			
		Mass doubling time, T_d (min)	Fraction of cells with constriction, F(x) (min)	Constriction time, t_c (min)	Constriction as % of cell cycle[c]
WT	2.93 ± 0.60	92	0.33	38	41.5
*ftsL**	2.50 ± 0.48	94	0.32	37	39.5

TB28 [*wt*] and MT10 [*ftsL**] were grown to steady-state in minimal M9 medium supplemented with 0.2% maltose at 30°C. The OD_{600} of the cultures was monitored at regular time intervals to determine the mass doubling time of each strain. At OD_{600} ~ 0.1, the cells were visualized on 2% agarose pads with either phase constrast or DIC optics. The mean cell length was determined from the phase contrast images using MicrobeTracker. The presence of a constriction was determined manually from the DIC images using the imaging software NIS-Elements (Nikon).

Given that the cultures were in steady-state growth, the period of visible constriction was determined as described [19]. Briefly, the constriction time (t_c) was calculated using: [$t_c = (T_d * \ln [1 + F(x)]) / \ln 2$], where T_d is the mass doubling time and F(x) is the fraction of cells with a visible constriction.

[a] Shown is the mean cell length ± standard deviation for a single experiment with 400 cells analyzed for each strain

[b] Shown is the average values from two independent experiments, with 800 cells total analyzed for each strain

[c] % = (t_c / T_d) * 100%

FtsL* causes a divisome malfunction

We suspected that the growth defect caused by the FtsL* variant under non-permissive conditions may stem from premature constriction initiation. We reasoned that if this was true, the defect should depend on an assembled divisome. Growth of *ftsL** cells in 0.5xLB-0N at 42°C was therefore monitored with or without production of the FtsZ antagonist and division inhibitor SulA prior to shifting the cells to non-permissive conditions. After three hours of growth in the presence of IPTG to induce the *sulA* expression construct, wild-type cells displayed a mild growth defect relative to the uninduced control (**Figure 2.6A**). As expected, these cells also formed long filaments indicative of a complete division block by SulA (**Figure 2.6B-C**). Strikingly, induction of *sulA* had the opposite effect on the growth of the *ftsL** mutant, with cells overexpressing *sulA* growing better than those lacking inducer (**Figure 2.6A**). Notably, although the induction of *sulA* still impaired division in the *ftsL** mutant, the division block appeared to be less robust than in wild-type cells. This observation suggests that the Z-ring may be more resistant to SulA in this background. Because blocking cell division relieved the negative effects of FtsL* on growth, we conclude that the variant protein is altering divisome function to induce the observed phenotypes.

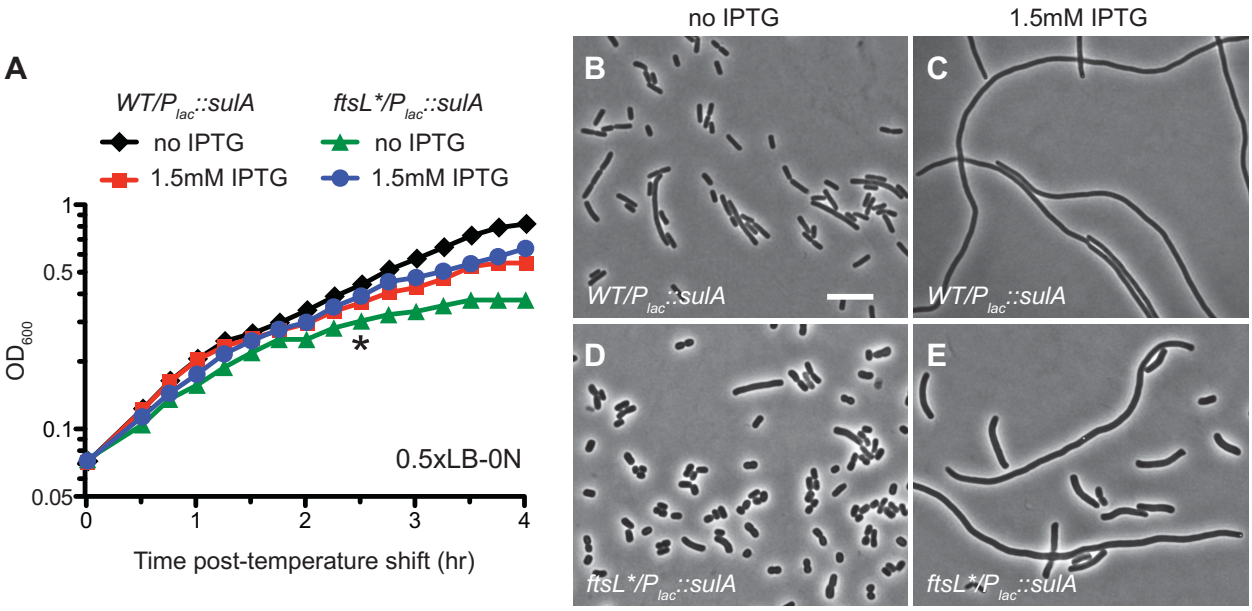

Figure 2.6. Overexpression of *sulA* suppresses the growth defect of the *ftsL mutant.** (**A**) Overnight cultures of TB28/pMT74 [WT/*P*$_{lac}$*::sulA*] and MT10/pMT74 [*ftsL*/ *P*$_{lac}$*::sulA*] were diluted in 0.5xLB-0N and grown to mid-log at 30°C. They were then diluted to a starting OD_{600} of ~ 0.015 in fresh 0.5xLB-0N medium with or without 1.5 mM IPTG and grown at 30°C for 1h before shifting to 42°C at time t = 0. (**B-E**) Cells were removed from the TB28/pMT74 (**B, C**) and MT10/pMT74 (**D, E**) cultures at the time point indicated by the asterisk and examined by phase contrast microscopy. Bar = 10µm.

In order to learn more about the division defect induced by *ftsL**, we selected for suppressors capable of growing on 0.5xLB-0N at 42°C following transposon mutagenesis of MT10 [*ftsL**]. Surviving colonies were purified and the positions of the transposon insertions were mapped. The insertion alleles were also transduced to a fresh MT10 [*ftsL**] background to confirm that suppression was indeed linked to the transposon. Several of the confirmed suppressors contained a transposon insertion in genes encoding divisome components implicated in the function and/or stability of the

machine, such as *ftsN*, *ftsK*, *dedD,* and *ftsP* [26, 40, 45-47] (**Figure 2.7A-B**). Three others had insertions in the complex *dcw* cluster of genes present at the two minute locus of the chromosome: two in *ddlB* and one at the 3' end of *murD* (**Figure 2.7A-B**). These insertions are likely to negatively impact division by affecting the expression of the many division genes located in this large operon. The final suppressor isolated was in *proQ*, which encodes an RNA-chaperone that post-transcriptionally regulates the osmoregulatory transporter ProP [48] (**Figure 2.7A-B**). This suppression is not due to polar effects on the downstream gene *prc*. Therefore, this allele is likely to suppress the sensitivity of *ftsL** cells to growth in medium with low osmolarity. Relative to the parental MT10 [*ftsL**] strain, derivatives with transposon insertions in genes with division related functions appeared longer, approaching the length of wild-type cells or even longer when they were grown in 0.5xLB-0N at 42°C (**Figure 2.7C-J**). Thus, as with *sulA* overexpression, transposon insertions that impair cell division suppress the growth phenotype of the *ftsL** mutation. These findings along with the above microscopic analyses strongly suggest that the growth defect and morphological changes induced by the FtsL* protein are mediated by a malfunctioning of the divisome that promotes the premature initiation of cell constriction.

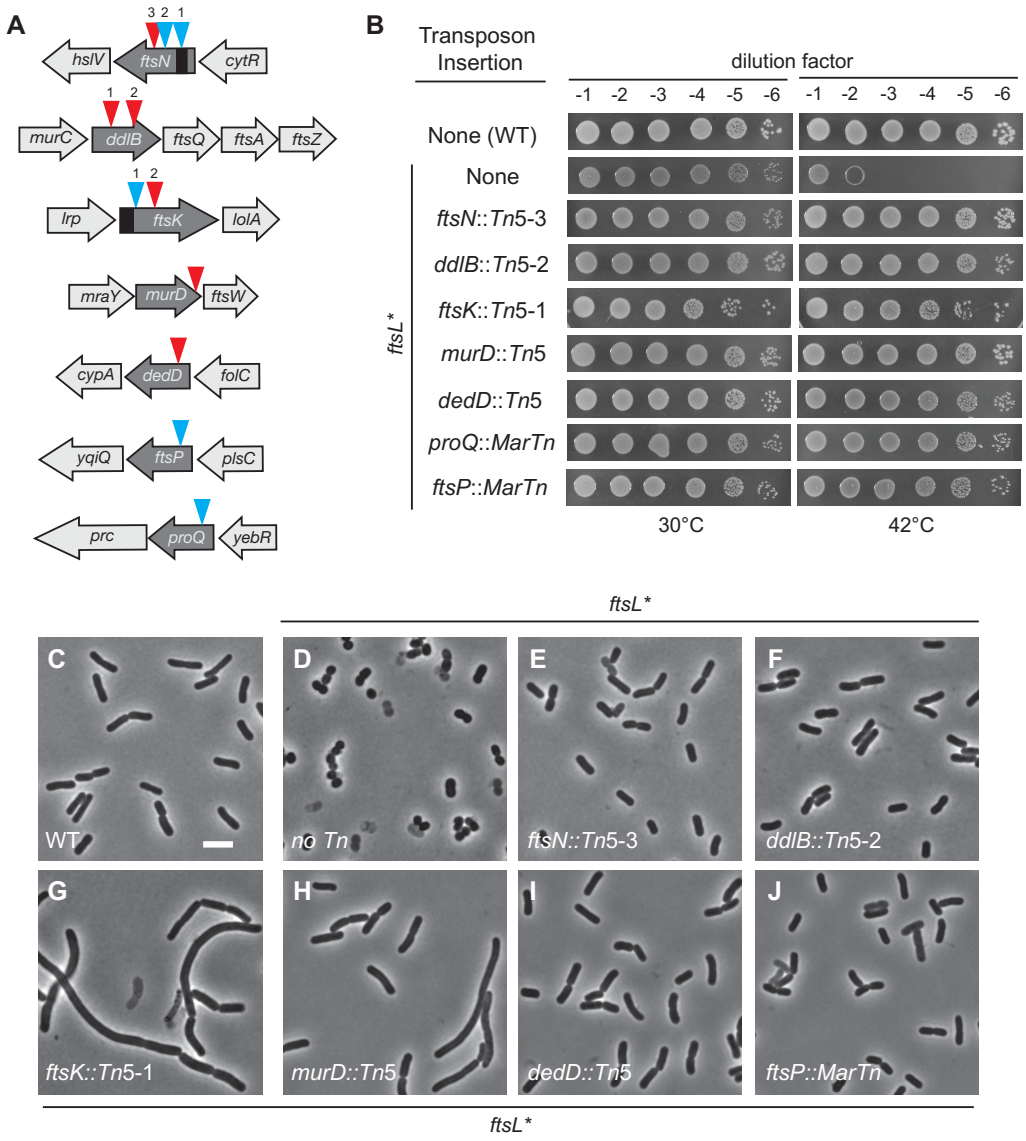

Figure 2.7. Transposon insertions that suppress the shape and growth defect of the *ftsL mutant.** (**A**) Shown is a diagram of the gene context and approximate positions of the unique transposon insertion mutants isolated in the suppressor selection. The triangles indicate the position of the transposon. Red, the direction of transcription in the kanamycin resistance cassette of the transposon is in the same orientation as disrupted gene; blue, opposite direction. The black segments denote the essential domains of FtsN and FtsK. (**B**) Cells of TB28 [WT], MT10 [*ftsL*(E88K)*], and MT10 derivatives with the indicated transposon insertions were grown in LB broth at

Figure 2.7 (Continued). 30°C. Following normalization for cell density (OD_{600} = 2), the resulting cultures were serially diluted (10^{-1} to 10^{-6}), and 5 µl of each dilution was spotted on 0.5xLB-0N agar. The plates were incubated overnight at the indicated temperature and photographed. *Tn5* and *MarTn* denote the two different transposons used for mutagenesis (see Experimental Procedures). (**C-J**) Overnight cultures of the strains from (B) were diluted in 0.5xLB-0N broth and grown to mid-log at 30°C. They were then diluted to a starting OD_{600} of ~ 0.02 in fresh 0.5xLB-0N and grown at 42°C to an OD_{600} of 0.3 - 0.5 before they were visualized on 2% agarose pads by phase contrast microscopy. Bar = 4µm.

FtsL* bypasses the essential functions of FtsK and FtsN

FtsK and FtsN both contain multiple domains with only a portion of the protein being essential for cell division. FtsK has three identifiable domains: (i) a polytopic transmembrane domain at its N-terminus, (ii) a long cytoplasmic linker domain, and (iii) a C-terminal AAA ATPase domain that functions as a DNA pump and also stimulates chromosome dimer resolution [49]. Only the N-terminal domain of FtsK is essential for cell division, but its function remains unknown [50, 51]. FtsN is a bitopic membrane protein with a flexible linker in the periplasm followed by a C-terminal SPOR domain with PG-binding activity [52, 53]. The essential domain of FtsN has been narrowed down to a small region of the periplasmic domain near the N-terminal transmembrane helix [40].

Of the *ftsL** suppressors isolated, we were intrigued by the *ftsK*::*Tn*5-1 and *ftsN*::*Tn*5-1 alleles because the insertions mapped within or very near the essential domains of FtsK and FtsN (**Figure 2.7A**). Further investigation showed that the *ftsK*::*Tn*5-1 insertion could only be transduced into a wild-type background on M9

minimal medium. On LB agar, the insertion resulted in a lethal division block (**Figure 2.8A**). This growth defect was completely suppressed by the *ftsL** mutation (**Figure 2.8A**), suggesting that this allele was capable of promoting cell division in cells lacking the essential N-terminal domain of FtsK [51]. To test this, we constructed an *ftsK* deletion strain possessing a second copy of the gene at an ectopic locus under control of the *lac* promoter (P_{lac}). As expected, in an otherwise wild-type background, this strain was dependent on IPTG induction for growth on both rich and minimal medium (**Figure 2.8B**). However, introduction of the *ftsL** mutation into this background resulted in IPTG independent growth regardless of the medium. We were also able to delete *ftsK* in the presence of the *ftsL** allele in a strain lacking the *ftsK* expression construct provided the strain was maintained on minimal medium (data not shown). We thus conclude that the *ftsL** mutation can bypass the essential function of FtsK.

Similar to the results with *ftsK*::*Tn*5-1, we found that the *ftsN*::*Tn*5-1 allele, in which the insertion disrupts the essential domain of FtsN [40], could only be transduced into a wild-type background if it possessed a second copy of *ftsN* under P_{lac} control. Such transductants were completely dependent on IPTG for growth, but again this dependence could be suppressed upon introduction of the *ftsL** mutation (**Figure 2.9A**). To test whether *ftsL** could suppress a more complete loss of FtsN function, we constructed an FtsN depletion strain that was deleted for the native *ftsN* gene and possessed the P_{lac}::*ftsN* expression construct. In an otherwise wild-type background, the strain was dependent on IPTG for growth. Following introduction of the *ftsL** allele, however, cell growth again became IPTG independent (**Figure 2.9B**). Similar to the

situation with *ftsK*, we could transduce an *ftsN* deletion into an *ftsL** strain lacking the P_{lac}::*ftsN* expression construct. However, the resulting strain grew very poorly, even on minimal medium (data not shown). We thus conclude that, as with FtsK, the *ftsL** allele can bypass the loss of FtsN function.

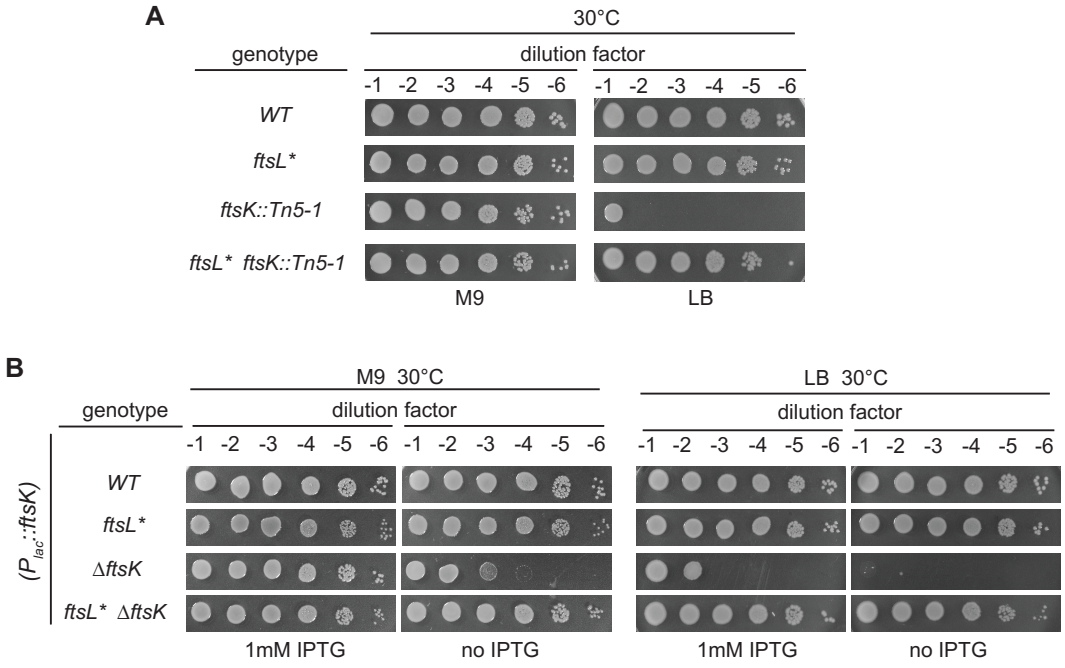

Figure 2.8. The *ftsL allele suppresses the essentiality of *ftsK*.** (**A**) Cells of TB28 [WT], MT10 [*ftsL**], MT38 [*ftsK::Tn*5-1] and MT30 [*ftsL* ftsK::Tn*5-1] were grown overnight in M9 maltose medium at 30°C. Following normalization for cell density (OD_{600} = 2), the resulting cultures were serially diluted (10^{-1} to 10^{-6}), and 5 µl of each dilution was spotted on the indicated medium. The plates were incubated overnight at 30°C and photographed. (**B**) Cells of TB28, MT10, MT75 [*ΔftsK*] and MT76 [*ftsL* ΔftsK*] containing the integrated *att*HKMT117 plasmid (*P_{lac}::ftsK*) were grown overnight in M9 maltose medium supplemented with 1mM IPTG, processed as in A, and spotted on the indicated medium with or without 1mM IPTG. The plates were incubated overnight at 30°C and photographed.

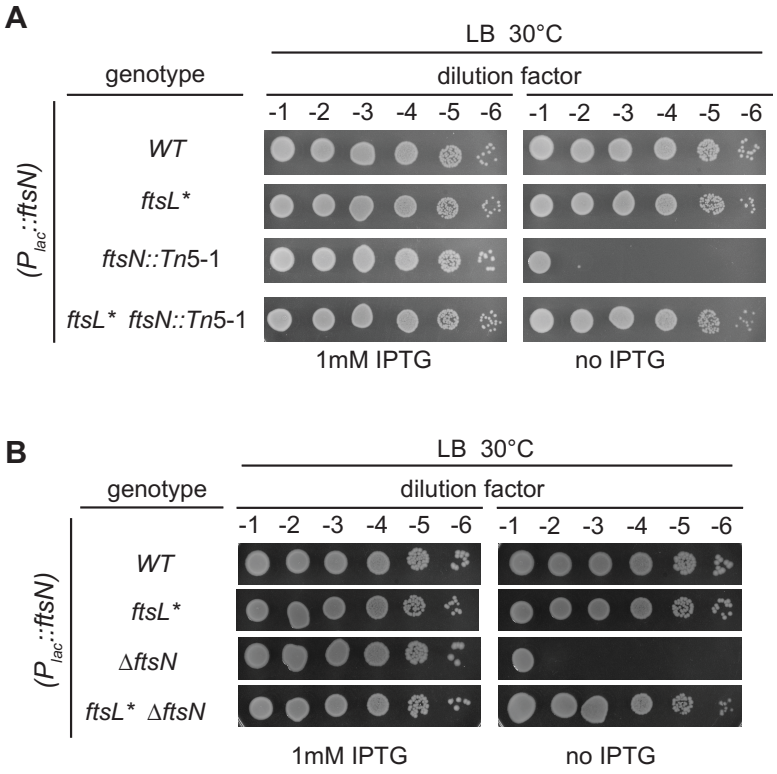

Figure 2.9. FtsL* bypasses the essential function of FtsN. (**A**) Cells of TB28 [WT], MT10 [*ftsL**], MT39 [*ftsN::Tn*5-1] and MT31 [*ftsL* ftsN::Tn*5-1] containing the integrated *att*HKNP102 plasmid (*P*$_{lac}$*::ftsN*) were grown overnight in LB broth supplemented with 1 mM IPTG at 30°C. Following normalization for cell density (OD_{600} = 2), the resulting cultures were serially diluted (10^{-1} to 10^{-6}), and 5 µl of each dilution was spotted on LB plates with or without 1 mM IPTG. The plates were incubated overnight at 30°C and photographed. (**B**) Cells of TB28, MT10, MT70 [*ΔftsN*] and MT71 [*ftsL* ΔftsN*] containing the integrated *att*HKNP102 plasmid (*P*$_{lac}$*::ftsN*) were processed as in A.

FtsL* largely bypasses the essential function of FtsA

Our results with *ftsL** were reminiscent of studies from Margolin and co-workers with an allele of *ftsA* called *ftsA**, which encodes FtsA(R286W) [39]. Cells with the *ftsA**

mutation are shorter than normal and do not require the essential functions of several division proteins including *ftsK*, *ftsN* and *zipA* [39, 42, 54]. To further investigate the similarity between *ftsA** and *ftsL** phenotypes, we assessed the ability of *ftsL** to suppress the essentiality of *zipA*. Indeed, we found that a *zipA* deletion could be transduced into a strain containing either the *ftsA** or *ftsL** alleles but not wild-type (data not shown).

Given the phenotypic similarities displayed by cells with the *ftsL** and *ftsA** alleles, FtsL and FtsA may lie within the same genetic pathway that modulates divisome activation and constriction initiation, possibly with FtsK, FtsN and ZipA acting upstream. If so, FtsL might either serve as an intermediary between FtsK/FtsN/ZipA and FtsA, or function downstream of FtsA to activate septal PG synthesis and cell constriction. To differentiate between these possibilities, we investigated the potential of *ftsL** mutants to bypass the essential function of FtsA. For these experiments, we employed a previously characterized strain in which FtsA could be depleted by growth at low temperature (30°C) [7]. Cells of this strain harbor a frameshift mutation in the native *ftsA* gene, indicated as $ftsA^0$, and possess a second copy of *ftsA* on a low copy plasmid under the control of the lambda P_R promoter and a temperature-sensitive CI repressor (CI857). Thus, at 37°C, the repressor is inactivated, *ftsA* is expressed, and cells divide more or less normally. However, shifting the cells to 30°C restores repressor function and division is inhibited due to the depletion of FtsA. The observed phenotypes of the strain at 30°C: (i) division block, (ii) growth defect, and (iii) FtsA protein depletion as monitored by immunoblotting, were all observed regardless of whether cells were grown in minimal

or rich medium, although the phenotypes were most severe in LB broth (**Figure 2.10**). Strikingly, introduction of the *ftsL** allele into the *ftsA*^{0}/P_R::*ftsA* strain dramatically improved its ability to divide at 30°C in both media types and completely restored plating efficiency at 30°C on M9 minimal agar without affecting the level of FtsA depletion achieved (**Figure 2.10**). We were unable to transduce the *ftsA*^{0} allele into an *ftsL** strain in the absence of the low-copy vector expressing *ftsA* (data not shown), suggesting that although the FtsA-requirement is dramatically reduced, a residual level of FtsA remains important for cell division in the presence of FtsL*. We thus conclude that the FtsL* protein largely bypasses the essential activity of FtsA. FtsL is therefore likely to be functioning downstream of FtsA in the proposed divisome activation pathway.

Figure 2.10. The *ftsL mutation suppresses the growth defect resulting from FtsA depletion.** (**A**) Overnight cultures of MT78/pDB355 [*ftsA*^{0}/P_R*::ftsA cI*^{TS}] or MT79/pDB355 [*ftsL* ftsA*^{0}/P_R*::ftsA cI*^{TS}] cells were diluted in fresh LB or M9 maltose medium and grown at 37°C or shifted to 30°C. Growth at 30°C results in the repression of the P_R promoter by CI and the concomitant depletion of wild-type FtsA. (**B-G**) Cells were removed from the MT78/pDB355 (**B, C, D**) and MT79/pDB355 (**E, F, G**) cultures at the time points indicated by the asterisks in (A) and examined by phase contrast microscopy. Bar = 10 µm. (**H**) At the time points indicated by the asterisks, cells were also harvested for whole-cell extract preparation. Proteins in the resulting extracts were separated by SDS-PAGE, transferred to PVDF, and FtsA was detected with anti-FtsA antisera. (**I**) Cells of MT78/pDB355 [*ftsA*^{0}/P_R*::ftsA cI*^{TS}] or MT79/pDB355 [*ftsL* ftsA*^{0}/P_R*::ftsA cI*^{TS}] were grown overnight in M9 maltose medium supplemented with spectinomycin at 37°C. Following normalization for cell density (OD_{600} = 2), the resulting cultures were serially diluted (10^{-1} to 10^{-6}), and 5 µl of each dilution was spotted on LB or M9 maltose agar. The plates were incubated at 37°C or 30°C and photographed after 12 - 36 hours depending on the medium.

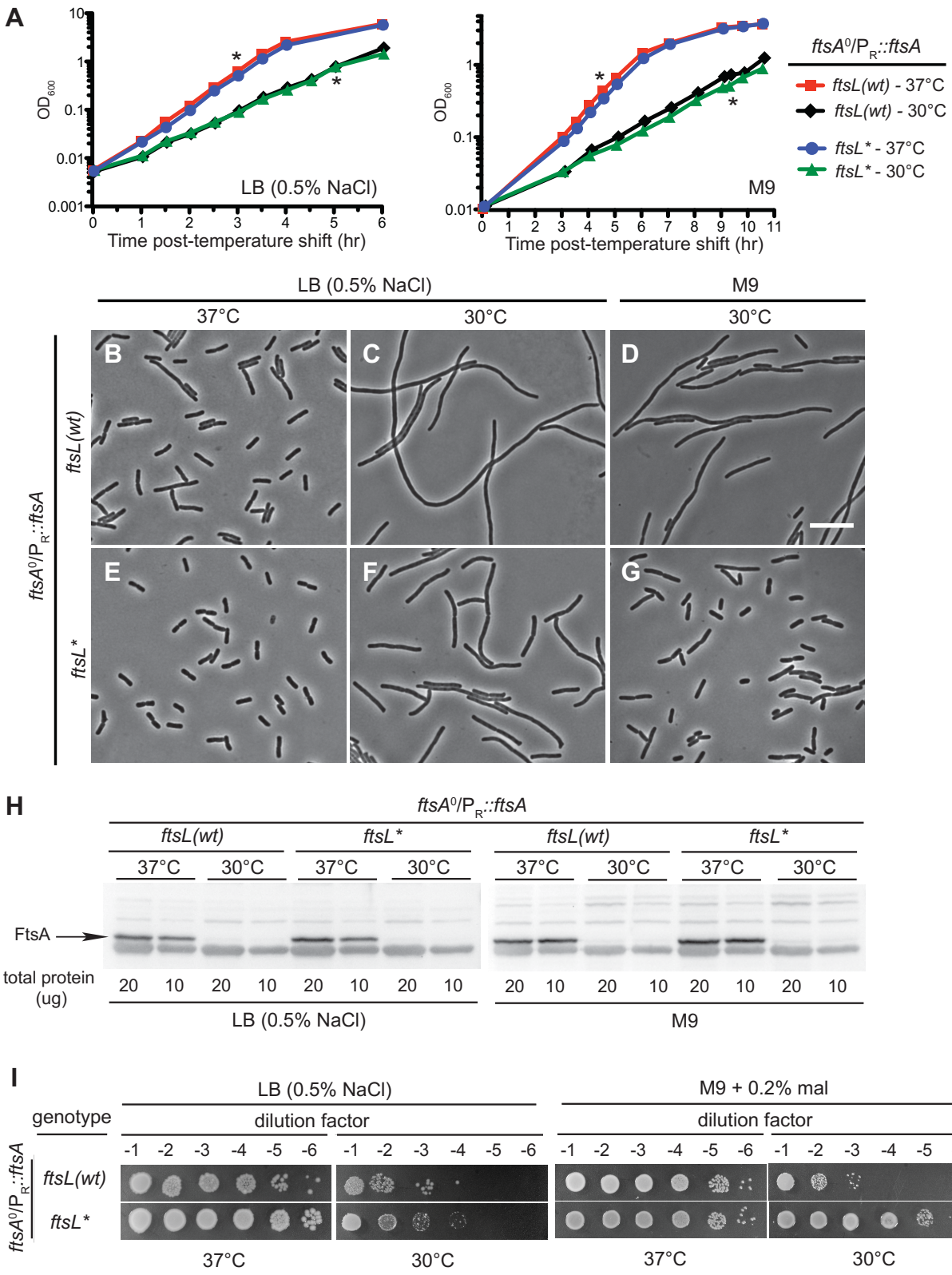

Figure 2.10 (Continued).

Section 2.4: Discussion

In *E. coli*, FtsL lies in the middle of the linear dependency pathway of divisome assembly and is a late recruit to the cytokinetic ring structure [19, 55]. It forms a complex with FtsB and FtsQ prior to localizing to the divisome [33]. Outside of the observation that these factors are essential for division, the function of FtsL and its partners in the FtsQLB complex remains unclear. Here, we studied the properties of a unique *ftsL* mutant we call *ftsL** in an effort to better understand how FtsL promotes cell division. Unlike most mutant alleles of the essential *fts* genes that cause a division block and the formation of smooth filamentous cells at the non-permissive temperature, *ftsL** [*ftsL*(E88K)] was reported to induce cell lysis [30, 31]. This observation suggested that *ftsL** may encode a mutant protein that fails during the process of cell constriction rather than at a step prior to initiation. We therefore reconstructed an *ftsL** strain and examined its growth and morphology under permissive (LB or M9 medium at all temperatures) or non-permissive (0.5xLB-0N at 42°C) growth conditions. In all media tested, the *ftsL** mutant appeared significantly shorter and wider than the wild-type control strain, with the greatest differential between the two displayed in 0.5xLB-0N at 42°C. We did not observe a precipitous drop in culture optical density when the *ftsL** mutant was shifted to non-permissive growth conditions, but lysed cell ghosts were apparent in the culture upon microscopic analysis. Although this lysis phenotype was relatively mild in liquid medium, we assume that it is likely to be exacerbated on solid 0.5xLB-0N agar at 42°C, resulting in the severe defect in plating efficiency observed under these conditions.

All of our microscopic and genetic results suggest that the *ftsL** size and growth phenotypes stem from an accelerated division process, most likely via the premature initiation of cell constriction. It is less clear why the mutant also appears to have a wider cell width and undergoes lysis under non-permissive conditions. However, given the importance of PG biogenesis for cell shape and integrity, these phenotypes probably result from defects in the assembly of the cell wall layer that are exacerbated upon growth in medium of low osmolarity at high temperatures. The problems with PG biogenesis in the mutant may be directly related to accelerated division, for example by the initiation of certain cell wall remodeling processes out of sequence or before the proper controls are in place. Alternatively, the shape and lysis phenotypes may result from an indirect and negative effect of a hyperactive divisome on the cell elongation machinery, possibly via a competition for cell wall precursors or protein components shared between the complexes. In either case, our findings point to a role for FtsL in the control of divisome function.

Previous studies in *Bacillus subtilis* have implicated FtsL as a possible point of regulation in the activity of the divisome [56, 57]. FtsL is highly unstable in *B. subtilis* and subject to degradation by the membrane protease YluC, a member of the site-2-protease family of proteases involved in regulated intramembrane proteolysis [56]. Importantly, inactivation of YluC or alterations of FtsL that prevent its turnover result in a short-cell phenotype, suggesting that FtsL levels are limiting for division [56]. This turnover of FtsL has also been implicated in blocking cell division in response to problems with DNA replication [57]. Given these results in *B. subtilis*, a simple

explanation for the early division phenotype of the *ftsL** mutant in *E. coli* is that the variant protein is stabilized and accumulates to higher than normal levels. However, although the steady-state level of FtsL* as assessed by immunoblot appears to be slightly higher than that of the wild-type protein, our genetic analysis indicates that the phenotypes are unlikely to be related to FtsL protein levels and/or stability. Overproduction of wild-type FtsL was not found to result in premature cell division. Furthermore, the expression of wild-type *ftsL* in the presence of *ftsL** restored normal division and growth on 0.5xLB-0N at 42°C. Therefore, rather than affecting FtsL protein levels, the E88K substitution in the periplasmic coiled-coil domain of FtsL* is likely to result in an altered conformation of the protein that prematurely stimulates cell division.

How the altered protein achieves this activation is not clear. One possibility is that it causes the FtsQLB complex to be recruited to the divisome early, thereby accelerating divisome maturation and the subsequent initiation of constriction. However, it is hard to envisage how merely speeding up the normal divisome assembly process could have such dramatic effects on cell shape and osmotic stability. We therefore favor an alternative explanation in which the FtsL* variant exerts its effects by short-circuiting the normal controls preventing the initiation of septal PG biogenesis and cell constriction prior to the proper completion of divisome assembly. The existence of a signaling process required for stimulating septal PG biogenesis following divisome assembly is consistent with recent work in *Caulobacter cresentus* showing that small membrane proteins produced in response to DNA damage can block division at the level of FtsI and FtsW activation [58, 59]. The FtsQLB complex is an attractive candidate for

mediating this activation given its presence upstream of FtsW and FtsI in the recruitment dependency pathway [4] and the potential interactions between these proteins suggested by two-hybrid analysis [14]. The properties of the FtsL* variant are consistent with a model in which the FtsQLB complex exists in one of two conformational states upon recruitment to the division site, “OFF” or “ON”, and that its conformation is somehow sensitive to the status of divisome assembly. Normally, the complex may only switch to the ON conformation to stimulate downstream events like septal PG synthesis once it “senses” that divisome assembly is complete. However, in the presence of FtsL*, the complex might spontaneously convert to the ON state such that it stimulates constriction before the division machinery is capable of safely initiating the process, thus causing problems with septal PG biogenesis and remodeling and rendering cells sensitive to low osmolarity and extremes of temperature.

What signals might FtsQLB receive for its potential role in monitoring divisome assembly? Some clues were provided from our analysis of *ftsL** suppressors as well as the recent literature. Because the essential functions of FtsN, FtsK and FtsA are completely or partially bypassed by the FtsL* variant, we propose that these proteins might communicate the status of divisome assembly to the FtsQLB complex. The bitopic membrane protein FtsN has long been thought to play a role in initiating constriction [13] due to its status as the last essential protein to be recruited to the divisome in the dependency pathway [45] and the ability of FtsN overexpression to stimulate division and suppress defects in numerous components of the divisome [51, 54, 60-62]. This idea was reinforced with the demonstration that FtsN is recruited to the divisome in a

self-enhancing process involving its small, membrane-proximal, essential domain (^{E}FtsN) and its C-terminal, PG-binding SPOR domain (^{S}FtsN) [40]. Based on this observation, a model for a positive feedback loop that drives cell constriction was proposed in which ^{E}FtsN stimulates septal PG synthesis and remodeling to create the recruitment signal for ^{S}FtsN, which brings more ^{E}FtsN to the division site to stimulate more septal PG synthesis, and so on [40]. The similarities between the phenotypes of FtsN overproduction and FtsL* in addition to the ability of FtsL* to bypass ^{E}FtsN function suggests the possibility that the accumulation of ^{E}FtsN above a critical threshold at midcell acts as one of the signals that divisome assembly is complete and either directly or indirectly converts the FtsQLB complex to an active complex that promotes septal PG synthesis and cell constriction.

Importantly, the isolation and analysis of *ftsA* mutants that bypass the normal requirement for other essential division proteins, including FtsN, indicates that the constriction initiation mechanism involves more than ^{E}FtsN recruitment [39, 42, 54, 61]. One of these mutants, *ftsA*(R286W),* is particularly relevant because it results in a short cell phenotype and has been shown to bypass the same set of divisome proteins as *ftsL** [39, 54, 63]. Thus, similar to our proposal for the FtsQLB complex, FtsA may also exist in one of two possible conformations, OFF and ON, that may participate in the control of constriction initiation. Recent results from Pichoff and Lutkenhaus suggest that this conformational change may be related to the polymeric status of FtsA with the polymeric form being inhibitory and the monomeric or reduced polymeric form being stimulatory for division. In addition, evidence from the Margolin group has been

accumulating indicating that the cytoplasmic N-terminal tail of FtsN interacts directly with FtsA in such a way that it would compete with the formation of FtsA polymers [13, 16, 64, 65]. Taken together, these results suggest that the N-terminal region of FtsN promotes a conformation of FtsA that can stimulate constriction [16, 64]. The observation that FtsL* can largely bypass the need for FtsA in addition to FtsN suggests that the FtsQLB complex is downstream of FtsA in the putative signaling pathway (**Figure 2.11**) and may be sensing FtsA conformation in addition to ^{E}FtsN recruitment as a means of assessing the status of divisome assembly prior to stimulating constriction. Additional support for this working model for the control of constriction initiation can be found in the accompanying report from Liu and coworkers [43]. What is missing from these models is a definitive role for FtsK. Defects in FtsK are suppressed by increased expression of FtsN, FtsB, FtsQ as well as the *ftsA** and *ftsL** alleles [54], suggesting its essential N-terminal domain is providing an input upstream of the FtsQLB complex in the putative signaling pathway. However, whether it is working through an effect on FtsA, an interaction with the FtsQLB complex [50], or both is unclear.

It is important to note that, based on the results with FtsN from the de Boer lab [40], the entire signaling system proposed in **Figure 2.11** is likely to be self-enhancing and intimately connected with the recruitment of the relevant components to the divisome. Thus, it may only be a few molecules of each factor that are recruited to midcell to initiate the cycle, but their activity is expected to be rapidly amplified to attract additional components and stimulate a sustained and visible constriction of the cell envelope. Such a possibility may explain the observed two-step divisome assembly

process and the near simultaneous arrival of the late proteins coincident with the onset of constriction [19].

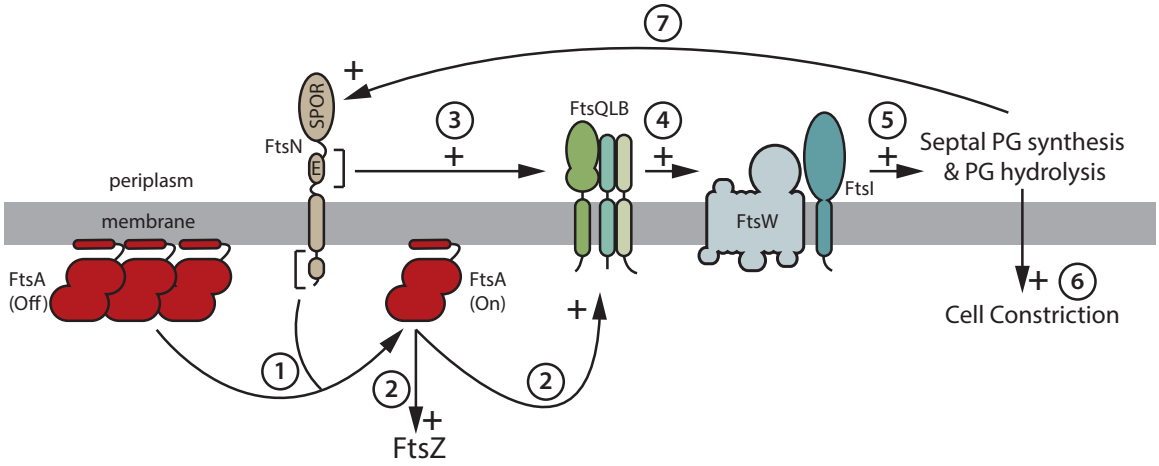

Figure 2.11. A potential signaling system involved in controlling constriction initiation. Shown is an illustration highlighting the major features of a model for a signaling pathway involved in controlling the initiation of cell constriction by the divisome. The transition of FtsA from an OFF to an ON conformation appears to be one of the major signals and may involve a change in polymerization state (step 1). The ON conformation of FtsA may then promote an altered, more stable, form of the Z-ring as well as directly or indirectly signaling its altered status to the FtsQLB complex (step 2). Because reduced FtsA self-interaction bypasses the essential functions of FtsN, FtsN may normally facilitate the disruption of FtsA polymers to stimulate constriction (step 1). The essential domain of FtsN (E) is also likely to either communicate the status of divisome assembly directly to the FtsQLB complex to stimulate constriction (step 3) or stimulate the synthesis of septal PG by activating the septal PG biogenesis machinery (FtsW and FtsI) directly in a manner that is redundant with FtsQLB activity (not shown). Similarly, given that FtsA and FtsL variants can bypass FtsK function, FtsK may also play a role in modulating FtsA conformation and or the communication of divisome assembly status directly to FtsQLB (not shown). The input from upstream signals

Figure 2.11 (Continued). received by FtsQLB is likely to cause a conformational change in the complex that is, in turn, communicated to FtsW, FtsI, and the rest of the PG synthetic apparatus to stimulate cell wall remodeling and cell constriction (steps 4, 5, and 6). The entire process is likely to be reinforced by positive feedback loops involving FtsN recruitment (step 7) and possibly other as yet to be identified feedbacks. See text for details, and also the accompanying paper from Liu and co-workers for additional support for this general scheme [43].

In summary, studies of division mutants with phenotypes other than filamentation such as *ftsA** [39] and *ftsL** are revealing what appears to be a complex signaling pathway that promotes the initiation of cell constriction by the divisome. The isolation and characterization of additional alleles in this class as well as other types of mutants that fail post-initiation is likely to shed additional light on the function of essential divisome components and the mechanism of cell constriction.

Section 2.5: Experimental procedures

Media, bacterial strains and plasmids

Cells were grown in LB (1% tryptone, 0.5% yeast extract, 0.5% NaCl), 0.5xLB-0N (0.5% tryptone, 0.25% yeast extract) or minimal M9 medium [66] supplemented with 0.2% casamino acids and 0.2% maltose. Unless otherwise indicated, antibiotics were used at 25 (chloramphenicol; Cm), 25 (kanamycin; Kan), 10 (tetracycline; Tet) or 50 (spectinomycin, Spec) µg/ml. For M9 medium, 50µg/ml Kan and 12.5µg/ml Tet were used.

The bacterial strains used in this study are listed in **Table 2.5**. All *E. coli* strains used in the reported experiments are derivatives of MG1655 [67]. Plasmids used in this study are listed in **Table 2.6**. PCR was performed using KOD polymerase (Novagen) for cloning purposes and *Taq* DNA polymerase (NEB) for diagnostic purposes, both according to the manufacturer's instructions. Unless otherwise indicated, MG1655 chromosomal DNA was used as the template. Plasmid DNA and PCR fragments were purified using the Zyppy plasmid miniprep kit (Zymo Research) or the Qiaquick PCR purification kit (Qiagen), respectively.

Table 2.5. Strains used in this study.

Strain	Genotype[a]	Source/Reference[b]
DH5α	*F– hsdR17 deoR recA1 endA1 phoA supE44 thi-1 gyrA96 relA1 Δ(lacZYA-argF)U169 ϕ80dlacZΔM15*	Gibco BRL
MG1655	*rph-1 ilvG rfb-50*	[67]
TB28	MG1655 *ΔlacIZYA*::*frt*	[68]
CH2	*dadR trpE trpA tna ftsA(0) recA::Tn10*	[7]
CH34	TB28 *ΔftsN::kan*^{R}	[40]
CH43	TB28 *leu::Tn10*	from de Boer lab
HC261	TB28 *zapA*-GFP *cm*^{R}	[20]
MT10	TB28 *ftsL(E88K)*	Allelic replacement
MT13	TB28 *leu::Tn10 ftsL(E88K)*	P1(CH43) x MT10
MT23	TB28 *ftsL(E88K) proQ::MarTn*	This Study (Isolated Suppressor)
MT24	TB28 *ftsL(E88K) ftsP::MarTn*	This Study (Isolated Suppressor)

Table 2.5 (Continued).

Strain	Genotype[a]	Source/Reference[b]
MT28	TB28 *ftsL(E88K) ftsN::Tn5-3*	This Study (Isolated Suppressor)
MT29	TB28 *ftsL(E88K) ddlB::Tn5-2*	This Study (Isolated Suppressor)
MT30	TB28 *ftsL(E88K) ftsK::Tn5-1*	This Study (Isolated Suppressor)
MT31	TB28 *ftsL(E88K) ftsN::Tn5-1*	This Study (Isolated Suppressor)
MT32	TB28 *ftsL(E88K) murD::Tn5*	This Study (Isolated Suppressor)
MT35	TB28 *ftsL(E88K) dedD::Tn5*	This Study (Isolated Suppressor)
MT38	TB28 *ftsK::Tn5-1*	P1(MT30) x TB28
MT39	TB28 *ftsN::Tn5-1*	P1(MT31) x TB28
MT70	TB28 *ΔftsN::kan^R*	P1(CH34) x TB28
MT71	TB28 *ftsL(E88K) ΔftsN::kan^R*	P1(CH34) x MT10
MT75	TB28 *ΔftsK::kan^R*	λRed
MT76	TB28 *ftsL(E88K) ΔftsK::kan^R*	P1(MT75) x MT10
MT78	TB28 *zapA*-GFP *frt leu::Tn10 ftsA(0)*	P1(MT13) x NP180
MT79	TB28 *zapA*-GFP *frt leu::Tn10 ftsL(E88K) ftsA(0)*	P1(MT13) x NP180
MT90	TB28 *ftsL(E88K) zapA*-GFP *cm^R*	P1 (HC261) x MT10
MT102	TB28 *ftsL(E88K) zapA-mCherry cm^R*	P1 (TU211) x MT10
NP1	TB28 *zapA*-GFP *frt*	[20]
NP179	TB28 *zapA*-GFP *frt leu::Tn10*	P1(CH43) x NP1
NP180	TB28 *zapA*-GFP *frt ftsA(0)*	P1(CH2) x NP179
TU211	TB28 *zapA-mCherry cm^R*	[20]

Table 2.5 (Continued).

[a] The Kan^R and Cm^R cassettes are flanked by *frt* sites for removal by FLP recombinase. An *frt* scar remains following removal of the cassette using FLP expressed from pCP20.

[b] Strain constructions by P1 transduction are described using the shorthand: P1(donor) x recipient. Transductants were selected on Kan, Tet, Cm, or minimal medium with no casamino acids plates where appropriate. Allelic replacement and λRec indicates strains were constructed by allelic exchange and recombineering respectively (see Experimental Procedures for details).

Table 2.6. Plasmids used in this study.

Plasmid	Genotype[a]	Origin	Source or Reference
pDB355	*aadA cI857(ts)* $P_{\lambda R}$*::ftsA*	pSC101	[7]
pDS132	*cat mobRP4 sacB*	R6K	[69]
pDY31	*cat araC* P_{ara}*::amiB*	pACYC/p15A	[21]
pKD46	*bla repA101(ts) araC* P_{ara}*::γ-β-exo*	pSC101	[70]
pMG20	*cat araC* P_{ara}*::*^{ss}*torA-bfp-ftsN(71-105)*	pACYC/p15A	[40]
pMM61	*att*HK022 *tetA tetR lacI*^{q} P_{lac}*::gfp-slmA*	R6K	This study
pMT15	*att*HK022 *tetA tetR lacI*^{q} P_{lac}*::ftsL*	R6K	This study
pMT16	*att*HK022 *tetA tetR lacI*^{q} P_{lac}*::ftsL(E88K)*	R6K	This study
pMT17	*cat mobRP4 sacB mraZ-mraW-ftsL(E88K)-ftsI*	R6K	This study
pMT23	*tetA tetR lacI*^{q} P_{lac}*::nlpD*	R6K	This study
pMT27	*cat araC* P_{ara}*::ftsL*	pACYC/p15A	This study
pMT28	*cat araC* P_{ara}*::ftsL(E88K)*	pACYC/p15A	This study
pMT35	*att*HK022 *tetA tetR lacI*^{q} P_{lac}*::gfp-ftsL*	R6K	This study
pMT36	*att*HK022 *tetA tetR lacI*^{q} P_{lac}*::gfp-ftsL(E88K)*	R6K	This study
pMT74	*tetA tetR lacI*^{q} P_{lac}*::sulA*	pBR/ColE1	This study

Table 2.6 (Continued)

Plasmid	Genotype[a]	Origin	Source or Reference
pMT117	*tetA tetR lacI*^{q} P$_{lac}$*::ftsK*	R6K	This study
pNP20	*att*HK022 *tetA tetR lacI*^{q} P$_{lac}$*::nlpD-mCherry*	R6K	[20]
pNP102	*att*HK022 *tetA tetR lacI*^{q} P$_{lac}$*::ftsN*	R6K	This study
pTB102	*cat repA(ts) cI857(ts)* P$_{\lambda R}$*::int(HK022)*	pSC101	[71]

[a] $P_{\lambda R}$, P_{lac}, and P_{ara} indicate the phage λR, lactose, and arabinose promoters, respectively.

Allelic replacement

A strain harboring the chromosomal *ftsL** mutation was constructed by allelic exchange using a modification of a procedure that was previously described [69]. The *pir*-dependent suicide plasmid pMT17 [*sacB* Cm^{R}] contained the *ftsL** gene with large regions of flanking homology. It was introduced into the recipient strain TB28(*att*HKMT15) [WT(P$_{lac}$*::ftsL* Tet^{R})] by conjugative transfer from the donor strain SM10(*λpir*). Briefly, 100 µl each of overnight cultures of the donor and recipient strains were mixed with fresh LB broth. After approximately 6 hours of incubation at 37°C, cells were diluted in fresh LB broth and plated on minimal M9 maltose plates supplemented with chloramphenicol, tetracycline and 1mM IPTG to select for TB28(*att*HKMT15) exconjugants with pMT17 integrated into the chromosome via a single cross-over. After incubation at 30°C for approximately 36 hours, one colony from this plate was picked, diluted in 10 mM $MgSO_4$ and serial dilutions were plated on minimal M9 maltose plates

with 1 mM IPTG and 6% sucrose. After incubation at 30°C for several days, 30 isolates were purified on minimal M9 maltose plates supplemented with 1mM IPTG and either chloramphenicol or 6% sucrose. The Suc^R Cm^S isolates were tested for a temperature-sensitive growth defect on 0.5xLB-0N indicative of the *ftsL** allele replacing the wild-type copy of *ftsL* at the native chromosomal locus. Presence of the allele was then confirmed by PCR and sequencing. Strain MT10 was obtained by P1-mediated transduction of the *ftsL** allele from the primary isolate into the chromosome of CH43 [*leu*::*Tn*10] by selecting for Leu^+ transductants and screening for temperature-sensitive growth on 0.5xLB-0N medium.

Recombineering

The *ΔftsK::kan^R* allele was constructed by replacing the region between the 2nd codon and the 7th codon from the stop codon of *ftsK* with the *kan^R* cassette as described previously [72, 73]. The *kan^R* cassette was amplified from pKD13 [70] using the primers 5'-ATCGGGCAGGAAAAGCCTGTAACCTGGAGAGCCTTTCTTGATTCCGGGGATCCGTCGACC-3' and 5'-CCGGCATACGATGCATTAGTTAGTCAAACGGCGGTGGGGCTGTAGGCTGGAGCTGCTTCG-3'. The resulting PCR product was purified and electroporated into strain TB28(attHKMT117)/pKD46 as described previously [68] and the recombinants were selected at 30°C on a minimal M9 plate containing 50 µg/ml kanamycin and 1 mM IPTG to generate the chromosomal deletion.

Suppressor selection

To select for suppressors of the lytic temperature sensitive phenotype of MT10 [*ftsL**], the strain was mutagenized either with the EzTn5-Kan2 transposome (Epicentre) or with a Mariner-based transposon as previous described [68, 74]. Mutants were selected for kanamycin resistance at 30°C, yielding a library of ~ 70,000 or ~ 300,000 independent transposon insertions, respectively. The mutant libraries were plated on 0.5xLB-0N agar and incubated at 42°C to identify mutants capable of growing under these non-permissive conditions. The frequency at which survivors arose was approximately 10^{-5} for spontaneous suppressors and 10^{-4} for the transposon libraries. The sites of the transposon insertions in the suppressors were identified by arbitrarily primed PCR followed by sequencing [68], and the transposons were transduced into a fresh MT10 background to confirm that the suppression phenotype was linked to the insertion in question.

Microscopy and image analyses

Both light and fluorescence microscopy were performed as described previously [75]. See figure legends for specific growth conditions employed for each experiment.

For the determination of constriction time shown in Figure 2.3 and Table 2.4, overnight cultures of TB28 [WT] and MT10 [*ftsL**] were diluted to a starting OD_{600} of ~ 0.03 in minimal M9 medium supplemented with 0.2% maltose and grown at 30°C until an OD_{600} of ~ 0.15 was reached. These cultures were then back-diluted to OD_{600} of ~

0.005 in fresh M9-maltose and growth was continued at 30°C. The OD_{600} of the cultures was monitored at regular time intervals to determine the mass doubling time of each strain. At specific time points, cells were imaged on 2% agarose pads using phase contrast optics and cell length was measured using MicrobeTracker. Cultures were considered to be at steady state if the cell length distribution remained constant over time. At $OD_{600} \sim 0.1$, the cells were visualized on 2% agarose pads with DIC optics. The presence of a constriction was determined manually using the imaging software NIS-Elements (Nikon). Given that the cultures were in steady-state growth, the period of visible constriction was determined as described [19]. Briefly, the constriction time (t_c) was calculated using the formula [$t_c = (T_d * \ln [1 + F(x)]) / \ln 2$], where T_d is the mass doubling time and F(x) is the fraction of cells with a visible constriction.

Time-Lapse Analysis

Overnight cultures of HC261 [*WT zapA-gfp*] and MT90 [*ftsL* zapA-gfp*] were diluted in minimal M9 medium supplemented with 0.2% maltose and grown at 30°C until an OD_{600} of ~ 0.15 - 0.3. The cells were spotted on two separate halves of a 2% agarose pad containing 1X M9 salts, 0.02% casamino acids and 0.2% maltose, the coverslip was sealed and a timelapse of both strains grown at 30°C (using a heated objective) was obtained using phase contrast and GFP optics, with frames taken every 1.5 min. The timelapse was analyzed using MicrobeTracker and SpotFinderZ to determine the total cell cycle time, as well as the division time. SpotFinderZ was used to identify diffraction-limited ZapA-GFP spots within each cell. Division time is defined as

the time between the formation of a stable Z-ring (using ZapA-GFP as a proxy for FtsZ) and the end of constriction. The criteria for a stable Z-ring is two ZapA-GFP spots that are aligned perpendicular to the long axis of the cell and that remain for at least three consecutive frames. During the segmentation, the end of constriction was manually determined as the moment when no ZapA-GFP spot was visible at the division site.

Immunoblotting

Strains were grown as described in the figure legends. At the designated times, cells were harvested and whole-cell extracts were prepared as described previously [7]. The protein concentration of each extract was determined using the non-interfering protein assay (Genotech) according to the manufacturer's instructions. Protein concentrations were normalized between extracts and the indicated amount of total protein from each extract was separated on a 12% or 15% SDS-PAGE gel. Proteins were transferred to a PVDF membrane (Whatman) and the membrane was blocked with Rapid-Block (Amresco) for 5 minutes. The membrane was incubated with primary antibodies diluted in Rapid-Block (either 1:10,000 dilution for anti-FtsA antibodies or 1:2,500 dilution for anti-FtsL antibodies) overnight at 4°C. In the case of the anti-FtsA antibodies, the same primary antibody solution was re-used for incubation with multiple blots. The next day, the primary antibody solution was removed and the membrane was quickly rinsed with TBST (10mM Tris-HCl pH 7.5, 100mM NaCl, 0.1% Tween-20) and then thoroughly washed three times with 25ml TBST for 10 minutes each wash. Following the final wash, the membrane was incubated with the secondary goat anti-

rabbit antibodies conjugated to horseradish peroxidase (Rockland) diluted 1:40,000 in Rapid-Block for 1 hour with gentle agitation at room temperature. After this incubation period, the secondary antibody solution was discarded and the membrane was again quickly rinsed with TBST and then thoroughly washed an additional four times with 25ml TBST for 10 minutes each. The blot was developed using the Super Signal West Pico system (Pierce) according to the manufacturer's protocol. Chemiluminescence was detected using a BioRad Chemidoc system.

Acknowledgements

The authors would like to thank all members of the Bernhardt and Rudner laboratories for helpful comments and suggestions. We would also like to thank Piet de Boer for strains, the anti-FtsA antiserum, helpful comments, and for communicating results prior to publication. Thanks also to Jon Beckwith and the Beckwith lab for providing the anti-FtsL antiserum. This work was supported by the National Institute of Allergy and Infections Diseases of the National Institutes of Health (R01 AI083365).

Section 2.6: References

1. Tsang, M.-J., and Bernhardt, T. G. (2015). A role for the FtsQLB complex in cytokinetic ring activation revealed by an ftsL allele that accelerates division. Mol Microbiol *95*, 925–944.

2. Lutkenhaus, J., Pichoff, S., and Du, S. (2012). Bacterial cytokinesis: From Z ring to divisome. Cytoskeleton *69*, 778–790.

3. Bi, E. F., and Lutkenhaus, J. (1991). FtsZ ring structure associated with division in Escherichia coli. Nature *354*, 161–164.

4. Goehring, N. W., and Beckwith, J. (2005). Diverse paths to midcell: assembly of the bacterial cell division machinery. Curr Biol *15*, R514–26.

5. Chen, J. C., and Beckwith, J. (2001). FtsQ, FtsL and FtsI require FtsK, but not FtsN, for co-localization with FtsZ during Escherichia coli cell division. Mol Microbiol *42*, 395–413.

6. Buddelmeijer, N., Judson, N., Boyd, D., Mekalanos, J. J., and Beckwith, J. (2002). YgbQ, a cell division protein in Escherichia coli and Vibrio cholerae, localizes in codependent fashion with FtsL to the division site. Proc Natl Acad Sci USA *99*, 6316–6321.

7. Hale, C. A., and de Boer, P. A. (1999). Recruitment of ZipA to the septal ring of Escherichia coli is dependent on FtsZ and independent of FtsA. J Bacteriol *181*, 167–176.

8. Schmidt, K. L., Peterson, N. D., Kustusch, R. J., Wissel, M. C., Graham, B., Phillips, G. J., and Weiss, D. S. (2004). A predicted ABC transporter, FtsEX, is needed for cell division in Escherichia coli. J Bacteriol *186*, 785–793.

9. Wang, L., Khattar, M. K., Donachie, W. D., and Lutkenhaus, J. (1998). FtsI and FtsW are localized to the septum in Escherichia coli. J Bacteriol *180*, 2810–2816.

10. Weiss, D. S., Chen, J. C., Ghigo, J. M., Boyd, D., and Beckwith, J. (1999). Localization of FtsI (PBP3) to the septal ring requires its membrane anchor, the Z ring, FtsA, FtsQ, and FtsL. J Bacteriol *181*, 508–520.

11. Mercer, K. L. N., and Weiss, D. S. (2002). The Escherichia coli cell division protein FtsW is required to recruit its cognate transpeptidase, FtsI (PBP3), to the division site. J Bacteriol *184*, 904–912.

12. Hale, C. A., and de Boer, P. A. J. (2002). ZipA is required for recruitment of FtsK, FtsQ, FtsL, and FtsN to the septal ring in Escherichia coli. J Bacteriol *184*, 2552–2556.

13. Corbin, B. D., Geissler, B., Sadasivam, M., and Margolin, W. (2004). Z-ring-independent interaction between a subdomain of FtsA and late septation proteins as revealed by a polar recruitment assay. J Bacteriol *186*, 7736–7744.

14. Karimova, G., Dautin, N., and Ladant, D. (2005). Interaction network among Escherichia coli membrane proteins involved in cell division as revealed by bacterial two-hybrid analysis. J Bacteriol *187*, 2233–2243.

15. Di Lallo, G., Fagioli, M., Barionovi, D., Ghelardini, P., and Paolozzi, L. (2003). Use of a two-hybrid assay to study the assembly of a complex multicomponent

protein machinery: bacterial septosome differentiation. Microbiology (Reading, Engl) *149*, 3353–3359.

16. Busiek, K. K., Eraso, J. M., Wang, Y., and Margolin, W. (2012). The Early Divisome Protein FtsA Interacts Directly through Its 1c Subdomain with the Cytoplasmic Domain of the Late Divisome Protein FtsN. J Bacteriol *194*, 1989–2000.

17. Alexeeva, S., Gadella, T. W. J., Verheul, J., Verhoeven, G. S., and Blaauwen, den, T. (2010). Direct interactions of early and late assembling division proteins in Escherichia coli cells resolved by FRET. Mol Microbiol *77*, 384–398.

18. Goehring, N. W., Gueiros-Filho, F., and Beckwith, J. (2005). Premature targeting of a cell division protein to midcell allows dissection of divisome assembly in Escherichia coli. Genes Dev *19*, 127–137.

19. Aarsman, M. E. G., Piette, A., Fraipont, C., Vinkenvleugel, T. M. F., Nguyen-Distèche, M., and Blaauwen, den, T. (2005). Maturation of the Escherichia coli divisome occurs in two steps. Mol Microbiol *55*, 1631–1645.

20. Peters, N. T., Dinh, T., and Bernhardt, T. G. (2011). A fail-safe mechanism in the septal ring assembly pathway generated by the sequential recruitment of cell separation amidases and their activators. J Bacteriol *193*, 4973–4983.

21. Yang, D. C., Tan, K., Joachimiak, A., and Bernhardt, T. G. (2012). A conformational switch controls cell wall-remodelling enzymes required for bacterial cell division. Mol Microbiol *85*, 768–781.

22. Uehara, T., Parzych, K. R., Dinh, T., and Bernhardt, T. G. (2010). Daughter cell separation is controlled by cytokinetic ring-activated cell wall hydrolysis. EMBO J *29*, 1412–1422.

23. Yang, D. C., Peters, N. T., Parzych, K. R., Uehara, T., Markovski, M., and Bernhardt, T. G. (2011). An ATP-binding cassette transporter-like complex governs cell-wall hydrolysis at the bacterial cytokinetic ring. Proc Natl Acad Sci USA *108*, E1052–60.

24. Begg, K. J., Hatfull, G. F., and Donachie, W. D. (1980). Identification of new genes in a cell envelope-cell division gene cluster of Escherichia coli: cell division gene ftsQ. J Bacteriol *144*, 435–437.

25. Khattar, M. M., Begg, K. J., and Donachie, W. D. (1994). Identification of FtsW and characterization of a new ftsW division mutant of Escherichia coli. J Bacteriol *176*, 7140–7147.

26. Begg, K. J., Dewar, S. J., and Donachie, W. D. (1995). A new Escherichia coli cell division gene, ftsK. J Bacteriol *177*, 6211–6222.

27. Allen, J. S., Filip, C. C., Gustafson, R. A., Allen, R. G., and Walker, J. R. (1974). Regulation of bacterial cell division: genetic and phenotypic analysis of temperature-sensitive, multinucleate, filament-forming mutants of Escherichia. J Bacteriol *117*, 978–986.

28. Hirota, Y., Mordoh, J., and Jacob, F. (1970). On the process of cellular division in Escherichia coli. J Mol Biol *53*, 369–387.

29. van de Putte, P., Dillewijn, J. V., and Rorsch, A. (1964). The Selection of Mutants of Escherichia coli with Impaired Cell Division at Elevated Temperature. Mutat Res *1*, 121–128.

30. Ishino, F., Jung, H., Ikeda, M., Doi, M., Wachi, M., and Matsuhashi, M. (1989). New mutations fts-36, lts-33, and ftsW clustered in the mra region of the Escherichia coli chromosome induce thermosensitive cell growth and division. J Bacteriol *171*, 5523–5530.

31. Ueki, M., Wachi, M., Jung, H. K., Ishino, F., and Matsuhashi, M. (1992). Escherichia coli mraR gene involved in cell growth and division. J Bacteriol *174*, 7841–7843.

32. Guzman, L. M., Barondess, J. J., and Beckwith, J. (1992). FtsL, an essential cytoplasmic membrane protein involved in cell division in Escherichia coli. J Bacteriol *174*, 7716–7728.

33. Buddelmeijer, N., and Beckwith, J. (2004). A complex of the Escherichia coli cell division proteins FtsL, FtsB and FtsQ forms independently of its localization to the septal region. Mol Microbiol *52*, 1315–1327.

34. Robichon, C., Karimova, G., Beckwith, J., and Ladant, D. (2011). Role of leucine zipper motifs in association of the Escherichia coli cell division proteins FtsL and FtsB. J Bacteriol *193*, 4988–4992.

35. Khadria, A. S., and Senes, A. (2013). The Transmembrane Domains of the Bacterial Cell Division Proteins FtsB and FtsL Form a Stable High-Order Oligomer. Biochemistry *52*, 7542–7550.

36. Gonzalez, M. D., Akbay, E. A., Boyd, D., and Beckwith, J. (2010). Multiple interaction domains in FtsL, a protein component of the widely conserved bacterial FtsLBQ cell division complex. J Bacteriol *192*, 2757–2768.

37. Lutkenhaus, J. (2009). FtsN--trigger for septation. J Bacteriol *191*, 7381–7382.

38. Pichoff, S., Shen, B., Sullivan, B., and Lutkenhaus, J. (2012). FtsA mutants impaired for self-interaction bypass ZipA suggesting a model in which FtsA's self-interaction competes with its ability to recruit downstream division proteins. Mol Microbiol *83*, 151–167.

39. Geissler, B., Elraheb, D., and Margolin, W. (2003). A gain-of-function mutation in ftsA bypasses the requirement for the essential cell division gene zipA in Escherichia coli. Proc Natl Acad Sci USA *100*, 4197–4202.

40. Gerding, M. A., Liu, B., Bendezú, F. O., Hale, C. A., Bernhardt, T. G., and de Boer, P. A. J. (2009). Self-enhanced accumulation of FtsN at Division Sites and Roles for Other Proteins with a SPOR domain (DamX, DedD, and RlpA) in Escherichia coli cell constriction. J Bacteriol *191*, 7383–7401.

41. Goehring, N. W., Robichon, C., and Beckwith, J. (2007). Role for the nonessential N terminus of FtsN in divisome assembly. J Bacteriol *189*, 646–649.

42. Bernard, C. S., Sadasivam, M., Shiomi, D., and Margolin, W. (2007). An altered FtsA can compensate for the loss of essential cell division protein FtsN in Escherichia coli. Mol Microbiol *64*, 1289–1305.

43. Liu, B., Persons, L., Lee, L., and de Boer, P. A. J. (2015). Roles for both FtsA and the FtsBLQ subcomplex in FtsN-stimulated cell constriction in Escherichia coli. Mol Microbiol *95*, 945–970.

44. Sliusarenko, O., Heinritz, J., Emonet, T., and Jacobs-Wagner, C. (2011). High-throughput, subpixel precision analysis of bacterial morphogenesis and intracellular spatio-temporal dynamics. Mol Microbiol *80*, 612–627.

45. Addinall, S. G., Cao, C., and Lutkenhaus, J. (1997). FtsN, a late recruit to the septum in Escherichia coli. Mol Microbiol *25*, 303–309.

46. Arends, S. J. R., Williams, K., Scott, R. J., Rolong, S., Popham, D. L., and Weiss, D. S. (2010). Discovery and characterization of three new Escherichia coli septal ring proteins that contain a SPOR domain: DamX, DedD, and RlpA. J Bacteriol *192*, 242–255.

47. Samaluru, H., SaiSree, L., and Reddy, M. (2007). Role of SufI (FtsP) in cell division of Escherichia coli: evidence for its involvement in stabilizing the assembly of the divisome. J Bacteriol *189*, 8044–8052.

48. Chaulk, S. G., Smith Frieday, M. N., Arthur, D. C., Culham, D. E., Edwards, R. A., Soo, P., Frost, L. S., Keates, R. A. B., Glover, J. N. M., and Wood, J. M. (2011). ProQ is an RNA chaperone that controls ProP levels in Escherichia coli. Biochemistry *50*, 3095–3106.

49. Massey, T. H., Mercogliano, C. P., Yates, J., Sherratt, D. J., and Löwe, J. (2006). Double-stranded DNA translocation: structure and mechanism of hexameric FtsK. Mol Cell *23*, 457–469.

50. Dubarry, N., Possoz, C., and Barre, F.-X. (2010). Multiple regions along the Escherichia coli FtsK protein are implicated in cell division. Mol Microbiol *78*, 1088–1100.

51. Draper, G. C., McLennan, N., Begg, K., Masters, M., and Donachie, W. D. (1998). Only the N-terminal domain of FtsK functions in cell division. J Bacteriol *180*, 4621–4627.

52. Ursinus, A., van den Ent, F., Brechtel, S., de Pedro, M., Höltje, J.-V., Löwe, J., and Vollmer, W. (2004). Murein (peptidoglycan) binding property of the essential cell division protein FtsN from Escherichia coli. J Bacteriol *186*, 6728–6737.

53. Yang, J.-C., van den Ent, F., Neuhaus, D., Brevier, J., and Löwe, J. (2004). Solution structure and domain architecture of the divisome protein FtsN. Mol Microbiol *52*, 651–660.

54. Geissler, B., and Margolin, W. (2005). Evidence for functional overlap among multiple bacterial cell division proteins: compensating for the loss of FtsK. Mol Microbiol *58*, 596–612.

55. Ghigo, J. M., Weiss, D. S., Chen, J. C., Yarrow, J. C., and Beckwith, J. (1999). Localization of FtsL to the Escherichia coli septal ring. Mol Microbiol *31*, 725–737.

56. Bramkamp, M., Weston, L., Daniel, R. A., and Errington, J. (2006). Regulated intramembrane proteolysis of FtsL protein and the control of cell division in Bacillus subtilis. Mol Microbiol *62*, 580–591.

57. Goranov, A. I., Katz, L., Breier, A. M., Burge, C. B., and Grossman, A. D. (2005). A transcriptional response to replication status mediated by the conserved bacterial replication protein DnaA. Proc Natl Acad Sci USA *102*, 12932–12937.

58. Modell, J. W., Hopkins, A. C., and Laub, M. T. (2011). A DNA damage checkpoint in Caulobacter crescentus inhibits cell division through a direct interaction with FtsW. Genes Dev *25*, 1328–1343.

59. Modell, J. W., Kambara, T. K., Perchuk, B. S., and Laub, M. T. (2014). A DNA damage-induced, SOS-independent checkpoint regulates cell division in Caulobacter crescentus. PLoS Biol *12*, e1001977.

60. Dai, K., Xu, Y., and Lutkenhaus, J. (1993). Cloning and characterization of ftsN, an essential cell division gene in Escherichia coli isolated as a multicopy suppressor of ftsA12(Ts). J Bacteriol *175*, 3790–3797.

61. Goehring, N. W., Petrovska, I., Boyd, D., and Beckwith, J. (2007). Mutants, suppressors, and wrinkled colonies: mutant alleles of the cell division gene ftsQ point to functional domains in FtsQ and a role for domain 1C of FtsA in divisome assembly. J Bacteriol *189*, 633–645.

62. Reddy, M. (2007). Role of FtsEX in cell division of Escherichia coli: viability of ftsEX mutants is dependent on functional SufI or high osmotic strength. J Bacteriol *189*, 98–108.

63. Geissler, B., Shiomi, D., and Margolin, W. (2007). The ftsA* gain-of-function allele of Escherichia coli and its effects on the stability and dynamics of the Z ring. Microbiology (Reading, Engl) *153*, 814–825.

64. Busiek, K. K., and Margolin, W. (2014). A role for FtsA in SPOR-independent localization of the essential Escherichia coli cell division protein FtsN. Mol Microbiol *92*, 1212–1226.

65. Szwedziak, P., Wang, Q., Freund, S. M., and Löwe, J. (2012). FtsA forms actin-like protofilaments. EMBO J *31*, 2249–2260.

66. Miller, J. H. (1972). Experiments in molecular genetics. (Cold Spring Harbor Laboratory Press).

67. Guyer, M. S., Reed, R. R., Steitz, J. A., and Low, K. B. (1981). Identification of a sex-factor-affinity site in E. coli as gamma delta. Cold Spring Harb Symp Quant Biol *45 Pt 1*, 135–140.

68. Bernhardt, T. G., and de Boer, P. A. J. (2004). Screening for synthetic lethal mutants in Escherichia coli and identification of EnvC (YibP) as a periplasmic septal ring factor with murein hydrolase activity. Mol Microbiol *52*, 1255–1269.

69. Philippe, N., Alcaraz, J.-P., Coursange, E., Geiselmann, J., and Schneider, D. (2004). Improvement of pCVD442, a suicide plasmid for gene allele exchange in bacteria. Plasmid *51*, 246–255.

70. Datsenko, K. A., and Wanner, B. L. (2000). One-step inactivation of chromosomal genes in Escherichia coli K-12 using PCR products. Proc Natl Acad Sci USA *97*, 6640–6645.

71. Bernhardt, T. G., and de Boer, P. A. J. (2005). SlmA, a nucleoid-associated, FtsZ binding protein required for blocking septal ring assembly over Chromosomes in E. coli. Mol Cell *18*, 555–564.

72. Baba, T., Ara, T., Hasegawa, M., Takai, Y., Okumura, Y., Baba, M., Datsenko, K. A., Tomita, M., Wanner, B. L., and Mori, H. (2006). Construction of Escherichia coli K-12 in-frame, single-gene knockout mutants: the Keio collection. Mol Syst Biol *2*, 2006.0008.

73. Yu, D., Ellis, H. M., Lee, E. C., Jenkins, N. A., Copeland, N. G., and Court, D. L. (2000). An efficient recombination system for chromosome engineering in Escherichia coli. Proc Natl Acad Sci USA *97*, 5978–5983.

74. Chiang, S. L., and Rubin, E. J. (2002). Construction of a mariner-based transposon for epitope-tagging and genomic targeting. Gene *296*, 179–185.

75. Uehara, T., Dinh, T., and Bernhardt, T. G. (2009). LytM-domain factors are required for daughter cell separation and rapid ampicillin-induced lysis in Escherichia coli. J Bacteriol *191*, 5094–5107.

Chapter 3: A structure-function analysis of NlpD reveals a potential role for cell wall amidase activity in cytokinetic ring stability and positioning

Attributions

I designed and performed all the experiments presented in this chapter and generated the subsequent figures. I wrote the text with editorial assistance from Thomas Bernhardt. The proposed model implicating amidase activity and the divisome protein FtsN in Z-ring positioning is partly inspired and supported by independent work by Nick Peters on Z-ring dynamics.

Chapter 3: A structure-function analysis of NlpD reveals a potential role for cell wall amidase activity in cytokinetic ring stability and positioning

Mary-Jane Tsang[1] and Thomas G. Bernhardt[1*]

[1]Department of Microbiology and Immunobiology, Harvard Medical School, Boston, MA 02115

Section 3.1: Summary

Bacterial cells are surrounded by a continuous matrix known as the peptidoglycan (PG) cell wall. During cytokinesis, the so-called septal PG layer that will ultimately form the new cell poles is initially shared between the developing daughter cells. Consequently, the PG hydrolytic activity of the amidases is required to split this septal PG layer and allow cell separation. This stage of cell division is tightly regulated with the amidases requiring activation by another set of periplasmic proteins, the LytM factors EnvC and NlpD.

We performed a structure-function analysis of NlpD in order to identify the regions of the protein responsible for amidase activation and/or localization to the cytokinetic ring. We discovered that NlpD is recruited to the division site via its LysM domain, which is a PG-binding module. On the other hand, the degenerate dLytM domain required for NlpD function is not sufficient for proper cell separation. Instead, the production of a soluble periplasmic NlpD truncation containing only the dLytM domain induced mislocalized and aberrant amidase activity, which ultimately led to division

inhibition and cell filamentation. Our results therefore support a model in which septal PG processing by the amidases influences the stability and positioning of the cytokinetic ring.

Section 3.2: Introduction

Cytokinesis is mediated by a ring-shaped, multi-protein complex known as the divisome or septal ring [1]. The assembly of this molecular machine at the prospective site of division is organized by cytoskeletal polymers of the tubulin-like protein FtsZ. In gram-negative bacteria, like *Escherichia coli*, cell division requires the coordinated constriction of the different layers that make up the cell envelope: the cytoplasmic/inner membrane, the peptidoglycan (PG) cell wall, and the outer membrane [2]. The PG cell wall is a continuous polysaccharide matrix that encompasses the cytoplasmic membrane. This macromolecular structure is essential for cell integrity and is composed of glycan strands connected to one another by peptide crosslinks [3]. Consequently, an important function of the division machinery is to synthesize the new cell wall layer that will ultimately form the daughter cell poles. As this so-called septal PG layer is formed, it is initially shared by the developing daughter cells and must be split by hydrolytic enzymes to allow the invagination of the outer membrane and the completion of cell division.

The periplasmic LytC-type N-acetylmuramyl-L-alanine amidases (AmiA, AmiB, and AmiC) are the PG hydrolytic enzymes responsible for splitting the new septal PG layer in order to shape the new polar caps of the daughter cells [4, 5]. The amidases

cleave the bonds that link the attached peptides to the glycan strands, thus breaking the crosslinks within the PG meshwork to allow cell separation. Mutants lacking all three amidases are able to complete the constriction of the inner membrane, but fail to split the septal PG layer. Therefore, these strains propagate as long chains of cells linked by the shared septal PG layer and a partially constricted outer membrane layer.

Tight control over the activity of the amidases is essential to prevent the formation of lethal breaches in the cell wall structure that eventually results in cell lysis. The spatiotemporal regulation of the amidases results from the weak intrinsic PG hydrolytic activity of the amidases due to the presence of an autoinhibitory helix within the amidase active site [6]. Release of this helix is stimulated by two divisome-associated proteins with LytM-like domains, EnvC and NlpD. These LytM factors are not PG hydrolases themselves, but instead they function as specific activators of the PG amidases, with EnvC and NlpD activating AmiA/B and AmiC respectively [7-9]. Accordingly, loss of both EnvC and NlpD results in a similar chaining phenotype as that observed upon inactivation of all three amidases.

The founding members of the LytM family of proteins, LytM and lysostaphin, are zinc metallo-endopeptidases that cleave the pentaglycine cross-links in *Staphylococcus aureus* PG [10, 11]. The majority of LytM-containing proteins are PG hydrolases, but *E. coli* EnvC and NlpD appear to have lost this hydrolytic activity [8, 9]. These proteins possess a degenerate metallo-peptidase active site (dLytM domain) lacking some or all of the critical conserved residues involved in zinc binding and catalysis. Accordingly, the crystal structure of the dLytM domain of EnvC lacks a Zn^{2+} ion [9]. Instead, it appears

that EnvC, and potentially NlpD, may use this degenerate active site cleft to either directly or indirectly stimulate the release of the autoinhibitory helix of the amidases to promote septal PG hydrolysis.

The regulation of amidase activation by EnvC is relatively well-understood. EnvC is anchored to the outer face of the IM and recruited to division sites via a direct interaction between its coiled-coil (CC) domain and the ATP-binding cassette (ABC) transporter-like complex FtsEX [12]. However, in addition to its function in protein localization, the CC domain also seems to be involved in EnvC regulation [8]. One model proposes an auto-inhibition of EnvC activity by its coiled-coil (CC) domain. This inhibition may be relieved in response to the ATPase activity of FtsE, since FtsEX variants lacking ATPase activity still recruit EnvC to the division site but fail to promote septal PG splitting [8, 12].

Unlike EnvC, details about the function and regulation of NlpD *in vivo* are still lacking. We therefore performed a structure-function analysis of NlpD to gain molecular insight in its activity. We determined that a predicted PG-binding module within NlpD was necessary and sufficient for its recruitment to the septal ring. We further showed that only the full-length protein was functional. However, the expression of soluble periplasmic truncations containing only the dLytM domain resulted in mislocalized and unregulated amidase activity. Interestingly, in the absence of the other amidase activator EnvC, this mislocalized amidase activity ultimately led to Z-ring instability, division inhibition and cell filamentation, which were suppressed by the overexpression of the essential PG-binding divisome protein FtsN. These findings support a model in which

the denuded glycan strands produced in the periplasm upon amidase activation act as a positional marker that allows FtsN to promote proper Z-ring stability and positioning on the cytoplasmic side of the inner membrane during cytokinesis.

Section 3.3: Results

Domain organization of NlpD

NlpD is an outer membrane lipoprotein consisting of a lysin motif (LysM) domain [13-15] and a degenerate LytM (dLytM) domain [9], with two linker regions, one at the N-terminus and another between the LysM and dLytM domains. The linker regions are predicted to be disordered/unstructured by DISOPRED [16]. The LysM domain is a common motif with PG binding properties [14, 15]. The dLytM domain has been reported to mediate amidase activation by the other LytM factor EnvC [8, 9]. However, it is still unknown which regions of NlpD are responsible for its amidase activation function and/or localization to the cytokinetic ring. Therefore, in order to gain molecular insight into the activity of NlpD, We performed a structure-function analysis (**Figure 3.1**).

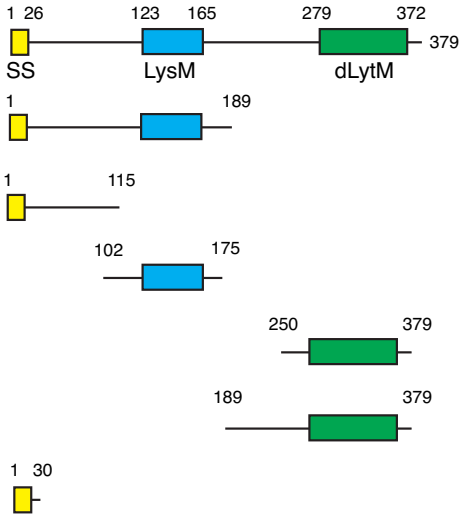

NlpD Residues	Localization	Functionality	Cell morphology in *ΔenvC*
$NlpD^{WT}$	+++	+	-
$NlpD^{(1-189)}$	+++	-	Chains
$NlpD^{(1-115)}$	+	-	-
$NlpD^{(102-175)}$	+++	ND	Short chains
$NlpD^{(250-379)}$	-	Lytic	Filaments
$NlpD^{(189-379)}$	-	Lytic	Filaments
$NlpD^{(1-30)}$	-	ND	ND

Figure 3.1. Structure-function analysis of NlpD. The domain organization of NlpD is illustrated. Indicated are the signal sequence (SS; yellow), lysin motif (LysM; blue), and the degenerate LytM domain (dLytM; green). Also shown are the NlpD truncations that were expressed under the control of the IPTG-inducible lactose promoter either as an untagged protein or as a C-terminal mCherry fusion. Truncations lacking $NlpD^{SS}$ are expressed as soluble periplasmic proteins fused to the DsbA signal peptide that is cleaved upon export to the periplasm via the Sec system. Columns indicate (i) the NlpD residues present in each truncation, (ii) whether the fusion to mCherry accumulated at division sites strongly (+++), poorly (+), or appeared evenly distributed along the periphery of the cell (-), (iii) whether the untagged truncation could (+++) or could not (-) compensate for the loss of endogenous NlpD, and finally (iv) whether it resulted in a change in cell morphology upon overexpression in a *ΔenvC* strain. ND, not determined.

The LysM domain of NlpD is necessary and sufficient for septal localization

In order to determine which region of NlpD is the localization determinant, we constructed different NlpD variants fused to the fluorescent protein mCherry at the C-

terminus (**Figure 3.1**). We expressed truncated versions of NlpD lacking either the dLytM domain or both the dLytM and LysM domains. Additionally, we also expressed soluble periplasmic variants containing only the dLytM domain ($NlpD^{dLytM}$) or only the LysM domain ($NlpD^{LysM}$). These domains were fused to the signal sequence of DsbA for Sec-mediated export into the periplasm. Finally, as control for a lipidated OM-localized protein, we expressed mCherry fused to the signal sequence of NlpD and 4 additional amino acids after the acylated cysteine. All the constructs were expressed under the control of the IPTG-inducible lactose promoter from an integrated plasmid in an *nlpD* null strain ($^{\Delta SS}$*nlpD*), which is described below. All fusion proteins were shown to be mostly intact by western blot analysis using antibodies against the mCherry fusion protein (**Figure 3.2**).

One minor complication with the *nlpD* null strain is the presence of a promoter for the downstream *rpoS* gene within the *nlpD* coding sequence. *rpoS* encodes an alternative sigma factor that regulates the expression of a large number of genes in response to a variety of stresses [17]. Consequently, deletion of the *nlpD* gene results in defects in *rpoS* expression [18]. In order to inactivate NlpD with minimal polar effects on *rpoS* expression, we replaced the N-terminal lipoprotein signal sequence of NlpD ($^{\Delta SS}$*nlpD*) to prevent its export to the periplasm where it normally functions. Importantly, $^{\Delta SS}$*nlpD* and *ΔnlpD* mutants displayed the same severe chaining phenotype when combined with a *ΔenvC* mutant (data not shown), suggesting that this strain behaves like an *nlpD* null strain with respect to amidase activation. We therefore used this $^{\Delta SS}$*nlpD* as our *nlpD* null strain throughout this study.

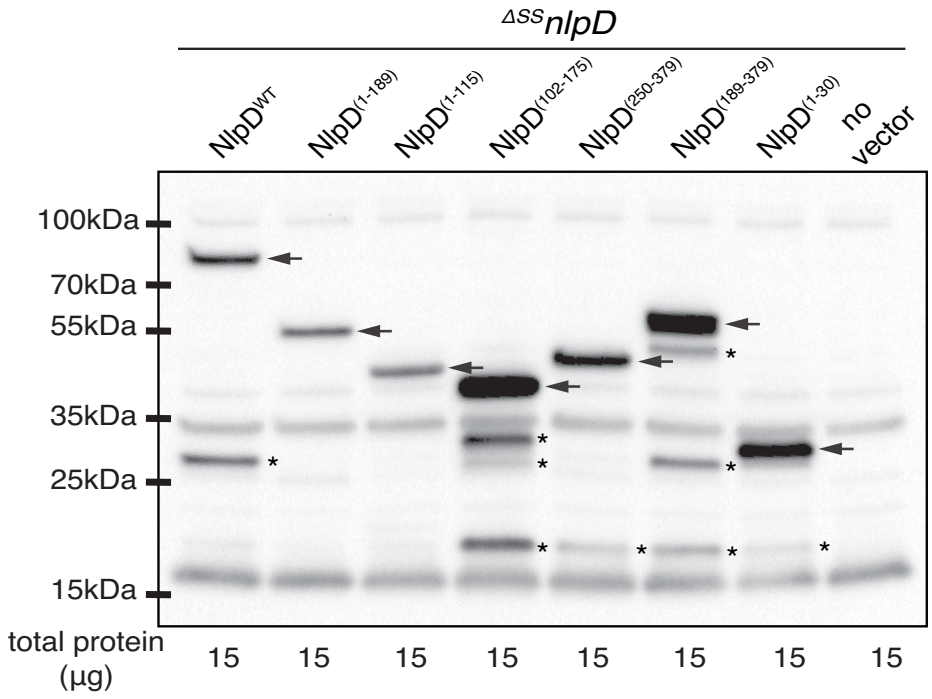

Figure 3.2. NlpD truncations fused to mCherry are expressed and mostly intact. Cells of MT47 (*ΔSSnlpD*) alone or expressing different NlpD-mCherry fusions from the integrated constructs attHKNP20 (*Plac::nlpDWT-mCherry*), attHKMT101 (*Plac::nlpD(1-189)-mCherry*), attHKMT103 (*Plac::nlpD(1-115)-mCherry*), attHKMT178 (*Plac::ssdsbA-nlpD(102-175)-mCherry*), attHKMT180 (*Plac::ssdsbA-nlpD(250-379)-mCherry*), attHKMT182 (*Plac::ssdsbA-nlpD(189-379)-mCherry*), or attHKMT149 (*Plac::nlpD(1-30)-mCherry*) were harvested for whole-cell extract preparation. Proteins in the resulting extracts were separated by SDS-PAGE, transferred to PVDF, and the mCherry fusion was detected with anti-mCherry antibodies. The arrows indicate the intact NlpD variant present in each strain. The asterisks denote possible degradation products of each variant.

Full-length NlpD localized to midcell at the site of future division or in actively constricting cells (**Figure 3.3A**). All constructs containing the LysM domain, whether lipidated or free-floating, also displayed midcell localization (**Figure 3.3B, D**), suggesting that the LysM domain is sufficient for localization. The N-terminal linker also appeared to have some affinity for the midcell, although the enrichment at the division site was much reduced compared to wild-type NlpD (**Figure 3.3C**). This localization was not due to the lipidation since a similarly-lipidated mCherry did not show this specific midcell localization (**Figure 3.3G**). Finally, the soluble periplasmic NlpD^{dLytM} variants (NlpD$^{(250\text{-}379)}$-mCherry and NlpD$^{(189\text{-}379)}$-mCherry) lacking both the LysM domain and N-terminal linker region were dispersed throughout the periplasm, suggesting that although this domain is responsible for amidase activation, it does not play any role in recruiting NlpD to the division site (**Figure 3.3E-F**). This observation is consistent with the timing of recruitment of the LytM factors and amidases as the LytM factors have been shown to localize to the division site prior to the amidases. Taken together, these results suggest that the LysM module of NlpD is both necessary and sufficient for proper localization to the septal ring.

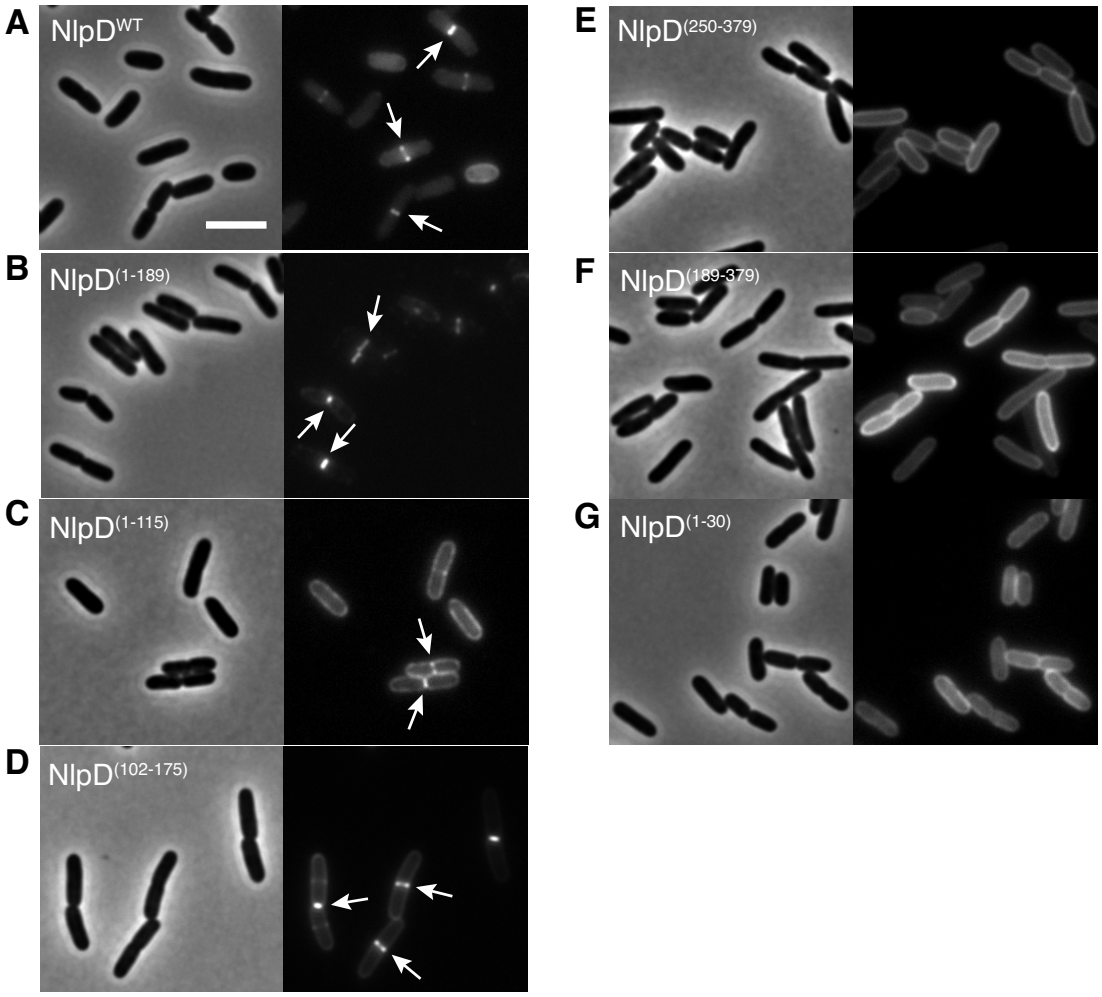

Figure 3.3. Localization of NlpD fusions in *$^{\Delta SS}$nlpD* cells. Overnight cultures of MT47 (*$^{\Delta SS}$nlpD*) harboring the integrated expression constructs (**A**) attHKNP20 (*P_{lac}::nlpD^{WT}-mCherry*), (**B**) attHKMT101 (*P_{lac}::nlpD$^{(1-189)}$-mCherry*), (**C**) attHKMT103 (*P_{lac}::nlpD$^{(1-115)}$-mCherry*), (**D**) attHKMT178 (*P_{lac}::^{ss}dsbA-nlpD$^{(102-175)}$-mCherry*), (**E**) attHKMT180 (*P_{lac}::^{ss}dsbA-nlpD$^{(250-379)}$-mCherry*), (**F**) attHKMT182 (*P_{lac}::^{ss}dsbA-nlpD$^{(189-379)}$-mCherry*), or (**G**) attHKMT149 (*P_{lac}::nlpD$^{(1-30)}$-mCherry*) were diluted in minimal M9-maltose medium supplemented with 25µM (**E-F**), 50µM (**A-B**), 100µM (**C-D**), or 150µM (**G**) IPTG. Cells were grown at 30°C to an OD_{600} of 0.15 - 0.25 before they were visualized on 2% agarose pads with phase contrast and mCherry optics. Arrows indicate localization of the protein fusion to division sites. Bar = 4µm.

The dLytM domain of NlpD is required for function but leads to increased cell lysis when expressed alone as a soluble periplasmic truncation

To investigate the functionality of NlpD, the truncations described previously were each expressed as an untagged protein under the control of the IPTG-inducible lactose promoter from an integrated plasmid in a strain lacking both LytM factors, NlpD and EnvC. In the absence of IPTG, this $^{\Delta SS}$*nlpD ΔenvC* strain grew as very long chains of cells that failed to separate (**Figure 3.4A**). Expression of wild-type NlpD from the integrated plasmid complemented the *nlpD* mutation, thus rescuing the cell chaining phenotype such that cells now only displayed the mild division defect of EnvC$^-$ cells (**Figure 3.4B-C**). Variants lacking the dLytM domain failed to suppress the cell chaining phenotype (**Figure 3.4D-E**). At least one of the variants (NlpD$^{(1\text{-}189)}$) was expressed and mostly intact, as assessed by Western blot analysis (**Figure 3.4H**). The other variant, NlpD$^{(1\text{-}115)}$, is likely not detected due to the lack of robust antigenic epitopes in this truncation. However, this variant may also be unstable. Overall, similarly to the other LytM factor EnvC, the dLytM domain of NlpD is required for amidase activation and cell separation.

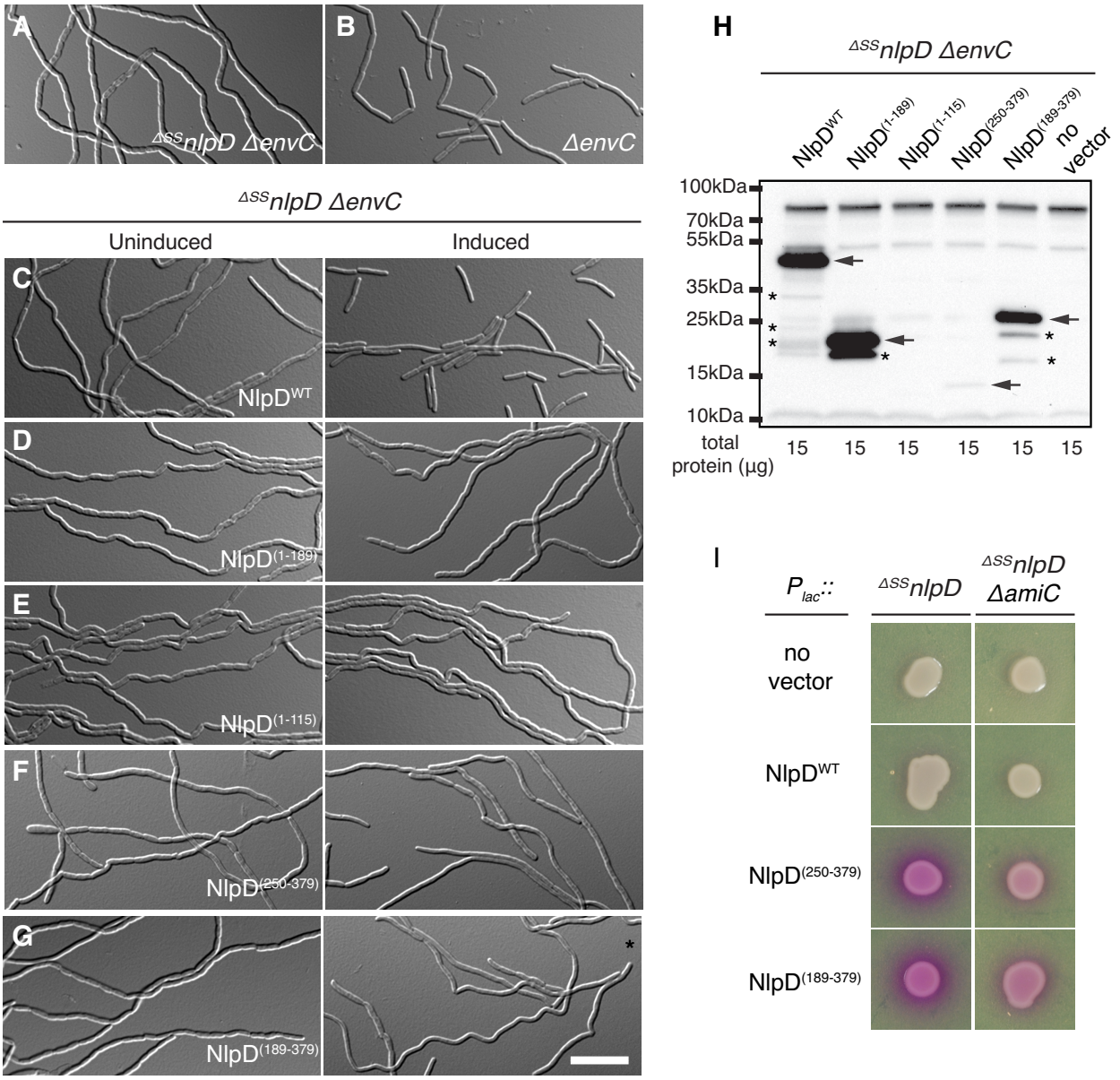

Figure 3.4. Only full-length NlpD properly and efficiently promotes cell separation. (**A-G**) Overnight cultures of (**A**) MT50 (*ΔSSnlpD ΔenvC*) or (**B**) TB140 (*ΔenvC*) alone or MT50 harboring the integrated expression constructs (**C**) attHKMT20 (P_{lac}*::nlpD*^{WT}), (**D**) attHKMT102 (P_{lac}*::nlpD*$^{(1-189)}$), (**E**) attHKMT104 (P_{lac}*::nlpD*$^{(1-115)}$), (**F**) attHKMT179 (P_{lac}*::*^{ss}*dsbA-nlpD*$^{(250-379)}$), or (**G**) attHKMT181 (P_{lac}*::*^{ss}*dsbA-nlpD*$^{(189-379)}$) were diluted in minimal M9-maltose medium and grown at 37°C. Mid-log cultures were then backdiluted into M9-maltose medium only or supplemented with 150μM (**C, F-G**) or 1mM (**D-E**)

Figure 3.4 (Continued). IPTG. Cells were further grown at 37°C to an OD_{600} of 0.2 - 0.3 before they were visualized on 2% agarose pads with DIC optics. Bar = 10µm. (**H**) Cells of the induced strains described above were harvested for whole-cell extract preparation. Proteins in the resulting extracts were separated by SDS-PAGE, transferred to PVDF, and NlpD was detected with affinity-purified anti-NlpD antibodies. The arrows indicate the intact NlpD variant present in each strain. The asterisks denote possible degradation products of each variant. (**I**) Cells of MT122 (*$^{\Delta SS}$nlpD*) and MT123 (*$^{\Delta SS}$nlpD ΔamiC*) alone or harboring the integrated constructs attHKMT20 (*P_{lac}::nlpD^{WT}*), attHKMT179 (*Pl_{ac}::^{ss}dsbA-nlpD$^{(250-379)}$*), or attHKMT181 (*P_{lac}::^{ss}dsbA-nlpD$^{(189-379)}$*) were grown in LB at 30°C. Following normalization for cell density (OD_{600} = 0.5), 5 µl of the resulting cultures was spotted on LB agar containing 150µM IPTG and 20µg/ml CPRG. The plates were incubated at 30°C and photographed after 14 hours.

Since the dLytM domain of NlpD is required for the activation of its cognate amidase AmiC, we tested whether it was also sufficient for NlpD activity. The expression of the soluble NlpD^{dLytM} variants (NlpD$^{(250-379)}$ and NlpD$^{(189-379)}$) did not suppress the chaining morphology of the *$^{\Delta SS}$nlpD ΔenvC* double mutant (**Figure 3.4F-G**), suggesting that the dLytM domain is not sufficient for NlpD function. Although only the NlpD$^{(189-379)}$ variant was strongly detected by Western blot in the double mutant strain (**Figure 3.4H**), expression of both NlpD^{dLytM} variants led to increased cell lysis and/or cell envelope permeability defects as shown by a positive red signal on medium containing chlorophenyl red-β-D-galactopyranoside (CPRG) (**Figure 3.4I**). This β-galactosidase substrate generally fails to penetrate the *E. coli* envelope and cannot be processed by cytoplasmic LacZ, unless cells lyse and/or become more permeable [19]. The CPRG^{+} phenotype observed is most likely due to the aberrant activation of amidases and

indeed, it was partially suppressed by the deletion of the NlpD-specific amidase, AmiC. Since the NlpD^{dLytM} variants showed diffused localization in the periplasm (**Figure 3.3E-F**), they may promote amidase activity away from the division site, thus inducing cell wall lesions throughout the cell. In summary, although the dLytM domain is required for NlpD function, it is not sufficient for cell separation. In fact, it appears to require further regulation, either through recruitment to the division site by the LysM domain and/or N-terminal linker region, or via its attachment to the outer membrane by the lipidated cysteine anchor.

Dominant negative effects of NlpD variants in *ΔenvC*

Interesting insights into the role of LytM factors and amidases were obtained by studying the phenotype of dominant negative NlpD variants. The NlpD truncations described above were expressed either as untagged proteins or as C-terminal mCherry fusions under IPTG-inducible lactose promoter from an integrated plasmid in a *ΔenvC* strain. Overexpression of wild-type NlpD or a variant lacking both the dLytM and LysM domains (NlpD$^{(1-115)}$) had no effect on the function of the endogenous wild-type NlpD protein (**Figure 3.5A-B, E**). On the other hand, NlpD variants lacking only the dLytM domain were dominant negative and led to severe chaining when expressed in the *ΔenvC* strain (**Figure 3.5C-D**). This dominant negative effect was also observed, although to a lesser extent, with a soluble periplasmic NlpD^{LysM} variant (NlpD$^{(102-175)}$) (**Figure 3.5F**). Since the LysM domain is the localization determinant of NlpD, the overexpression of variants containing the LysM module but missing the dLytM domain

may displace the endogenous wild-type NlpD from the division site, thus leading to the observed dominant negative effect. Alternatively, they may interact with potential regulators of NlpD, thus interfering with the proper function of the endogenous NlpD protein.

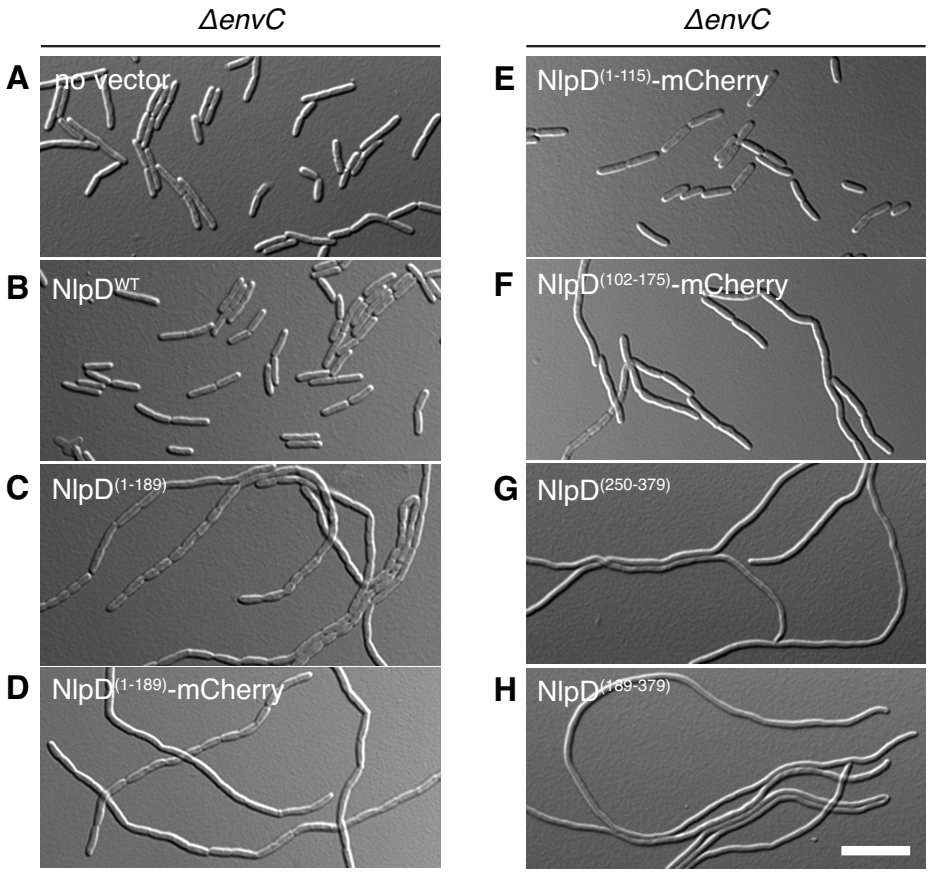

Figure 3.5. Dominant negative effects of untagged and mCherry-tagged NlpD truncations. Cells of (**A**) TB140 (*ΔenvC*) alone or harboring the integrated expression constructs (**B**) attHKMT20 (P_{lac}*::nlpD*^{WT}), (**C**) attHKMT102 (P_{lac}*::nlpD*$^{(1\text{-}189)}$), (**D**) attHKMT101 (P_{lac}*::nlpD*$^{(1\text{-}189)}$*-mCherry*), (**E**) attHKMT103 (P_{lac}*::nlpD*$^{(1\text{-}115)}$*-mCherry*), (**F**) attHKMT178 (P_{lac}*::*^{ss}*dsbA-nlpD*$^{(102\text{-}175)}$*-mCherry*), (**G**) attHKMT179 (Pl_{ac}*::*^{ss}*dsbA-nlpD*$^{(250\text{-}379)}$), or (**H**) attHKMT181 (P_{lac}*::*^{ss}*dsbA-nlpD*$^{(189\text{-}379)}$) were grown overnight in LB

Figure 3.5 (Continued). with 50μM IPTG. The overnight cultures were diluted in minimal M9-maltose medium supplemented with 100μM (**F**), 150μM (**A-D, G-H**), or 1mM (**E**) IPTG. Cells were grown at 30°C to an OD_{600} of 0.1 - 0.2 before they were visualized on 2% agarose pads with DIC optics. Bar = 10μm.

Surprisingly, the soluble periplasmic $NlpD^{dLytM}$ variants ($NlpD^{(250-379)}$ and $NlpD^{(189-379)}$) were also dominant negative. However, rather than causing a chaining phenotype, they induced the formation of smooth cell filaments (**Figure 3.5G-H**). In order to determine if these filaments were the result of a defect in constriction of the outer membrane alone or whether the constriction of all cell envelope layers was inhibited, we used cytoplasmic or periplasmic mCherry markers expressed from an constitutive promoter. Chains formed upon overexpression of an NlpD variant lacking the dLytM domain ($NlpD^{(1-189)}$) were similar to those of a $^{\Delta SS}$*nlpD ΔenvC* strain: these chains contained cells with separate cytoplasm (**Figure 3.6C**) but with a continuous periplasm, as observed with the periplasmic mCherry marker that formed transverse bands where cell division occurred and the inner membrane invaginated (**Figure 3.6D**). However, the soluble $NlpD^{dLytM}$ variants led to the formation of filaments with a continuous cytoplasm (**Figure 3.6E**, data not shown) and little to no transverse bands of periplasmic mCherry fluorescence (**Figure 3.6F**, data not shown), suggesting that the inner membrane invagination was incomplete and that cell division was inhibited.

Figure 3.6. A soluble periplasmic NlpD^{dLytM} variant induces cell filamentation in *ΔenvC*. Cells of TB140 (*ΔenvC*) harboring the integrated expression constructs (**A-B**) attHKMT20 (P_{lac}*::nlpD*^{WT}), (**C-D**) attHKMT102 (P_{lac}*::nlpD*$^{(1\text{-}189)}$), or (**E-F**) attHKMT181 (P_{lac}*::*^{ss}*dsbA-nlpD*$^{(189\text{-}379)}$) and either pAAY71 (P_{syn135}*::mCherry*) (**A, C, E**) or pAAY65 (P_{syn135}*::*^{ss}*dsbA-mCherry*) (**B, D, E**) were grown overnight in LB with 50μM IPTG. The overnight cultures were diluted in minimal M9-maltose medium supplemented with 50μM (**E-F**), or 150μM (**A-D**) IPTG. Cells were grown at 30°C to an OD_{600} of 0.1 - 0.2 before they were visualized on 2% agarose pads with phase contrast and mCherry optics. Bar = 10μm.

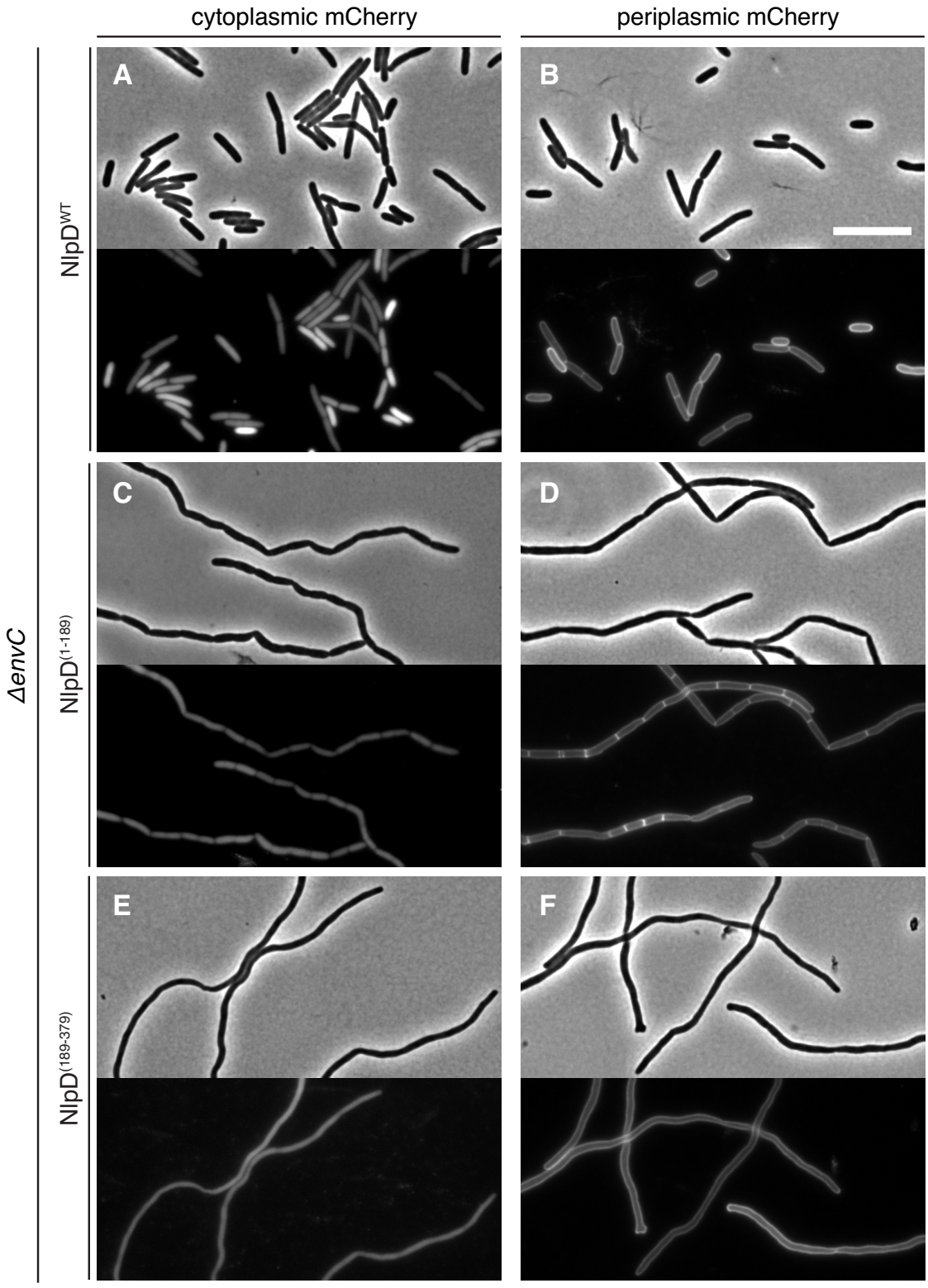

Figure 3.6 (Continued).

Interestingly, the same filamentation phenotype was not observed when the soluble NlpD^{dLytM} variants were expressed in an *nlpD* null strain, in which wild-type EnvC was still present (**Figure 3.7B-C**). The cells appeared slightly longer and thinner than cells overexpressing wild-type NlpD (**Figure 3.7A**), but did not display the dramatic filamentation observed with *ΔenvC* cells, suggesting that the division inhibition induced by the soluble NlpD^{dLytM} variants is exacerbated in the absence of the other amidase activator EnvC and therefore, AmiA/B activity.

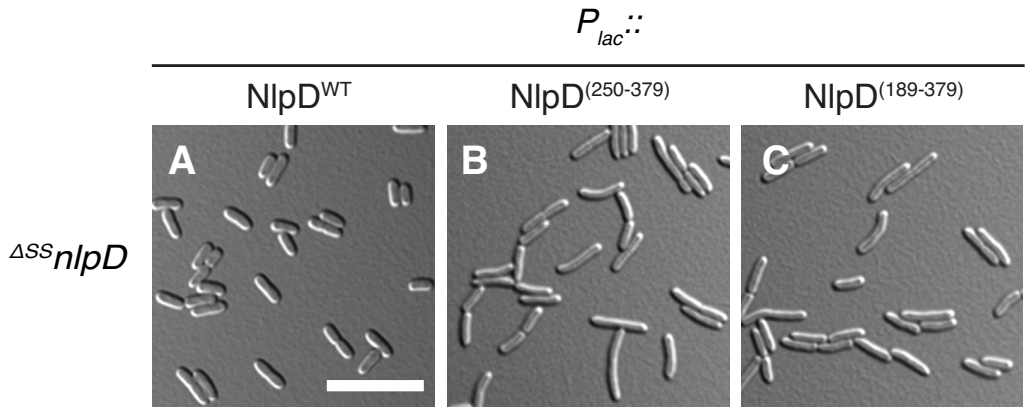

Figure 3.7. The soluble periplasmic NlpD^{dLytM} variants have only mild effects in $^{\Delta SS}$*nlpD*. Cells of MT47 ($^{\Delta SS}$*nlpD*) harboring the integrated expression constructs (**A**) attHKMT20 (P_{lac}*::nlpD*^{WT}), (**B**) attHKMT179 (P_{lac}*::*^{ss}*dsbA-nlpD*$^{(250-379)}$), or (**C**) attHKMT181 (P_{lac}*::*^{ss}*dsbA-nlpD*$^{(189-379)}$) were grown overnight in LB with 50μM IPTG. The overnight cultures were diluted in minimal M9-maltose medium supplemented with 1mM IPTG. Cells were grown at 30°C to an OD_{600} of 0.1 - 0.2 before they were visualized on 2% agarose pads with DIC optics. Bar = 10μm.

Mislocalized activity of the amidases affects Z-ring stability

Since the soluble NlpD^{dLytM} variants are dispersed around the cell periphery (**Figure 3.3E-F**), we hypothesize that they induce aberrant amidase activity throughout the cell, which has a negative effect on cell division and constriction. According to this model, the division inhibition is dependent on the presence of the amidases. A strain lacking all amidase activity exhibits a severe chaining phenotype because cells are able to constrict the inner membrane but fail to separate (**Figure 3.8D**). Accordingly, if the filamentation phenotype observed upon overexpression of the soluble NlpD^{dLytM} variants is due to aberrant amidase activity, the deletion of the amidases would suppress the constriction defect, although the resulting strain would grow as chains due to the lack of amidase activity. Alternatively, cells would still filament if the division inhibition was a simple consequence of protein overexpression. As predicted, the inactivation of all three amidases suppressed the cell constriction defect induced by the overexpression of the soluble NlpD^{dLytM} variants (**Figure 3.8B-C, E-F**). These results are therefore consistent with the model whereby mislocalized amidase activity inhibits cell division, thus inducing cell filamentation.

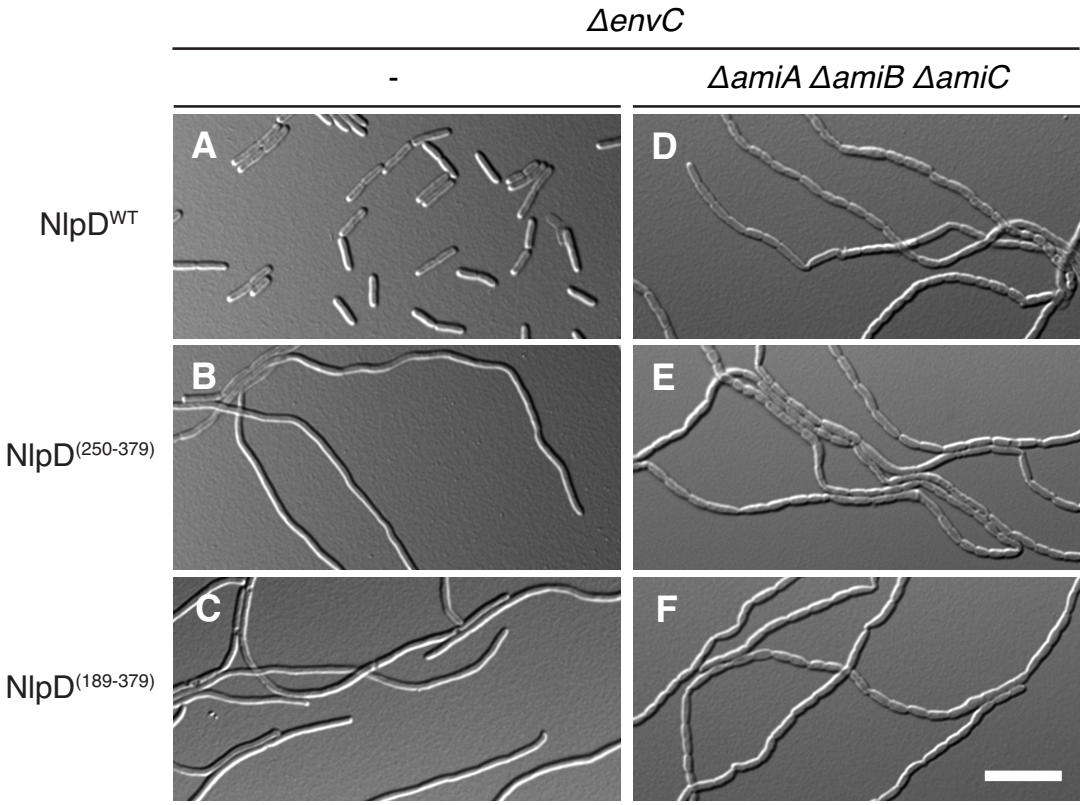

Figure 3.8. Mislocalized amidase activity induces cell filamentation in *ΔenvC* cells. Cells of (**A-C**) TB140 (*ΔenvC*), or (**D-F**) MT143 (*ΔenvC ΔamiA ΔamiB ΔamiC)* harboring the integrated expression constructs (**A, D**) attHKMT20 (P_{lac}*::nlpD*^{WT}), (**B, E**) attHKMT179 (Pl_{ac}*::*^{ss}*dsbA-nlpD*$^{(250-379)}$), or (**C, F**) attHKMT181 (P_{lac}*::*^{ss}*dsbA-nlpD*$^{(189-379)}$) were grown overnight in LB with 50μM IPTG. The overnight cultures were diluted in minimal M9-maltose medium supplemented with 150μM IPTG. Cells were grown at 30°C to an OD_{600} of 0.1 - 0.2 before they were visualized on 2% agarose pads with DIC optics. Bar = 10μm.

The first step of cell division is the assembly of the cytoskeletal ring-like structure known as the Z-ring, which consists of the bacterial tubulin homolog FtsZ. This structure

then recruits the other components of the division machine or divisome, including the septal PG synthase FtsI/PBP3 [1]. Consequently, the dynamics of the Z-ring provides useful information on the division process. ZapA-sfGFP encoded at the endogenous chromosomal locus can be used as a proxy for cellular FtsZ dynamics. ZapA-sfGFP mostly localized as single rings or bands at the midcell position in a *ΔenvC* strain overexpressing wild-type NlpD (**Figure 3.9A**). Inhibition of the PG synthase FtsI upon treatment with the β-lactam cephalexin resulted in division inhibition and filamentation. While rings of ZapA-sfGFP were still present along the filaments, the distance between consecutive rings was greater compared to untreated cells (**Figure 3.9A-B**). Therefore, Z-ring formation is not inhibited in filamentous cells that fail to constrict. ZapA-sfGFP mostly localized as single rings or bands at midcell in chaining *ΔenvC* cells that failed to separate due to the expression of a dominant negative NlpD variant, ($NlpD^{(1-189)}$) (**Figure 3.9C**). Surprisingly, when the soluble $NlpD^{dLytM}$ variants variants were expressed in *ΔenvC*, very few ZapA-sfGFP rings or bands were observed along the resulting filaments (**Figure 3.9D-E**). Instead of single rings/bands, ZapA-sfGFP frequently localized as a dispersed structures or as double/multi-rings in close proximity to each other, which is an indication of increased instability of the Z-ring structure and possibly of the divisome as a whole. The formation of contiguous double or multiple Z-rings also suggests a potential loss of Z-ring positioning information.

Figure 3.9. Mislocalized amidase activity leads to increase Z-ring instability. Cells of HC268 (*ΔenvC zapA-sfGFP*) harboring the integrated expression constructs (**A-B**) attHKMT20 (P_{lac}*::nlpD*^{WT}), (**C**) attHKMT102 (P_{lac}*::nlpD*$^{(1-189)}$), (**D**) attHKMT179 (P_{lac}*::*^{ss}*dsbA-nlpD*$^{(250-379)}$), or (**E**) attHKMT181 (P_{lac}*::*^{ss}*dsbA-nlpD*$^{(189-379)}$) were grown overnight in LB with 50μM IPTG. The overnight cultures were diluted in minimal M9-maltose medium supplemented with 150μM IPTG without (**A, C-E**) or with (**B**) 10μg/ml cephalexin. Cells were grown at 30°C to an OD_{600} of 0.1 - 0.2 before they were visualized on 2% agarose pads with phase contrast and GFP optics. Asterisks indicate ZapA-sfGFP localization as dispersed structures or double/multi-rings in close proximity to each other. Bar = 10μm.

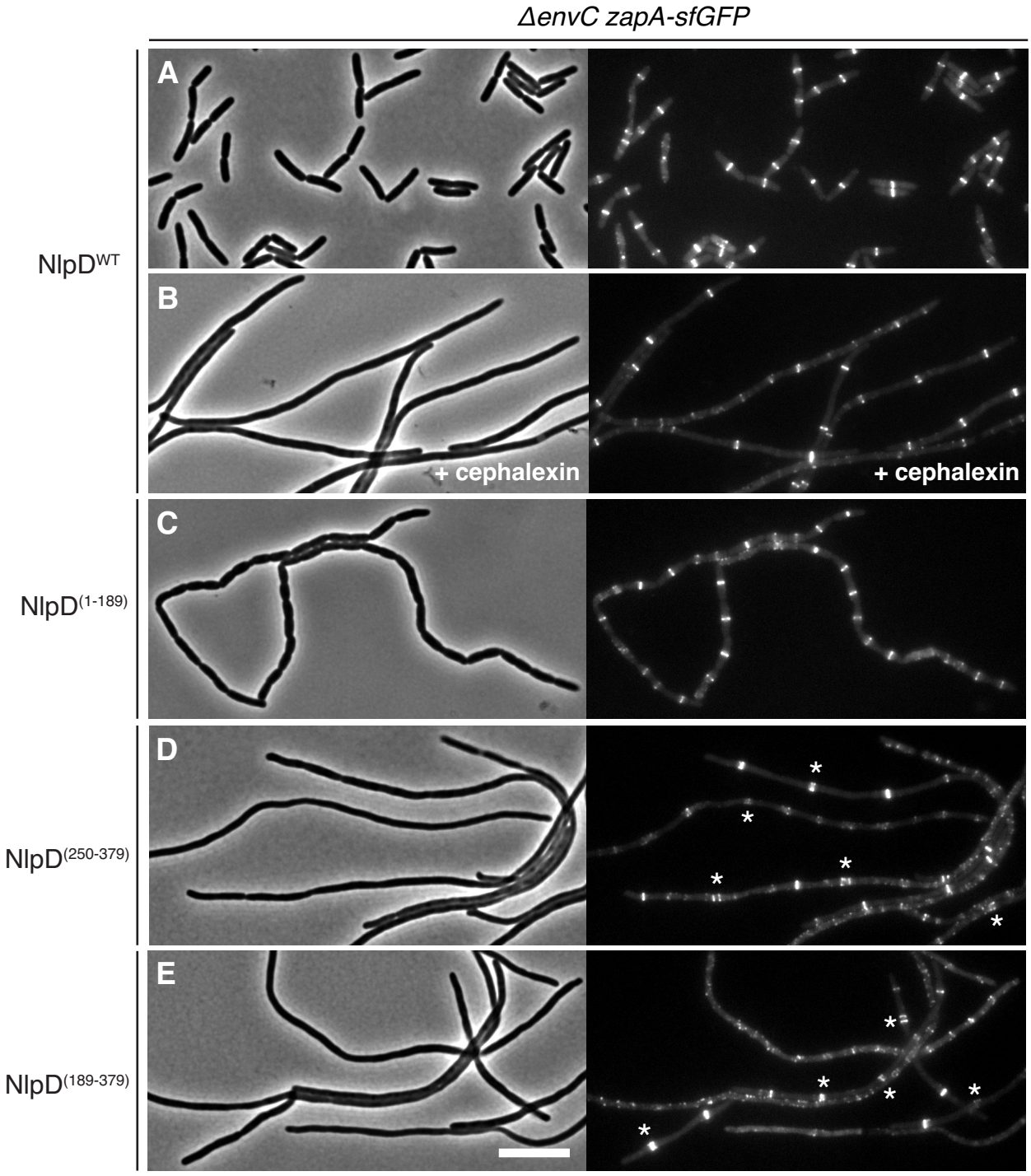

Figure 3.9 (Continued).

Excess FtsN suppress the constriction defect upon mislocalized amidase activity

FtsN is a bitopic inner membrane protein and an essential divisome component. Its localization to the division site is enhanced by the ability of its C-terminal SPOR domain to bind to denuded glycan strands produced by the amidases [20, 21]. The division inhibition observed upon overexpression of the dispersed soluble NlpD^{dLytM} variants (NlpD$^{(250\text{-}379)}$ and NlpD$^{(189\text{-}379)}$) is consistent with a model wherein mislocalized amidases activity recruits FtsN away from divisome complexes assembled at potential division sites. This would result in a failure to properly divide and ultimately lead to filamentation. If this model is correct, overexpression of FtsN may compensate for its delocalization from divisome complexes upon aberrant amidase activity, thus allowing cell constriction to proceed and suppressing the filamentation phenotype.

Indeed, the concurrent overexpression of the functional GFP-FtsN fusion protein in *ΔenvC* cells expressing the soluble NlpD^{dLytM} variants suppressed the cell constriction defect (**Figure 3.10C-D**). Therefore, the Z-ring instability that was previously observed may be due to the delocalization of FtsN away from divisome complexes. Although cell constriction is no longer inhibited in the presence of excess FtsN, it appears that the *ΔenvC* cells now fail to separate, potentially due to the inability of the endogenous wild-type NlpD to activate its cognate amidase AmiC. Consistent with this hypothesis, the same chaining phenotype was observed upon GFP-FtsN overexpression in a *ΔenvC* strain overexpressing wild-type NlpD (**Figure 3.10A**), but not in wild-type cells in which EnvC is present and able to promote cell separation (**Figure 3.10E**). The exact reason why excess FtsN has such a negative effect on NlpD/AmiC function is still unclear.

Figure 3.10. FtsN overexpression suppresses the constriction defect due to mislocalized amidase activity. Cells of TB140 (*ΔenvC*) harboring both pCH201 (P_{lac}*::gfp-ftsN*) and the integrated constructs (**A**) attHKMT20 (P_{lac}*::nlpD*^{WT}), (**B**) attHKMT102 (P_{lac}*::nlpD*$^{(1-189)}$), (**C**) attHKMT179 (Pl_{ac}*::*^{ss}*dsbA-nlpD*$^{(250-379)}$), or (**D**) attHKMT181 (P_{lac}*::*^{ss}*dsbA-nlpD*$^{(189-379)}$) were grown overnight in LB with 50μM IPTG. As control, (**E**) TB28 (*wt*) cells with pCH201 were also grown overnight under the same conditions. The overnight cultures were diluted in minimal M9-maltose medium supplemented with 150μM IPTG and grown at 30°C to an OD_{600} of 0.1 - 0.2. Cells were then visualized on 2% agarose pads with phase contrast and GFP optics. Bar = 10μm.

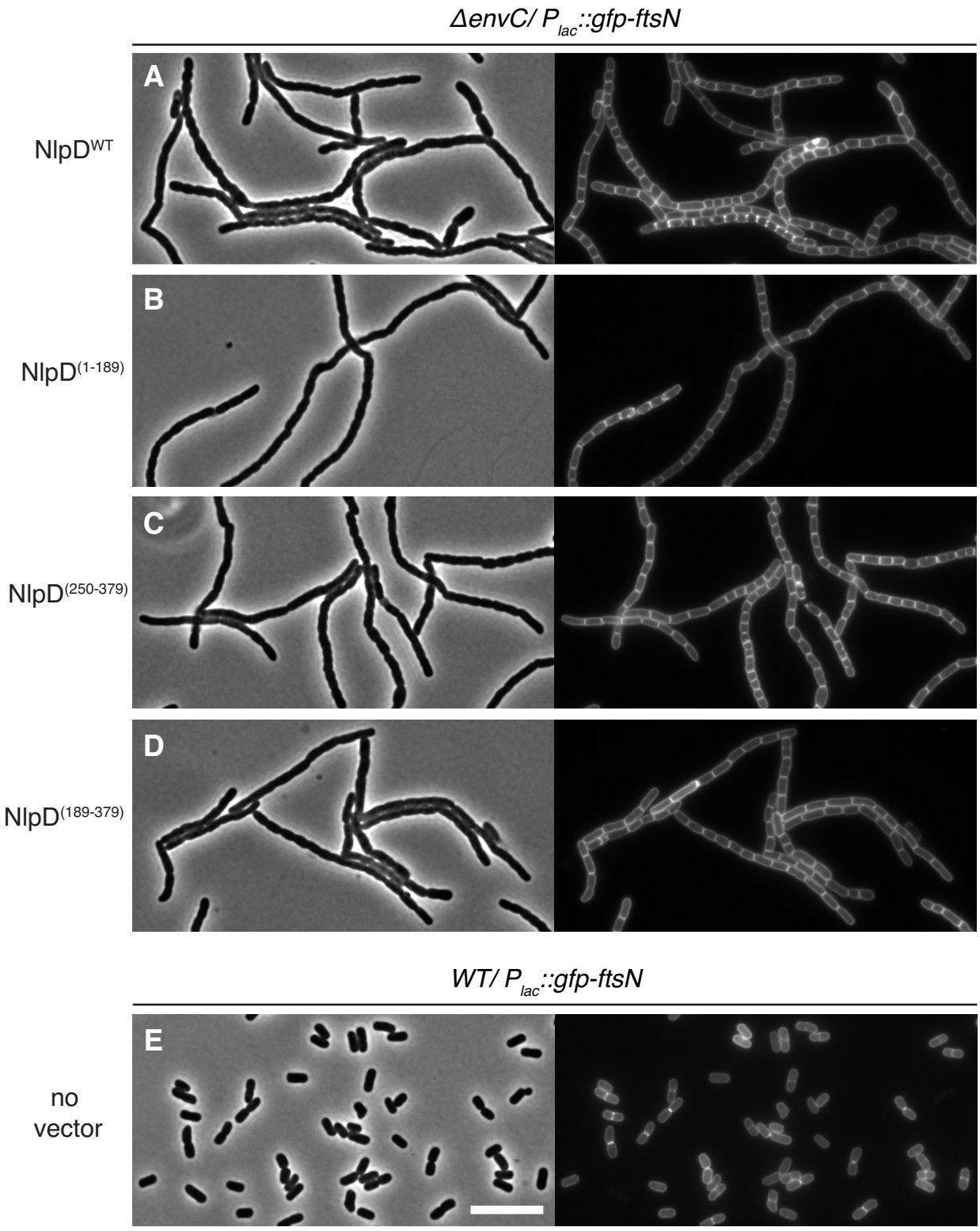

Figure 3.10 (Continued).

Section 3.4: Discussion

In this study, we performed a structure-function analysis of NlpD, one of two LytM-containing factors responsible for amidase activation during cell division. An understanding of the roles of the different subdomains of this protein has provided us with insights into its activity. Additionally, we uncovered a potential link between the formation of denuded glycan strands by the amidases in the periplasm and Z-ring stability and potentially positioning in the cytoplasm.

The peptidoglycan-binding LysM domain of NlpD is necessary and sufficient for its recruitment to the septal ring, suggesting that PG binding may recruit NlpD to the division site. This may be a general recruitment mechanism as similar LysM domains have been shown to have affinity for the cell poles and septa in other bacteria [14, 22, 23]. A lipidated NlpD truncation including both the N-terminal linker and the LysM domain displayed potent dominant negative effects and resulted in the formation of long chains of cells when expressed in a *ΔenvC* background. One possible explanation for this phenotype is that the septal localization of this NlpD truncation displaces the native full-length protein from the division site, thus inhibiting septal PG splitting and cell separation. However, the cell chaining phenotype upon expression of a soluble NlpD truncation containing only the LysM domain was less severe, yet this NlpD variant robustly localized to the septal ring. Consequently, we hypothesize that the lipidated NlpD truncation not only displaces the native protein from the division site, but it may also interact with and sequester a potential regulator of NlpD that is important for cell separation.

The subdomain of NlpD required for cell separation is its degenerate LytM (dLytM) domain, but this domain alone ($NlpD^{dLytM}$) is not sufficient for cell separation. Instead, soluble periplasmic $NlpD^{dLytM}$ variants were mislocalized throughout the cell, resulting in aberrant amidase activity and increased cell lysis. The inactivation of AmiC, the cognate amidase of NlpD, did not completely abolish the lytic phenotype (**Figure 3.4I**), suggesting that when mislocalized and overexpressed, $NlpD^{dLytM}$ may be promiscuous and therefore activate the other amidases, AmiA and/or AmiB. Although the LytM factors are generally specific to their cognate amidases, there are situations where promiscuity has been observed. One such example is a mutant of AmiB that no longer requires EnvC for activation but is now activated by NlpD *in vivo* [6]. How amidase specificity is achieved is an interesting question that is still largely unanswered.

How NlpD is regulated *in vivo* is also unclear. Results from our domain analysis indicate that the activity of the dLytM domain may be restricted either through recruitment to the division site by the LysM domain and/or N-terminal linker region, or via its attachment to the outer membrane by the lipidated cysteine anchor. One interesting possibility is that the OM localization of NlpD maintains it physically separate from the PG layer at the division site, thus holding the protein and its cognate amidase AmiC inactive. However, upon constriction of the OM, NlpD is brought closer to the PG layer where it can activate AmiC and promote septal PG splitting. Alternatively, the potential binding of the LysM domain to PG at the septum may position NlpD such that the activated AmiC is able to access and cleave septal PG. These are all interesting models that require further investigation.

In addition to its role in cell separation, the localized amidase activity induced by the LytM factors EnvC and NlpD at the division site is thought to promote cell constriction (**Figure 3.11A**). This idea came about following the demonstration that FtsN is recruited to the divisome in a self-enhancing process involving its small, membrane-proximal, essential domain (^{E}FtsN) and its C-terminal, PG-binding SPOR domain (^{S}FtsN) [20] (**Figure 3.11B**). Based on this observation, it was proposed that cell constriction is driven by a positive feedback loop in which ^{E}FtsN stimulates the synthesis and concomitant remodeling of cell wall material at the division site by the amidases, thus creating the denuded glycan strands that serve as the recruitment signal for ^{S}FtsN. This in turn brings more ^{E}FtsN to the division site to stimulate more cell wall synthesis and remodeling and so on, to ultimately drive cell constriction. The binding of ^{S}FtsN to denuded glycan strands which are produced almost exclusively at the division site specifically recruits FtsN [21]. However, the initial recruitment of FtsN to the septal ring may involve a direct interaction between its cytoplasmic N-terminal region (^{N}FtsN) and the early divisome component FtsA, which interacts with FtsZ to tether the Z-ring to the cytoplasmic side of the inner membrane [24, 25].

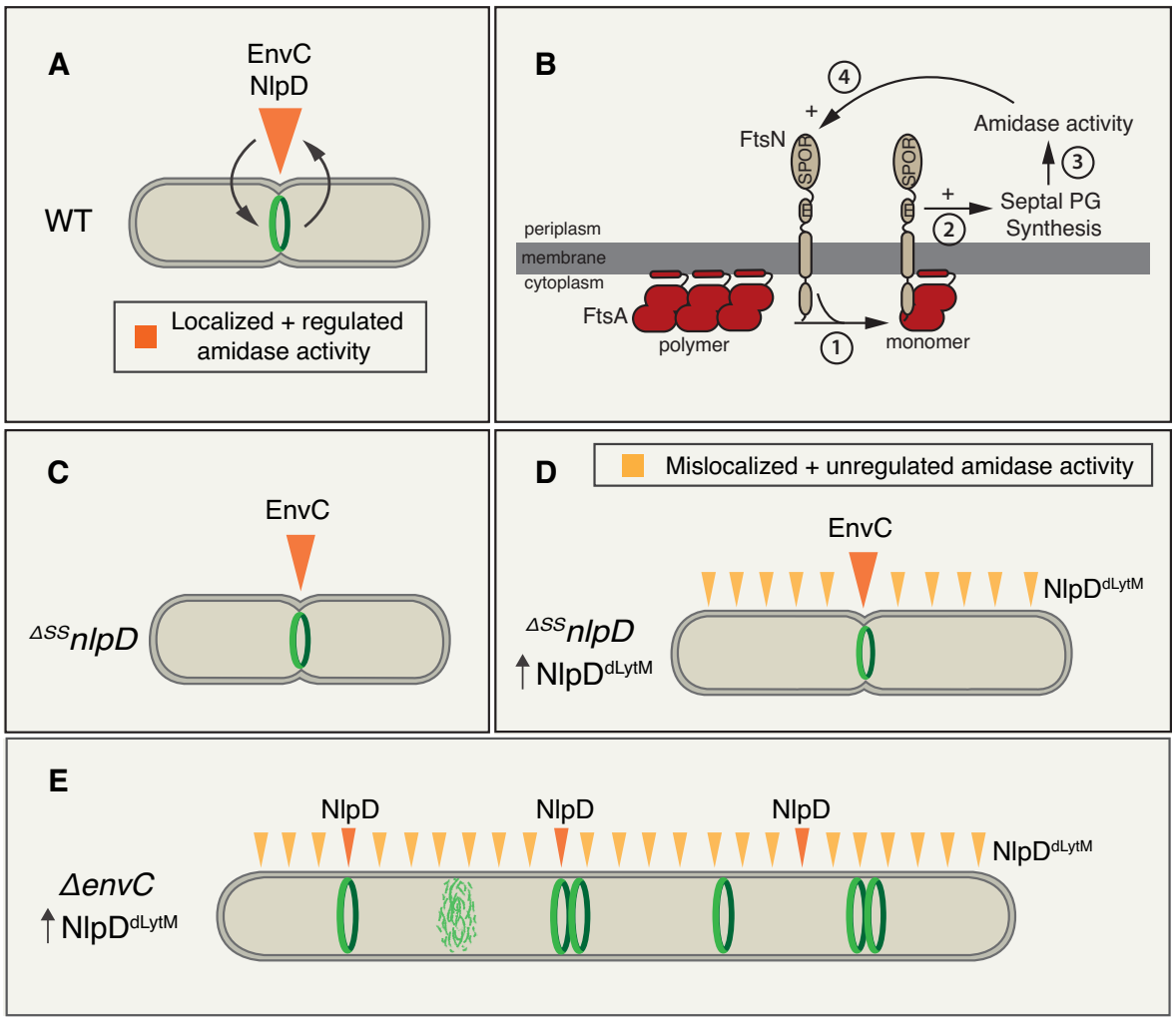

Figure 3.11. A potential role for amidase activity in Z-ring stability and positioning. (**A**) During cell division, the septal PG layer is split and remodeled by the amidases, which require activation by the LytM factors EnvC and NlpD. The orange triangle indicates regulated amidase activation at the division site, with the size reflecting the amount of denuded glycan strands produced by the amidases. The Z-ring or divisome is represented as a ring at midcell. Highlighted with the black arrows is a possible connection and back-and-forth regulation between amidase activity and Z-ring and/or divisome stability and positioning. (**B**) Shown is a diagram depicting a positive feedback loop that may drive cell constriction. The initial recruitment of FtsN to the septal ring may involve a direct interaction between its cytoplasmic N-terminal region (^{N}FtsN) and

Figure 3.11 (Continued). the early divisome component FtsA, which anchors the Z-ring to the membrane (step 1). Within the septal ring, the small, membrane-proximal, essential domain of FtsN (^{E}FtsN) stimulates the synthesis of septal PG at the division site (step 2). This new cell wall material is remodeled by the amidases (step 3), leading to the production of denuded glycan strands that serve as the recruitment signal for the C-terminal, PG-binding SPOR domain of FtsN (^{S}FtsN) (step 4). This in turn brings more ^{E}FtsN to the division site to stimulate more cell wall synthesis and remodeling and so on, to ultimately drive cell constriction. (**C**) In the absence of NlpD, proper cell separation is mediated by EnvC and its specific activation of AmiA and AmiB at division sites. (**D**) A soluble NlpD^{dLytM} variant is mislocalized and induces unregulated amidase activity throughout the cell, as indicated by the yellow triangles. Cell constriction proceeds relatively normally in an *nlpD* null background as EnvC provides enough of a division-specific "signal" to counterbalance the mislocalized amidase activity (orange triangle). The size of the triangles reflect the amount of denuded glycan strands produced in each case. In this case, the Z-ring and divisome still localize to the midcell position. (**E**) In the absence of EnvC, the division-specific "signal" mediated by NlpD (orange) cannot counterbalance the mislocalized amidase activity (yellow), thus leading to the instability of Z-rings and/or divisomes. This ultimately results in division inhibition and cell filamentation.

In this study, we discovered that the expression of a soluble truncated version of NlpD containing only the dLytM domain (NlpD^{dLytM}) results in division inhibition and cell filamentation in a *ΔenvC* background, but not in an *nlpD* null background where EnvC is present. In the *nlpD* null strain, proper cell separation is mediated by EnvC and its specific activation of AmiA and AmiB at division sites (**Figure 3.11C**). Consequently, the activity of EnvC would result in the formation of enough denuded glycan strands at the midcell to provide a division-specific "signal" that allows proper cytokinesis to occur,

even in the presence of the mislocalized amidase activity induced by the soluble NlpD^{dLytM} variant (**Figure 3.11D**). However in the absence of EnvC, the specific activation of AmiC at division sites by the endogenous NlpD does not generate a strong enough “signal” to counterbalance the mislocalized amidase activity induced by the dispersed NlpD^{dLytM} variant. This lack of positional information results in Z-ring and potentially divisome instability, which ultimately inhibits cell constriction (**Figure 3.11E**).

Denuded glycan strands have been shown to be enriched in septal PG and may therefore serve as a division-specific “signal” for SPOR domain-containing proteins, such as FtsN [21]. Therefore, the mislocalized amidase activity induced by the soluble NlpD^{dLytM} variant may sequester FtsN from divisomes assembled at potential division sites, thus resulting in a division block and cell filamentation. Accordingly, the concurrent overexpression of functional GFP-FtsN compensated for this potential FtsN delocalization and suppressed the defect in cell constriction. Interestingly, this potential delocalization of FtsN resulted in Z-ring instability. FtsN depletion has been previously reported to affect the stability of the divisome; even ring structures formed by the early divisome proteins FtsZ, FtsA, and ZipA, are destabilized to a certain extent in the absence of FtsN [26]. These observations suggested a potential role for FtsN in Z-ring stability. However, the observed destabilization may be a general consequence of division inhibition as reduced Z-ring frequency is also observed in mutants defective in some late divisome proteins [26-29] and in cells in which septal PG synthesis is inhibited with cephalexin (**Figure 3.9B**).

In addition to reduced Z-ring frequency, we also observed the formation of double or multiple Z-rings in close proximity. This finding is consistent with increased Z-ring instability or a potential loss of Z-ring positioning information. Double Z-rings may result from the reassembly of existing rings at both the original position but also at a site in close proximity. Since these events are rarely observed in wild-type cells, we hypothesize that mechanisms exist within the divisome to ensure that the Z-ring only reassembles at its original position. One possible mechanism involves a physical link between the cytoplasmic Z-ring and the PG structure in the periplasm. We propose that FtsN may provide this physical connection through its interactions with FtsA, which anchors the Z-ring to the membrane, and denuded glycan strands present within the PG meshwork at the division site. In this model, the assembly of the septal ring stimulates septal PG remodeling by the amidases, thus providing a specific positional signal that marks and reinforces the position where the Z-ring first formed such that constriction occurs at this specific site and via a single septal ring (**Figure 3.11A**). According to this model, the absence of this signal may therefore lead to increased levels of misplaced Z-rings. However, a mutant lacking all amidase activity is viable and able to constrict, suggesting that this increase in Z-ring misplacement is not lethal on its own. However, this defect may become lethal when combined with defects in other systems responsible for Z-ring placement, such as the Min system or nucleoid occlusion. Indeed, the loss of the amidase activator EnvC is synthetically lethal with loss of the Min system [30].

In summary, we gained molecular insights into the activity of the amidase activator, NlpD, and also revealed a potential role for amidase activity in Z-ring stability and positioning. Our model suggests that the stimulation of septal PG synthesis and remodeling by the divisome may be a committed step in the cell constriction process and may play a critical role in the maintenance of the division site. In addition, it is a critical part of the self-enhancing recruitment of FtsN, which has been implicated in both constriction initiation and active constriction. Overall, our findings raises the possibility that once the division site is selected, mechanisms may exist within the divisome to ensure that constriction occurs at that specific site.

Acknowledgements

The authors would like to thank all members of the Bernhardt and Rudner laboratories for helpful comments and suggestions, particularly Chris Sham and Jackson Buss for reading this chapter and providing useful edits. Thanks also to David Rudner and the Rudner lab for providing the anti-mCherry antiserum.

Section 3.5: Experimental procedures

Media, bacterial strains and plasmids

Cells were grown in LB (1% tryptone, 0.5% yeast extract, 0.5% NaCl) or minimal M9 medium [31] supplemented with 0.2% casamino acids and 0.2% maltose. Unless otherwise indicated, antibiotics were used at 25 (chloramphenicol; Cm), 25 (kanamycin; Kan), 10 (tetracycline; Tet), 50 (ampicillin, Amp), or 5 (gentamicin, Gent) μg/ml.

The bacterial strains used in this study are listed in **Table 3.1**. All *E. coli* strains used in the reported experiments are derivatives of MG1655 [32]. All deletion alleles were either sourced from the Keio knockout collection [33] or constructed to resemble those in the collection. Plasmids used in this study are listed in **Table 3.2**. Plasmids that are derivatives of CRIM plasmids [34] were integrated into the HK022 phage attachment site using the helper plasmid pTB102 [35] as described [34]. PCR was performed using either KOD polymerase (Novagen) or Q5 polymerase (NEB) according to the manufacturer's instructions. Unless otherwise indicated, MG1655 chromosomal DNA was used as the template. Plasmid DNA and PCR fragments were purified using the Zyppy plasmid miniprep kit (Zymo Research) or the Qiaquick PCR purification kit (Qiagen) respectively. Sequencing reactions were carried out with an ABI3730xl DNA analyzer at the DNA Resource Core of Dana-Farber/Harvard Cancer Center (funded in part by NCI Cancer Center support grant 2P30CA006516-48).

Table 3.1. Strains used in this study

Strain	Genotype[a]	Source/Reference[b]
DH5α	*F– hsdR17 deoR recA1 endA1 phoA supE44 thi-1 gyrA96 relA1 Δ(lacZYA-argF)U169 ϕ80dlacZΔM15*	Gibco BRL
BL21(λDE3)	*ompT rB– mB– (PlacUV5::T7gene1)*	Novagen
MG1655	*rph-1 ilvG rfb-50*	[32]
TB10	MG1655 *λΔcro-bio nad::Tn10*	[36]
TB28	MG1655 *ΔlacIZYA*::*frt*	[30]
HC268	TB28 *ΔenvC::frt zapA-sfGFP cm^R*	P1(TU212) x TB140

Table 3.1 (Continued).

Strain	Genotype[a]	Source/Reference[b]
MT46	TB28 *ΔSSnlpD::kan^R*	P1(λRed) x TB28
MT47	TB28 *ΔSSnlpD::frt*	MT46/pCP20
MT50	TB28 *ΔSSnlpD::frt ΔenvC::kan^R*	P1(TB134) x MT47
MT121	MG1655 *ΔSSnlpD::kan^R*	P1(MT46) x MG1655
MT122	MG1655 *ΔSSnlpD::frt*	MT121/pCP20
MT123	MG1655 *ΔSSnlpD::frt ΔamiC::kan^R*	P1(TB137) x MT122
MT142	TB28 *ΔamiA::frt ΔamiB::frt ΔenvC::frt*	TU221/pCP20
MT143	TB28 *ΔamiA::frt ΔamiB::frt ΔenvC::frt ΔamiC::Kan^R*	P1(TB137) x MT142
TB134	TB28 *ΔenvC::kan^R*	[7]
TB137	TB28 *ΔamiC::kan^R*	[7]
TB140	TB28 *ΔenvC::frt*	[7]
TU207	TB28 *ΔamiA::frt ΔamiB::frt*	[8]
TU212	TB28 *zapA-sfGFP cmR*	P1(λRed) x TB28
TU221	TB28 *ΔamiA::frt ΔamiB::frt ΔenvC::kan^R*	P1(TB134) x TU207

[a] The Kan^R and Cm^R cassettes are flanked by *frt* sites for removal by FLP recombinase. An *frt* scar remains following removal of the cassette using FLP expressed from pCP20. *sfGFP* encodes for superfolder GFP.

[b] Strain constructions by P1 transduction are described using the shorthand: P1(donor) x recipient. Transductants were selected on LB Kan, LB Cm or LB Tet plates where appropriate. λRed indicates strains constructed by recombineering (see Experimental Procedures for details). Strains resulting from the removal of a drug resistance cassette using pCP20 are indicated as: Parental strain/pCP20.

Table 3.2. Plasmids used in this study

Plasmid	Genotype[a]	Origin	Source or Reference
pAAY65	*aacC1* P_{syn135}*::*^{ss}*dsbA-mCherry*	pBBR1	[37]
pAAY71	*aacC1* P_{syn135}*::mCherry*	pBBR1	This study
pCH201	*bla lacI*^{q} P_{lac}*::gfp-ftsN*$^{(1-319)}$	pBR/ColE1	[20]
pCP20	*bla cat cI857(ts) repA(ts)* $P_{\lambda R}$*::flp*	pSC101	[38]
pHC467	*cat sfGFP*	R6K	This study
pMT20	*att*HK022 *tetA tetR lacI* P_{lac}*::nlpD*$^{(1-379)}$	R6K	This study
pMT101	*att*HK022 *tetA tetR lacI* P_{lac}*::nlpD*$^{(1-189)}$*-mCherry*	R6K	This study
pMT102	*att*HK022 *tetA tetR lacI* P_{lac}*::nlpD* $^{(1-189)}$	R6K	This study
pMT103	*att*HK022 *tetA tetR lacI* P_{lac}*::nlpD*$^{(1-115)}$*-mCherry*	R6K	This study
pMT104	*att*HK022 *tetA tetR lacI* P_{lac}*::nlpD*$^{(1-115)}$	R6K	This study
pMT149	*att*HK022 *tetA tetR lacI* P_{lac}*::nlpD*$^{(1-30)}$*-mCherry*	R6K	This study
pMT178	*att*HK022 *tetA tetR lacI* P_{lac}*::nlpD*$^{(102-175)}$*-mCherry*	R6K	This study
pMT179	*att*HK022 *tetA tetR lacI* P_{lac}*::*^{ss}*dsbA-nlpD*$^{(250-379)}$	R6K	This study
pMT180	*att*HK022 *tetA tetR lacI* P_{lac}*::*^{ss}*dsbA-nlpD*$^{(250-379)}$*-mCherry*	R6K	This study
pMT181	*att*HK022 *tetA tetR lacI* P_{lac}*::*^{ss}*dsbA-nlpD*$^{(189-379)}$	R6K	This study
pMT182	*att*HK022 *tetA tetR lacI* P_{lac}*::*^{ss}*dsbA-nlpD*$^{(189-379)}$*-mCherry*	R6K	This study
pNP20	*att*HK022 *tetA tetR lacI*^{q} P_{lac}*::nlpD*$^{(1-379)}$*-mCherry*	R6K	[39]
pTB102	*cat repA(ts) cI857(ts)* $P_{\lambda R}$*::int(HK022)*	pSC101	[35]
pTU119	*bla lacI*^{q} P_{T7}*::h-sumo-nlpD*$^{(27-379)}$	pBR/ColE1	[8]

[a] A 6xHis tag for purification is indicated by the letter *h*. *flp* encodes for FLP recombinase. ^{ss}*dsbA* corresponds to the first 24 codons of *dsbA* encoding its export signal to the periplasm. P_{T7}, $P_{\lambda R}$, and P_{lac} indicate the phage T7, λR, and lactose promoters, respectively. P_{syn135} is a synthetic lactose promoter with a consensus –35 element and no operators.

Recombineering

Since the promoter of *rpoS* is present within the coding sequence of *nlpD*, a gene knockout of *nlpD* is polar on *rpoS* expression. Therefore, in order to make an *nlpD* null strain, the N-terminal lipoprotein signal sequence of NlpD was replaced ($^{\Delta SS}$*nlpD*) to prevent its export to the periplasm where it normally functions. The $^{\Delta SS}$*nlpD::kan*^{R} allele was constructed by replacing the region between the 2nd codon and 27th codon of *nlpD* with the Kan^{R} cassette by λ recombineering as described previously [33, 40]. The Kan^{R} cassette was amplified from pKD13 [38] using the primers 5'-TGTCACTGGTTATTAACCAATTTTTCCTGGGGGATAAATGATTCCGGGGATCCGTCGACC-3' and 5'-TAACGGAGCTGACCGGTGCCGGTGGATTTGAAGTGTCAGATGTAGGCTGGAGCTGCTTCG-3'. The resulting PCR product was electroporated into strain TB10 and the recombinants were selected at 30°C on LB Kan to generate the chromosomal deletion as described previously [36]. The Kan^{R} cassette was removed using FLP recombinase expressed from pCP20 [38], leaving behind the *frt* site scar to act as the signal sequence of $^{\Delta SS}$*nlpD*.

To generate the marker for Z-ring, a *zapA-sfGFP* gene fusion was created at its native chromosomal locus by λ recombineering as described above. The *sfGFP* coding sequence and a linked Cm^{R} cassette flanked by a *zapA* 3'-end sequence and a sequence downstream of *zapA* were amplified using pHC467 as template and the primers 5'-ACAAGGTCGCATCACCGAAAAAACTAACCAAAACTTTGAACTCGAGGGTCCGGCTG

GTCTG-3' and 5'-

TTGTCTTCACGGTTACTCTACCACAGTAAACCGAAAAGTGGTGTAGGCTGGAGCTG

CTTCG-3'. The resulting fragment was electroporated into strain TB10 and the recombinants were selected at 30°C on LB Cm to generate the chromosomal fusion as described previously [36]. The *zapA-sfGFP* gene fusion linked to the Cm^R cassette was transferred between strains by P1 transduction. If necessary, the Cm^R cassette was removed using FLP recombinase expressed from pCP20 [38].

Microscopy

Cells were images on 2% agarose pads using a Nikon TE2000 inverted microscope outfitted with a Nikon Intensilight illuminator, a Coolsnap HQ2 CCD camera from Photometrics, a Nikon CFI Plan Apo VC 100x objective (1.4 NA) for differential interference contrast (DIC) imaging or a CFI Plan Apo DM 100x objective (1.4 NA) for phase contrast imaging. Please see figure legends for details about growth conditions used for specific experiments. Filter cubes for fluorescence image acquisition were from Chroma. mCherry and GFP fluorescence images were taken using the ET-mCherry filter set (Chroma 49008) and ET-GFP filter set (Chroma 49002) respectively. Images were captured using Nikon Elements software, exported and cropped for figure preparation in MetaMorph (Molecular Devices).

Protein purification

NlpD was overexpressed and purified with a 6xHis-SUMO (H-SUMO) tag fused to its N-terminus [41, 42]. The sequence of the affinity tag was MRGSHHHHHHMASG. The SUMO sequence was amplified from the *Saccharomyces cerevisiae genome* (gene Smt3) [43]. H-SUMO-NlpD(27-379) was purified from BL21(λDE3)/pTU119. Overnight cultures were diluted 1:200 into 1 L of LB supplemented with ampicillin (50 µg/ml) and cells were grown at 30°C to an OD_{600} of 0.5. IPTG was then added to 1 mM, growth was continued for an additional 3.5 hours, and the cells were harvested by centrifugation. Cell pellets were resuspended in 25 ml Buffer A (20 mM Tris-HCl, pH 7.4, 500 mM NaCl, 20 mM imidazole) and stored at -80°C prior to use for protein purification. For purification, the frozen resuspension was thawed, and the cells were disrupted by passing them through a french pressure cell twice at 15,000 psi. Cell debris were pelleted by centrifugation at 17,000 x g for 10 minutes at 4°C. The clarified lysate was incubated with Ni-NTA agarose beads (Qiagen) for 1 hour at 4°C and then loaded on a gravity flow column (BioRad). The column was washed with 10ml Buffer A and the H-SUMO-NlpD(27-379) was eluted with Buffer B (20 mM Tris-HCl, pH 7.4, 500 mM NaCl, 300 mM imidazole). Peak fractions were collected and dialyzed against 1 L of Buffer D (50 mM Tris-HCl, pH 7.4, 300 mM NaCl, 10% glycerol).

After purification of the H-SUMO fusion protein, the H-SUMO tag was removed using 6xHis-tagged SUMO protease (H-SP) [43]. Cleavage reactions were passed through Ni-NTA resin (Qiagen) to remove free H-SUMO and H-SP, yielding a pure preparation of

untagged NlpD without added non-native residues. Aliquots of both tagged and untagged versions of NlpD(27-379) were stored at -80°C prior to use.

Antibody preparation and affinity purification

Rabbit polyclonal antibodies against NlpD was prepared by Covance. Tagged NlpD protein prepared as described above was used in a custom antibody production service. The anti-NlpD antibodies were subsequently affinity purified using purified untagged NlpD conjugated to AminoLink Plus resin (Pierce), according to the manufacturer's instructions.

Immunoblotting

Strains were grown as described in the figure legends. At the designated times, cells were harvested and whole-cell extracts were prepared as described previously [44]. The protein concentration of each extract was determined using the non-interfering protein assay (Genotech) according to the manufacturer's instructions. Protein concentrations were normalized between extracts and the indicated amount of total protein from each extract was separated on a 4-20% Mini-PROTEAN® TGX™ precast protein gel (BioRad). Proteins were transferred to a PVDF membrane (Whatman) and the membrane was blocked with 2% skim milk in TBS-T (10mM Tris HCl, pH 7.5, 100mM NaCl, 0.1% Tween 20) for 1 hour at room temperature. The membrane was incubated with primary antibodies diluted in TBS-T with 0.2% skim milk (either 1:5,000 dilution for anti-mCherry antibodies or 1:10,000 dilution for affinity-purified anti-NlpD antibodies)

overnight at 4°C. When anti-mCherry antibodies were used, the blocking solution also contained cell lysate from the $^{\Delta SS}$*nlpD* strain. The next day, the primary antibody solution was removed and the membrane was quickly rinsed with TBS-T and then thoroughly washed three times with TBS-T for 5-10 minutes each wash. Following the final wash, the membrane was incubated with the secondary goat anti-rabbit antibodies conjugated to horseradish peroxidase (Rockland) diluted 1:40,000 in TBS-T with 0.2% skim milk for 1 hour with gentle agitation at room temperature. After this incubation period, the secondary antibody solution was discarded and the membrane was again quickly rinsed with TBS-T and then thoroughly washed an additional four times with TBS-T for 5-10 minutes each. The blot was developed using the Super Signal West Pico system (Pierce) according to the manufacturer's protocol. Chemiluminescence was detected using a BioRad Chemidoc system.

Section 3.6: References

1. Lutkenhaus, J., Pichoff, S., and Du, S. (2012). Bacterial cytokinesis: From Z ring to divisome. Cytoskeleton *69*, 778–790.

2. de Boer, P. A. (2010). Advances in understanding E. coli cell fission. Current Opin Microbiol *13*, 730–737.

3. Höltje, J. V. (1998). Growth of the stress-bearing and shape-maintaining murein sacculus of Escherichia coli. Microbiol Mol Biol Rev *62*, 181–203.

4. Heidrich, C., Templin, M. F., Ursinus, A., Merdanovic, M., Berger, J., Schwarz, H., de Pedro, M. A., and Höltje, J. V. (2001). Involvement of N-acetylmuramyl-L-alanine amidases in cell separation and antibiotic-induced autolysis of Escherichia coli. Mol Microbiol *41*, 167–178.

5. Priyadarshini, R., de Pedro, M. A., and Young, K. D. (2007). Role of peptidoglycan amidases in the development and morphology of the division septum in Escherichia coli. J Bacteriol *189*, 5334–5347.

6. Yang, D. C., Tan, K., Joachimiak, A., and Bernhardt, T. G. (2012). A conformational switch controls cell wall-remodelling enzymes required for bacterial cell division. Mol Microbiol *85*, 768–781.

7. Uehara, T., Dinh, T., and Bernhardt, T. G. (2009). LytM-domain factors are required for daughter cell separation and rapid ampicillin-induced lysis in Escherichia coli. J Bacteriol *191*, 5094–5107.

8. Uehara, T., Parzych, K. R., Dinh, T., and Bernhardt, T. G. (2010). Daughter cell separation is controlled by cytokinetic ring-activated cell wall hydrolysis. EMBO J *29*, 1412–1422.

9. Peters, N. T., Morlot, C., Yang, D. C., Uehara, T., Vernet, T., and Bernhardt, T. G. (2013). Structure-function analysis of the LytM domain of EnvC, an activator of cell wall remodelling at the Escherichia coli division site. Mol Microbiol *89*, 690–701.

10. Firczuk, M., Mucha, A., and Bochtler, M. (2005). Crystal structures of active LytM. J Mol Biol *354*, 578–590.

11. Firczuk, M., and Bochtler, M. (2007). Folds and activities of peptidoglycan amidases. FEMS Microbiol Rev *31*, 676–691.

12. Yang, D. C., Peters, N. T., Parzych, K. R., Uehara, T., Markovski, M., and Bernhardt, T. G. (2011). An ATP-binding cassette transporter-like complex governs cell-wall hydrolysis at the bacterial cytokinetic ring. Proc Natl Acad Sci USA *108*, E1052–60.

13. Bateman, A., and Bycroft, M. (2000). The structure of a LysM domain from E. coli membrane-bound lytic murein transglycosylase D (MltD). J Mol Biol *299*, 1113–1119.

14. Buist, G., Steen, A., Kok, J., and Kuipers, O. P. (2008). LysM, a widely distributed protein motif for binding to (peptido)glycans. Mol Microbiol *68*, 838–847.

15. Mesnage, S., Dellarole, M., Baxter, N. J., Rouget, J.-B., Dimitrov, J. D., Wang, N., Fujimoto, Y., Hounslow, A. M., Lacroix-Desmazes, S., Fukase, K., et al. (2014). Molecular basis for bacterial peptidoglycan recognition by LysM domains. Nat Commun *5*, 4269.

16. Ward, J. J., Sodhi, J. S., McGuffin, L. J., Buxton, B. F., and Jones, D. T. (2004). Prediction and functional analysis of native disorder in proteins from the three kingdoms of life. J Mol Biol *337*, 635–645.

17. Battesti, A., Majdalani, N., and Gottesman, S. (2011). The RpoS-Mediated General Stress Response in Escherichia coli. Annu Rev Microbiol *65*, 189–213.

18. Lange, R., and Hengge-Aronis, R. (1994). The nlpD gene is located in an operon with rpoS on the Escherichia coli chromosome and encodes a novel lipoprotein with a potential function in cell wall formation. Mol Microbiol *13*, 733–743.

19. Paradis-Bleau, C., Kritikos, G., Orlova, K., Typas, A., and Bernhardt, T. G. (2014). A Genome-Wide Screen for Bacterial Envelope Biogenesis Mutants Identifies a Novel Factor Involved in Cell Wall Precursor Metabolism. PLoS Genet *10*, e1004056.

20. Gerding, M. A., Liu, B., Bendezú, F. O., Hale, C. A., Bernhardt, T. G., and de Boer, P. A. J. (2009). Self-enhanced accumulation of FtsN at Division Sites and Roles for Other Proteins with a SPOR domain (DamX, DedD, and RlpA) in Escherichia coli cell constriction. J Bacteriol *191*, 7383–7401.

21. Yahashiri, A., Jorgenson, M. A., and Weiss, D. S. (2015). Bacterial SPOR domains are recruited to septal peptidoglycan by binding to glycan strands that lack stem peptides. Proc Natl Acad Sci USA *112*, 11347–11352.

22. Yamamoto, H., Kurosawa, S.-I., and Sekiguchi, J. (2003). Localization of the vegetative cell wall hydrolases LytC, LytE, and LytF on the Bacillus subtilis cell surface and stability of these enzymes to cell wall-bound or extracellular proteases. J Bacteriol *185*, 6666–6677.

23. Steen, A., Buist, G., Leenhouts, K. J., Khattabi, El, M., Grijpstra, F., Zomer, A. L., Venema, G., Kuipers, O. P., and Kok, J. (2003). Cell wall attachment of a widely distributed peptidoglycan binding domain is hindered by cell wall constituents. J Biol Chem *278*, 23874–23881.

24. Busiek, K. K., Eraso, J. M., Wang, Y., and Margolin, W. (2012). The Early Divisome Protein FtsA Interacts Directly through Its 1c Subdomain with the Cytoplasmic Domain of the Late Divisome Protein FtsN. J Bacteriol *194*, 1989–2000.

25. Busiek, K. K., and Margolin, W. (2014). A role for FtsA in SPOR-independent localization of the essential Escherichia coli cell division protein FtsN. Mol Microbiol *92*, 1212–1226.

26. Rico, A. I., García-Ovalle, M., Palacios, P., Casanova, M., and Vicente, M. (2010). Role of Escherichia coli FtsN protein in the assembly and stability of the cell division ring. Mol Microbiol *76*, 760–771.

27. Boyle, D. S., Khattar, M. M., Addinall, S. G., Lutkenhaus, J., and Donachie, W. D. (1997). ftsW is an essential cell-division gene in Escherichia coli. Mol Microbiol *24*, 1263–1273.

28. Pogliano, J., Pogliano, K., Weiss, D. S., Losick, R., and Beckwith, J. (1997). Inactivation of FtsI inhibits constriction of the FtsZ cytokinetic ring and delays the assembly of FtsZ rings at potential division sites. Proc Natl Acad Sci USA *94*, 559–564.

29. Chen, J. C., and Beckwith, J. (2001). FtsQ, FtsL and FtsI require FtsK, but not FtsN, for co-localization with FtsZ during Escherichia coli cell division. Mol Microbiol *42*, 395–413.

30. Bernhardt, T. G., and de Boer, P. A. J. (2004). Screening for synthetic lethal mutants in Escherichia coli and identification of EnvC (YibP) as a periplasmic septal ring factor with murein hydrolase activity. Mol Microbiol *52*, 1255–1269.

31. Miller, J. H. (1972). Experiments in molecular genetics. (Cold Spring Harbor Laboratory Press).

32. Guyer, M. S., Reed, R. R., Steitz, J. A., and Low, K. B. (1981). Identification of a sex-factor-affinity site in E. coli as gamma delta. Cold Spring Harb Symp Quant Biol *45 Pt 1*, 135–140.

33. Baba, T., Ara, T., Hasegawa, M., Takai, Y., Okumura, Y., Baba, M., Datsenko, K. A., Tomita, M., Wanner, B. L., and Mori, H. (2006). Construction of Escherichia coli K-12 in-frame, single-gene knockout mutants: the Keio collection. Mol Syst Biol *2*, 2006.0008.

34. Haldimann, A., and Wanner, B. L. (2001). Conditional-replication, integration, excision, and retrieval plasmid-host systems for gene structure-function studies of bacteria. J Bacteriol *183*, 6384–6393.

35. Bernhardt, T. G., and de Boer, P. A. J. (2005). SlmA, a nucleoid-associated, FtsZ binding protein required for blocking septal ring assembly over Chromosomes in E. coli. Mol Cell *18*, 555–564.

36. Johnson, J. E., Lackner, L. L., Hale, C. A., and de Boer, P. A. J. (2004). ZipA is required for targeting of DMinC/DicB, but not DMinC/MinD, complexes to septal ring assemblies in Escherichia coli. J Bacteriol *186*, 2418–2429.

37. Yakhnina, A. A., McManus, H. R., and Bernhardt, T. G. (2015). The cell wall amidase AmiB is essential for Pseudomonas aeruginosa cell division, drug resistance and viability. Mol Microbiol *97*, 957–973.

38. Datsenko, K. A., and Wanner, B. L. (2000). One-step inactivation of chromosomal genes in Escherichia coli K-12 using PCR products. Proc Natl Acad Sci USA *97*, 6640–6645.

39. Peters, N. T., Dinh, T., and Bernhardt, T. G. (2011). A fail-safe mechanism in the septal ring assembly pathway generated by the sequential recruitment of cell separation amidases and their activators. J Bacteriol *193*, 4973–4983.

40. Yu, D., Ellis, H. M., Lee, E. C., Jenkins, N. A., Copeland, N. G., and Court, D. L. (2000). An efficient recombination system for chromosome engineering in Escherichia coli. Proc Natl Acad Sci USA *97*, 5978–5983.

41. Mossessova, E., and Lima, C. D. (2000). Ulp1-SUMO crystal structure and genetic analysis reveal conserved interactions and a regulatory element essential for cell growth in yeast. Mol Cell *5*, 865–876.

42. Marblestone, J. G., Edavettal, S. C., Lim, Y., Lim, P., Zuo, X., and Butt, T. R. (2006). Comparison of SUMO fusion technology with traditional gene fusion systems: enhanced expression and solubility with SUMO. Protein Sci *15*, 182–189.

43. Bendezú, F. O., Hale, C. A., Bernhardt, T. G., and de Boer, P. A. J. (2009). RodZ (YfgA) is required for proper assembly of the MreB actin cytoskeleton and cell shape in E. coli. EMBO J *28*, 193–204.

44. Hale, C. A., and de Boer, P. A. (1999). Recruitment of ZipA to the septal ring of Escherichia coli is dependent on FtsZ and independent of FtsA. J Bacteriol *181*, 167–176.

Chapter 4: A potential link between outer membrane constriction and septal peptidoglycan remodeling in *E. coli*

Attributions

I designed and performed all the experiments presented in this chapter and generated the subsequent figures. I wrote the text with editorial assistance from Thomas Bernhardt. The flow cytometry-based cell sorting was done by the Division of Immunology's Flow Cytometry Facility at Harvard Medical School.

Chapter 4: A potential link between outer membrane constriction and septal peptidoglycan remodeling in *E. coli*

Mary-Jane Tsang[1] and Thomas G. Bernhardt[1*]

[1]Department of Microbiology and Immunobiology, Harvard Medical School, Boston, MA 02115

Section 4.1: Summary

In gram-negative bacteria like *E. coli*, cell division involves the coordinated constriction of the three layers that make up the cell envelope. Such coupling requires the efficient splitting of the septal peptidoglycan (PG) layer that is initially shared between the developing daughter cells in order to allow the outer membrane (OM) to invaginate in step with the inner membrane. However, not much is known about the potential mechanisms that may link OM invagination and septal PG remodeling.

Septal PG splitting requires the PG hydrolytic activity of the amidases, which are themselves activated by the LytM-containing factors, EnvC and NlpD. Although the regulation of EnvC is relatively well-understood, how the activity of the OM lipoprotein NlpD is regulated *in vivo* is still unclear. In this report, we determined that the OM localization of NlpD is important for its function and regulation. Using a flow cytometry-based cell sorting approach, we identified the OM lipoprotein YraP as a potential direct activator of NlpD and showed that YraP may be a new member of the division machinery. In addition, we uncovered a genetic connection between NlpD and the Tol-

Pal system, which has been implicated in OM constriction. Based on our genetic results, we postulate a regulatory connection between OM constriction and septal PG splitting to ensure the coordinated constriction of the cell envelope layers of *E. coli*.

Section 4.2: Introduction

Bacterial cells are surrounded by a polysaccharide matrix called the peptidoglycan (PG) cell wall. This macromolecular structure is essential for cell integrity and is composed of glycan strands connected by peptide crosslinks. Given the continuous nature of the PG cell wall structure, cell growth requires the activity of PG hydrolases to cleave bonds within the PG meshwork to allow its expansion [1]. The most clearly defined function for cell wall hydrolases is during cell division to shape the new polar caps and separate the two daughter cells. In gram-negative bacteria, like *E. coli*, cytokinesis requires the coordinated constriction of the three layers that make up the cell envelope: the inner membrane (IM) and outer membrane (OM) along with the PG layer sandwiched in between them [2]. This coordination is achieved by a multi-protein ring-shaped division machine known as the divisome or septal ring. The septal PG layer synthesized by the divisome is initially shared by the developing daughter cells and must be split by PG hydrolases to allow cell separation. Consequently, an important function of the divisome is to ensure tight control over the activity of these hydrolytic enzymes to prevent the formation of lethal breaches in the cell wall structure that can result in cell lysis [3, 4].

In *E. coli*, the periplasmic LytC-type N-acetylmuramyl-L-alanine amidases (AmiA, AmiB, and AmiC) are the PG hydrolytic enzymes responsible for splitting the newly-synthesized septal PG [5, 6]. They cleave the bonds that link the stem peptides to the glycan strands, thus breaking the crosslinks within the PG cell wall meshwork to allow cell separation. However, these enzymes have poor hydrolytic activity on their own due to the presence of an autoinhibitory helix within the amidase active site [7]. Consequently, amidase activation and proper cell separation require two divisome-associated proteins with LytM-like domains, EnvC and NlpD [8-10]. Mutants lacking all three amidases or both LytM factors fail to split the septal PG layer, thus forming long chains of cells with distinct cytoplasms connected by uncleaved septal PG layers and a partially constricted outer membrane.

These cell separation factors exist as two largely redundant PG-splitting systems with EnvC specifically activating AmiA and AmiB, whereas NlpD specifically activates AmiC [9, 10]. Importantly, the LytM factors themselves are subject to further regulation *in vivo*, potentially in order to ensure that amidase activation is ultimately coordinated with the many other activities of the division machinery. EnvC is regulated by an ATP-binding cassette (ABC) transporter-like complex composed of the divisome proteins FtsE and FtsX [11]. FtsEX directly recruits EnvC to the division site and anchors it to the inner membrane. Although the mechanistic details are still unclear, FtsEX may modulate EnvC activity and amidase activation in the periplasm through conformational changes induced by ATP hydrolysis in the cytoplasm.

Much less is known about the regulation of NlpD *in vivo*. Additionally, it is still unclear why *E. coli* possesses two largely redundant septal PG-splitting systems. Given that EnvC is anchored to the outer face of the IM and NlpD is thought to be an OM lipoprotein, an attractive hypothesis is that these two PG-splitting systems ensure proper coupling between septal PG hydrolysis and the invagination of their associated membranes. This is an attractive idea as the coordinated constriction of the cell envelope layers of *E. coli* likely requires efficient septal PG processing to allow the OM to invaginate in step with the IM. We therefore postulate the existence of a regulatory connection between amidase activation and OM constriction. By virtue of its localization within the OM, the amidase activator NlpD is perfectly positioned to couple these two important processes.

The OM has long been thought to passively follow the constriction of the other layers of the cell envelope through protein linkages between the OM and the PG [2, 12]. One of the main players believed to contribute to this passive process is the major lipoprotein, Lpp or Braun's lipoprotein. Lpp is an abundant PG-bound OM lipoprotein that physically tethers the OM to the PG layer, thus allowing contacts between the OM and PG around the cell periphery and at the division site. However, Lpp is uniformly distributed throughout the cell and therefore not specifically associated with the division machine [13]. Rather than a passive process, it has recently been proposed that efficient OM invagination requires the action of a conserved trans-envelope complex known as the Tol-Pal system [14]. The phenotypes of *tol-pal* mutants are consistent with a role for the system in OM invagination and cell separation: these mutants form chains

in rich medium with either low or high osmolarity, display increased periplasmic volume at the constriction sites and shed OM vesicles primarily from the division sites and cell poles [14, 15]. Additionally, members of the Tol-Pal complex localize to the septal ring, suggesting that they may play a specific role in the division process [14].

In this study, we investigated the regulatory mechanism(s) governing the ability of NlpD to activate its cognate amidase AmiC. We determined that the subcellular localization of NlpD to the OM allows it to efficiently and properly promote PG hydrolysis for cell separation. Using a flow cytometry-based cell sorting approach, we identified genes that may be required for proper NlpD activity *in vivo* as the inactivation of these genes phenocopies the loss of NlpD. We isolated multiple transposon insertions that mapped to *yraP*, which encodes for an OM lipoprotein that localizes to the division site. In addition, many transposon insertions mapped to genes encoding for members of the Tol-Pal system, which has been implicated in OM constriction. Overall, our results suggest a model in which OM constriction by the Tol-Pal system indirectly “activates” NlpD by pulling it close to the PG layer where YraP stimulates NlpD activity to promote AmiC-mediated septal PG splitting. Therefore, OM constriction and septal PG splitting may be coupled at multiple levels.

Section 4.3: Results

Localization of NlpD to the outer membrane is important for its proper function

The two LytM-containing factors in *E. coli* have different subcellular localization. EnvC is anchored to the outer leaflet of the inner membrane via a direct interaction with

its regulator FtsEX [11]. On the other hand, NlpD is thought to be an OM lipoprotein. One hypothesis is that the OM localization of NlpD plays a role in its proper function and regulation. In order to test this possibility, we constructed two NlpD variants with altered subcellular localization. Firstly, we mutated the residue at the +2 position after the acylated cysteine from serine to aspartate (NlpD$^{(S27D)}$) in order to exclude this variant from the Lol system and thus force its retention in the IM [16] (**Figure 4.1A**). We also expressed a soluble periplasmic NlpD variant (NlpD$^{(27\text{-}379)}$) in which the first 26 residues, including the lipidated cysteine, were replaced by the signal sequence of the DsbA protein for Sec-mediated export to the periplasm.

In order to assess whether the different variants localized as expected, a cytological assay was used [17]. Cells expressing each variant fused to mCherry at the C-terminus were hyperosmotically shocked to induce plasmolysis and subsequently visualized using both phase contrast and fluorescence microscopy. Upon plasmolysis, the cytoplasm shrunk and, as visualized by phase contrast microscopy, the IM pulled away from the rest of the cell envelope (**Figure 4.1B-D**). Wild-type NlpD-mCherry displayed a smooth peripheral fluorescence signal in the plasmolyzed cells consistent with an OM localization (**Figure 4.1B**). On the other hand, the fluorescence pattern of NlpD$^{(S27D)}$-mCherry followed the retracted IM, indicating that this variant is indeed retained in the IM (**Figure 4.1C**). Finally, the fluorescent signal of NlpD$^{(27\text{-}379)}$-mCherry accumulated in the increased periplasmic spaces of the plasmolyzed cells, which are generally phase-gray in the phase contrast images (**Figure 4.1D**). Based on these

cytological results, we conclude that the different NlpD variants are present in the expected subcellular localizations.

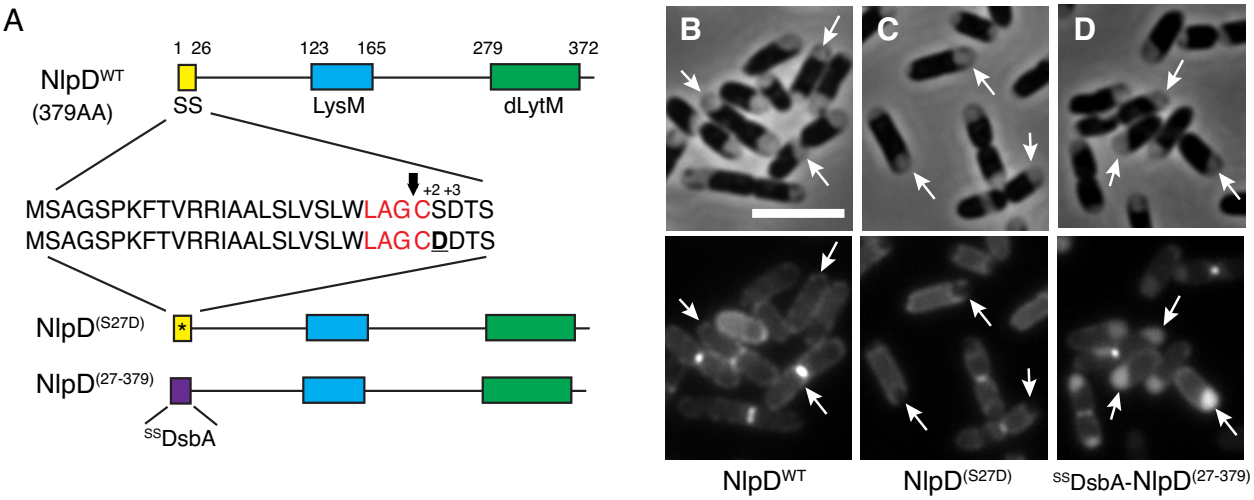

Figure 4.1. NlpD variants with altered subcellular localization. (**A**) The domain structure of NlpD is illustrated. Indicated are the signal sequence (SS; yellow), lysin motif (LysM; blue), and the degenerate LytM domain (dLytM; green). Details of the signal sequence are presented with the lipobox in red and the arrow indicating the cleavage site just before the acylated cysteine. The IM-retained variant (NlpD$^{(S27D)}$) contains a mutated signal sequence (indicated by the asterisk) with an aspartate at the +2 position after the acylated cysteine (bold and underlined). The soluble periplasmic variant (NlpD$^{(27-379)}$) is fused to the DsbA signal peptide (purple) that is cleaved upon export to the periplasm via the Sec system. (**B-D**) Cytological assay to determine the subcellular localization of the NlpD variants. Overnight cultures of MT47 (*$^{\Delta SS}$nlpD*) expressing different NlpD-mCherry fusions from the integrated constructs (**B**) attHKNP20 (*P$_{lac}$::nlpD^{WT}-mCherry*), (**C**) attHKMT21 (*P$_{lac}$::nlpD$^{(S27D)}$-mCherry*), or (**D**) attHKMT147 (*P$_{lac}$::^{ss}dsbA-nlpD$^{(27-379)}$-mCherry*) were diluted in minimal M9-maltose medium supplemented with 25µM (**D**) or 150µM (**B-C**) IPTG. Cells were grown at 30°C to an OD_{600} of 0.25 - 0.35, washed and then osmotically shocked by resuspension in

Figure 4.1 (Continued). plasmolysis buffer. The plasmolyzed cells were visualized on 1% agarose pads with 15% sucrose with phase contrast and mCherry optics. Arrows indicate signals that display smooth OM peripheral signal in (**B**), track with the IM in (**C**), or fill the increased periplasmic spaces in (**D**) in the plasmolyzed bays that are phase gray in the phase contrast images. Bar = 4μm.

Next, we determined whether the NlpD variants with altered localization were functional for amidase activation. The deletion of *nlpD* is polar on the downstream gene *rpoS*, which encodes for an alternative sigma factor that regulates a large number of genes in response to a variety of stresses [18, 19]. Therefore, in order to prevent polar effects, we replaced the signal sequence of NlpD ($^{\Delta SS}$*nlpD*) to trap NlpD in the cytoplasm, thus rendering it non-functional (see details in Chapter 3). We used this $^{\Delta SS}$*nlpD* as our *nlpD* null strain throughout this study. Each untagged variant was expressed under the control of the IPTG-inducible lactose promoter from an integrated plasmid in a strain lacking both LytM factors, NlpD and EnvC. In the absence of IPTG, this $^{\Delta SS}$*nlpD ΔenvC* strain grew as very long chains of cells that failed to separate due to lack of amidase activation (**Figure 4.2A, C-D**).

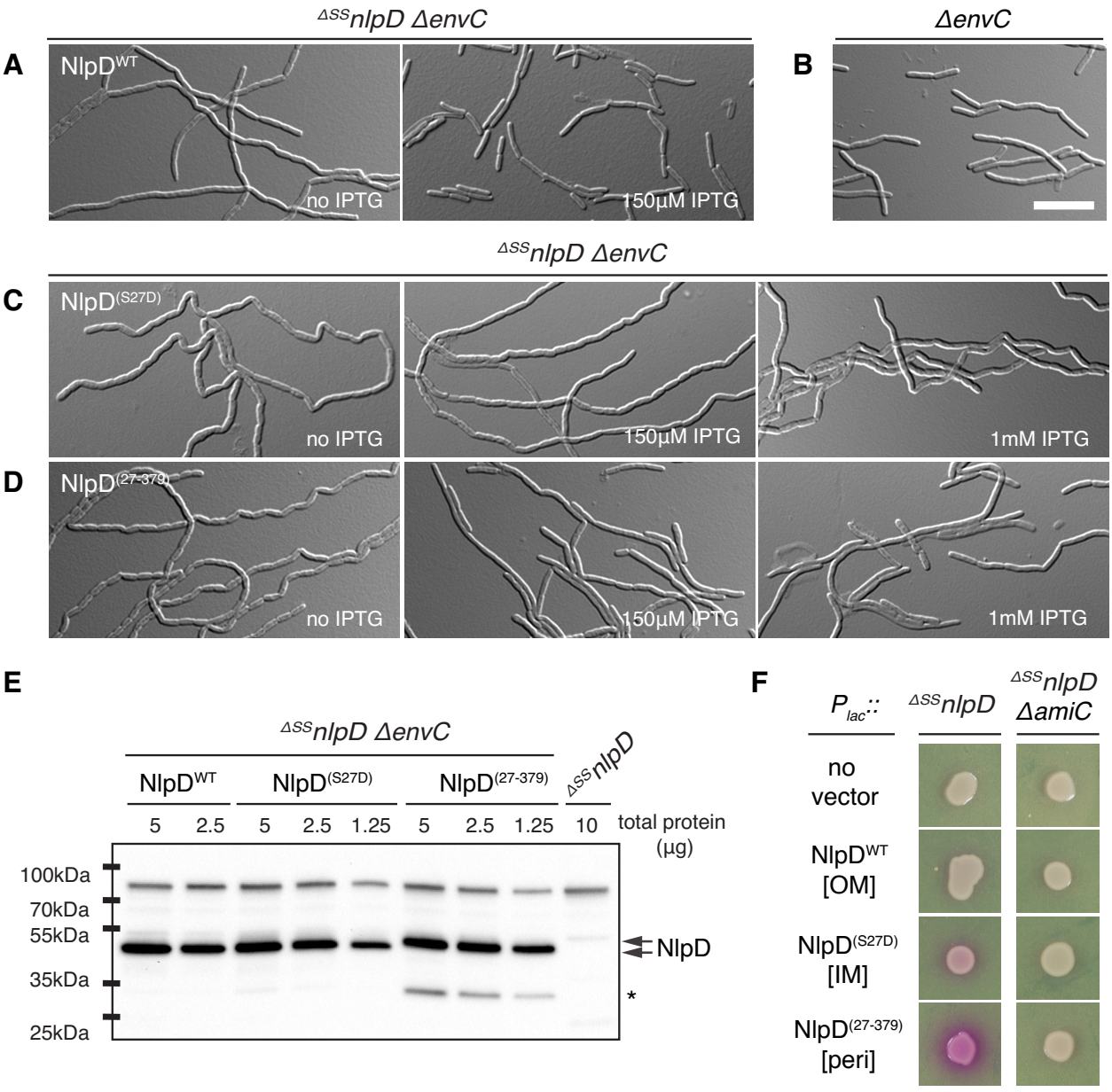

Figure 4.2. OM localization of NlpD is required for efficient and proper cell separation. (**A-D**) Overnight cultures of MT50 (*ΔSSnlpD ΔenvC*) harboring the integrated expression constructs (**A**) attHKMT20 (*Plac::nlpDWT*), (**C**) attHKMT12 (*Plac::nlpD (S27D)*), or (**D**) attHKMT121 (*Plac::ssdsbA-nlpD (27-379)*) were diluted in minimal M9-maltose medium and grown at 37°C until mid-log. Cultures were then backdiluted into M9-maltose only or supplemented with the indicated IPTG concentration. As control, (**B**) TB140 (*ΔenvC*)

Figure 4.2 (Continued). was also grown under the same conditions in medium lacking IPTG. The cells were grown at 37°C to an OD_{600} of 0.25 - 0.35 and then visualized on 2% agarose pads with DIC optics. Bar = 10µm. (**E**) The MT50 strains described above were grown in M9-maltose medium with 150µM IPTG. As control, MT47 (*$^{\Delta SS}$nlpD*) was also grown under similar conditions. Cells of these induced strains were harvested for whole-cell extract preparation. Proteins in the resulting extracts were separated by SDS-PAGE, transferred to PVDF, and NlpD was detected with affinity purified anti-NlpD antibodies. The arrows indicate the NlpD variant present in each strain. The asterisk denotes a degradation product of NlpD$^{(27\text{-}379)}$. (**F**) Cells of MT122 (*$^{\Delta SS}$nlpD*) and MT123 (*$^{\Delta SS}$nlpD ΔamiC*) alone or harboring the integrated constructs described above were grown in LB at 30°C. Following normalization for cell density (OD_{600} = 0.5), 5 µl of the resulting cultures was spotted on LB agar containing 150µM IPTG and 20µg/ml CPRG. The plates were incubated at 30°C and photographed after 14 hours. The subcellular localization of each NlpD variant is indicated in the square brackets: OM, outer membrane; IM, inner membrane; peri, periplasm.

Expression of wild-type NlpD rescued the chaining phenotype of the *$^{\Delta SS}$nlpD ΔenvC* double mutant such that cells displayed only the mild division defect of EnvC- cells (**Figure 4.2A-B**). However, the expression of either IM-retained NlpD (NlpD$^{(S27D)}$) or soluble periplasmic NlpD (NlpD$^{(27\text{-}379)}$) failed to suppress the chaining phenotype of the double mutant, even when fully induced from the lactose promoter (**Figure 4.2C-D**). Since both variants were intact and expressed at similar levels as the wild-type protein (**Figure 4.2E**), these results suggest that the OM localization of NlpD allows it to efficiently activate its cognate amidase AmiC. Interestingly, expression of the soluble periplasmic NlpD$^{(27\text{-}379)}$ variant led to a slight reduction in chain length of the *$^{\Delta SS}$nlpD ΔenvC* mutant (**Figure 4.2D**). However, this reduction is most likely due to increased

cell lysis induced by this periplasmic variant. Indeed, expression of NlpD$^{(27\text{-}379)}$ resulted in a positive red signal on medium containing chlorophenyl red-β-D-galactopyranoside (CPRG) (**Figure 4.2F**). This β-galactosidase substrate generally fails to penetrate the *E. coli* cell envelope and cannot be processed by cytoplasmic LacZ, unless cells lyse and/ or become more permeable [20]. The CPRG^{+} phenotype observed was suppressed by inactivating AmiC, indicating that the soluble periplasmic NlpD variant may aberrantly activate its cognate amidase. We therefore conclude that the OM localization of NlpD allows it to efficiently and properly promote PG hydrolysis for cell separation.

Identification of NlpD regulators using flow cytometry-based cell sorting

Cell separation in *E. coli* is mediated by two largely redundant PG-splitting systems, EnvC/AmiA/AmiB and NlpD/AmiC. Consequently, loss of either *nlpD* or *amiC* leads to a cell separation defect and formation of long chains of cells when combined with an *envC* deletion. If NlpD is activated *in vivo* by a yet unknown protein to promote PG hydrolysis, the loss of this putative activator would also lead to chaining in a *ΔenvC* background. Such chains can be isolated using flow cytometry-based cell sorting [21]. Since side scatter pulse width (SSC-W) increases with increasing cell length, chaining cells ($^{\Delta SS}$*nlpD ΔenvC*) could be distinguished from non-chaining cells (*ΔenvC*) at high SSC-W (**Figure 4.3A-B**). From a defined mixed population of chaining and non-chaining cells, cells with high SSC-W were isolated by cell sorting and found to be primarily chaining (data not shown). We therefore used this approach to isolate transposon mutants that resulted in chaining in a *ΔenvC* background.

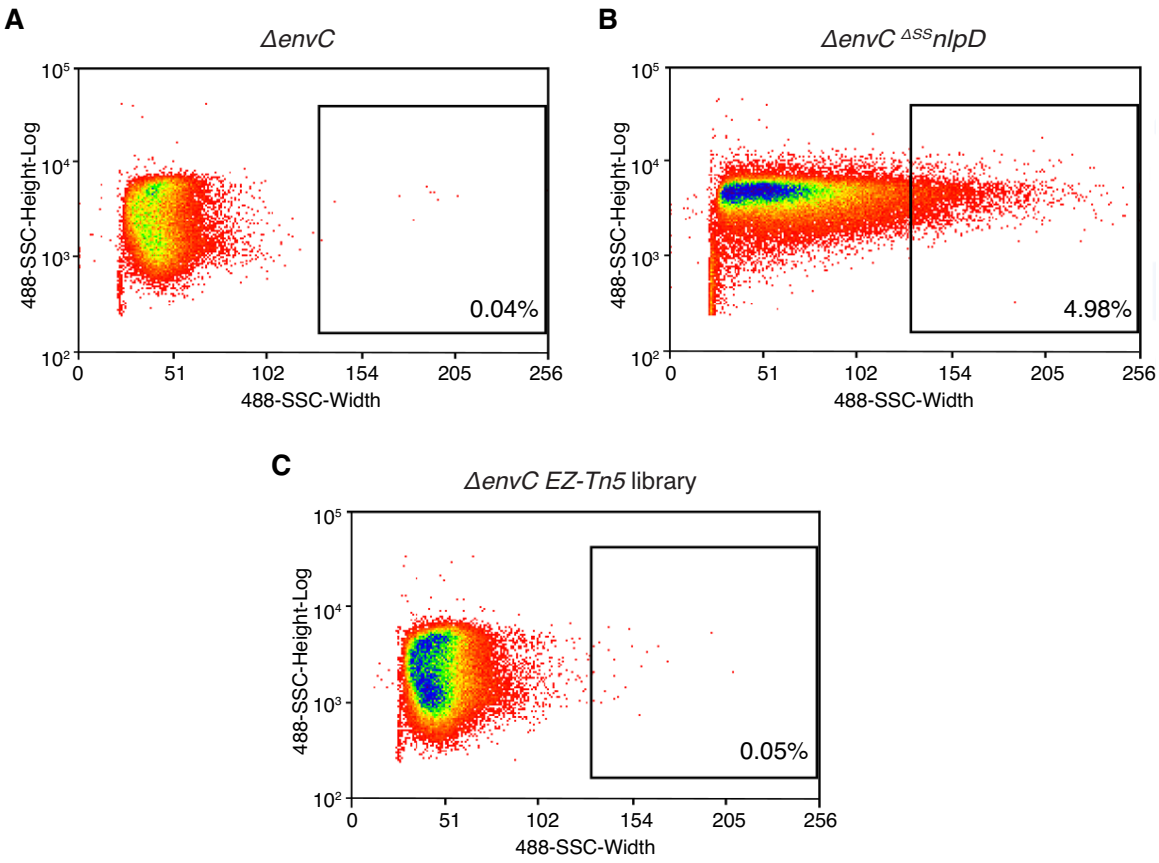

Figure 4.3. Flow cytometry analysis to distinguish chaining cells from non-chaining cells. Dot plots of (**A**) a control non-chaining strain, TB140 (*ΔenvC*), (**B**) a control chaining strain, MT50 (*ΔSSnlpD ΔenvC*), and (**C**) the TB140 transposon (EZ-Tn5 <Kan-2>) mutagenized library, with side scatter pulse height (SSC-H; y-axis) versus side scatter pulse width (SSC-W; x-axis). The gate used for sorting is shown on the plot, with the number of events present in that gate indicated as a percentage of the total population.

An EnvC-depletion strain was transposon-mutagenized and the plasmid containing the inducible *envC* gene was cured by the subsequent growth and transposon insertion selection at 37°C [22]. The resulting *ΔenvC* transposon library was sorted for cells with high SSC-W (gate shown in **Figure 4.3C**). Flow cytometry analysis

suggests a small increase in the events present in the selected gate from 0.04% of the total population for the unmutagenized control to 0.05% for the mutant library (increase of 25%) (**Figure 4.3A,C**). A second visual colony screen was used to distinguish cells with a severe chaining phenotype from non-chaining *ΔenvC* cells isolated as background. This secondary screen was based on the observation that colonies containing chaining cells are mucoid when grown at 37°C on minimal M9-maltose agar. Sorted cells were therefore plated under these conditions. The mucoid colonies were purified on LB, the chaining phenotype confirmed by phase contrast microscopy, and the positions of the transposon insertions were mapped. As expected, many of the transposon insertions were in *nlpD* or *amiC*. A high number of insertions also mapped to *tolB* and *pal*, with a few in *tolQ* and *tolA*. These genes encode for members of the Tol-Pal system, which has been implicated in OM integrity and OM invagination during cell constriction [14, 23, 24]. Finally, three insertions were found within *yraP*, which encodes for a predicted OM lipoprotein of unknown function [25].

We confirmed that the chaining phenotype observed was due to the inactivation of the genes mentioned above. A strain inactivated for both YraP and EnvC (*ΔyraP ΔenvC)* grew as very long chains of cells under both growth conditions tested (**Figure 4.4C,H**), similar to the $^{\Delta SS}$*nlpD ΔenvC* double mutant (**Figure 4.4B, G**). Since *ΔyraP* cells displayed no separation defect (**Figure 4.4C,H**), the severe chaining phenotype observed upon simultaneous inactivation of YraP and EnvC suggests that YraP may be required for NlpD-mediated cell separation.

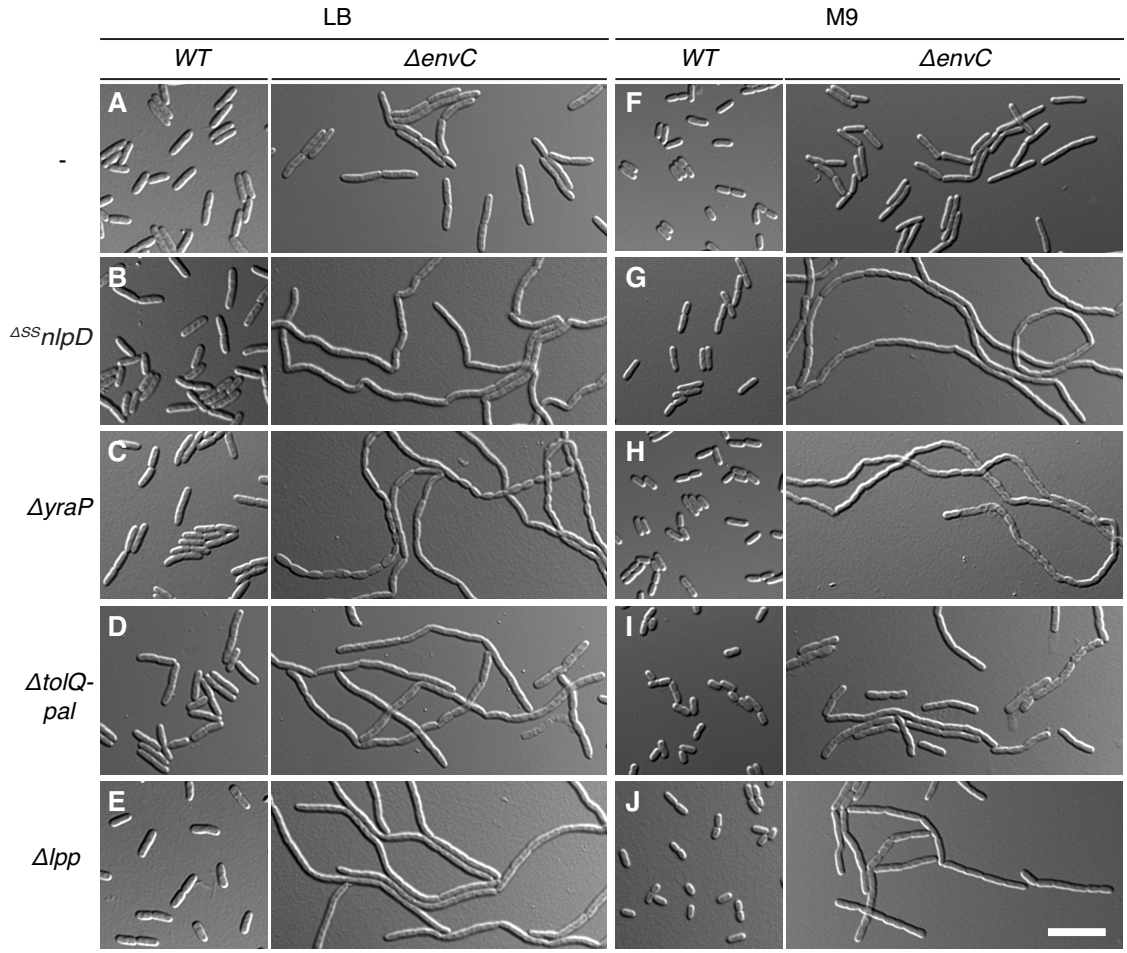

Figure 4.4. Cell morphology of potential regulators of NlpD. Overnight cultures of (**A, F**) TB28 (*WT*), TB140 (*ΔenvC*), (**B, G**) MT47 (*^{ΔSS}nlpD*), MT50 (*^{ΔSS}nlpD ΔenvC*), (**C, H**) MT140 (*ΔyraP*), MT135 (*ΔyraP ΔenvC*), (**D, I**) MT51 (*ΔtolQ-pal*), MT55 (*ΔtolQ-pal ΔenvC*), (**E, J**) TU163 (*Δlpp*), MT83 (*Δlpp ΔenvC*) were diluted in LB (**A-E**) or minimal M9-maltose (**F-J**) medium. Cells were grown at 30°C to an OD_{600} of 0.3 - 0.5 for the LB cultures or an OD_{600} of 0.1 - 0.2 for the M9 cultures before they were visualized on 2% agarose pads with DIC optics. Bar = 10μm.

Next, we assessed whether the Tol-Pal system may also function in the process of septal PG splitting with NlpD and AmiC. Mutants lacking both EnvC and the five main components of the Tol-Pal system (*ΔtolQ-pal ΔenvC)* displayed a severe chaining

phenotype in LB (**Figure 4.4D**). Surprisingly, this phenotype was partially suppressed when this mutant was grown in liquid minimal M9 medium (**Figure 4.4I**). Given the reported OM integrity defects of the *ΔtolQ-pal* mutant, the observed suppression may result from beneficial effects on OM integrity and OM invagination due to the presence of a higher concentration of Mg^{2+} in minimal M9 medium relative to standard LB [26, 27] and/or the slower overall growth rate of the cells. Lpp is an abundant PG-bound OM lipoprotein that physically tethers the OM to the PG layer and is believed to be generally involved in OM constriction. We therefore reasoned that if the chaining phenotype of *ΔtolQ-pal ΔenvC* is due to a defect in OM invagination, the loss of both Lpp and EnvC should also result in a similar chaining phenotype. This proved to be the case in LB and to a lesser extent in minimal M9 medium (**Figure 4.4E, J**). These findings suggest a model in which the induction of septal PG hydrolysis and splitting by NlpD/AmiC may be coupled with the constriction of the outer membrane (see Discussion).

NlpD localizes to the septal ring independently of YraP or the Tol-Pal system

A potential reason for the genetic connection between NlpD and YraP or Tol-Pal is that they may be required for the recruitment of NlpD to the septal ring. To investigate this possibility, we expressed an NlpD-mCherry fusion under IPTG-inducible lactose promoter control from an integrated plasmid in a strain lacking NlpD ($^{\Delta SS}$*nlpD*) alone or in combination with *ΔyraP* or *ΔtolQ-pal*. As control, we also expressed a lipidated mCherry fusion that localizes to the OM ($NlpD^{(1-30)}$-mCherry). In the $^{\Delta SS}$*nlpD* strain, NlpD-mCherry formed rings/bands at division sites, whereas the OM-localized mCherry

displayed a diffuse pattern along the cell periphery (**Figure 4.5A, D**). In cells lacking both NlpD and either YraP or the Tol-Pal system, NlpD-mCherry still showed strong accumulation at midcell, compared to the OM-localized mCherry control (**Figure 4.5B-C, E-F**). Interestingly, peripheral NlpD-mCherry signal was also higher in the absence of YraP, compared to the *$^{\Delta SS}$nlpD* strain. Overall, we conclude that YraP and the Tol-Pal system are not required for the recruitment of NlpD to the septal ring, although YraP may slightly enhance the septal localization of NlpD.

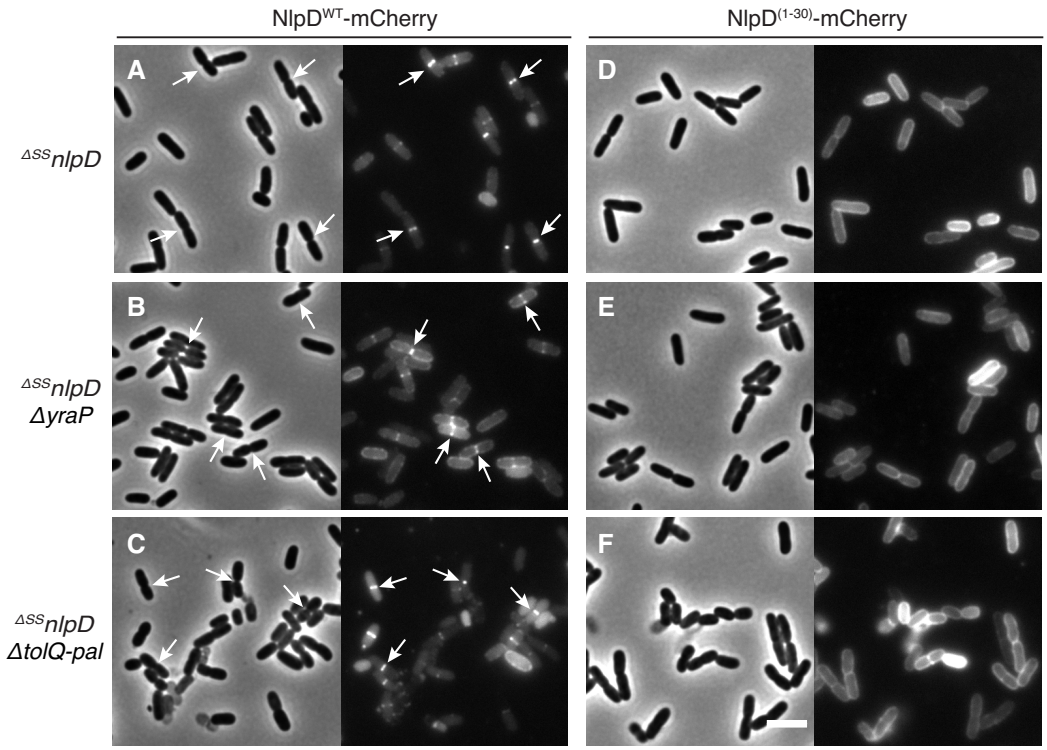

Figure 4.5. NlpD localizes to the septal ring independently of YraP or the Tol-Pal system. Overnight cultures of (**A, D**) MT47 (*$^{\Delta SS}$nlpD*), (**B, E**) MT141 (*$^{\Delta SS}$nlpD ΔyraP*), or (**C, F**) MT53 (*$^{\Delta SS}$nlpD ΔtolQ-pal*) harboring the integrated expression constructs attHKNP20 (*P_{lac}::nlpD^{WT}-mCherry*) (**A-C**) or attHKMT149 (*P_{lac}::nlpD$^{(1-30)}$-mCherry*) (**D-F**) were diluted in minimal M9-maltose medium supplemented with 50μM (**A-C**) or 150μM

Figure 4.5 (Continued). (**D-E**) IPTG. Cells were grown at 30°C to an OD_{600} of 0.2 - 0.3 before they were visualized on 2% agarose pads with phase contrast and mCherry optics. Arrows indicate localization of the protein fusion to division sites. Bar = 4μm.

YraP is a divisome protein that may activate the NlpD/AmiC PG-splitting system

We showed above that the simultaneous loss of EnvC and YraP resulted in severe cell chaining (**Figure 4.6B**), suggesting that YraP may be specifically required for NlpD-mediated cell separation. Since EnvC activates the amidases AmiA and AmiB, the combined inactivation of AmiA, AmiB, and YraP should also result in long chains of cells, as was indeed the case (**Figure 4.6C**). Mutants lacking both YraP and NlpD did not exhibit the same chaining phenotype because the EnvC/AmiA/AmiB pathway is still active (**Figure 4.6D**). These findings are consistent with YraP being specifically involved in the NlpD/AmiC system.

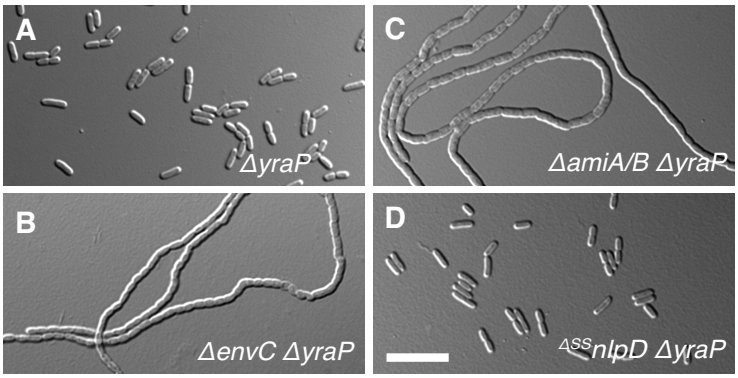

Figure 4.6. Loss of YraP leads to severe chaining in the absence of either EnvC or AmiA/B. Overnight cultures of (**A**) MT140 (*ΔyraP*), (**B**) MT135 (*ΔenvC ΔyraP*), (**C**) MT144 (*ΔamiA/B ΔyraP*), or (**D**) MT141 (*^{ΔSS}nlpD ΔyraP*) were diluted in minimal M9-maltose medium and grown at 30°C to an OD_{600} of 0.15 - 0.25. Cells were then visualized on 2% agarose pads with DIC optics. Bar = 10μm.

YraP is predicted to be an OM lipoprotein consisting of two bacterial OsmY and nodulation (BON) domains [28] (**Figure 4.7A**). We used the same cytological assay as with NlpD to experimentally determine whether YraP resides in the OM [17]. Upon plasmolysis, wild-type YraP-mCherry displayed the smooth peripheral fluorescence signal consistent with an OM localization (**Figure 4.7B**). On the other hand, an IM-retained YraP variant followed the retracted IM in plasmolyzed cells (**Figure 4.7C**). This variant was retained in the IM by mutating the residues at the +2 and +3 position after the lipidated cysteine from valine/alanine to aspartate/glutamate [16] (**Figure 4.7A**). These results demonstrate that YraP is indeed an OM lipoprotein.

We expressed wild-type YraP, either untagged or with a C-terminal mCherry fusion, under IPTG-inducible lactose promoter control from an integrated plasmid in a strain lacking both YraP and EnvC or YraP alone. Both wild-type YraP variants rescued the chaining phenotype of the *ΔyraP ΔenvC* strain such that cells only displayed an $EnvC^-$ phenotype (**Figure 4.7D-G**), suggesting that it is indeed the lack of the YraP protein that leads to NlpD inactivation. Interestingly, YraP-mCherry localized as bands at the division sites of both *ΔyraP ΔenvC* and *ΔyraP* cells (**Figure 4.8A-B**), indicating that YraP is recruited to the divisome or septal ring. On the other hand, a YraP variant that is retained in the IM failed to complement the chaining phenotype of the *ΔyraP ΔenvC* strain (**Figure 4.7H-I**), nor did it localize to the division site (**Figure 4.8C-D**). We thus conclude that YraP needs to be in the OM to associate with the division machine and promote septal PG splitting by NlpD and its cognate amidase AmiC.

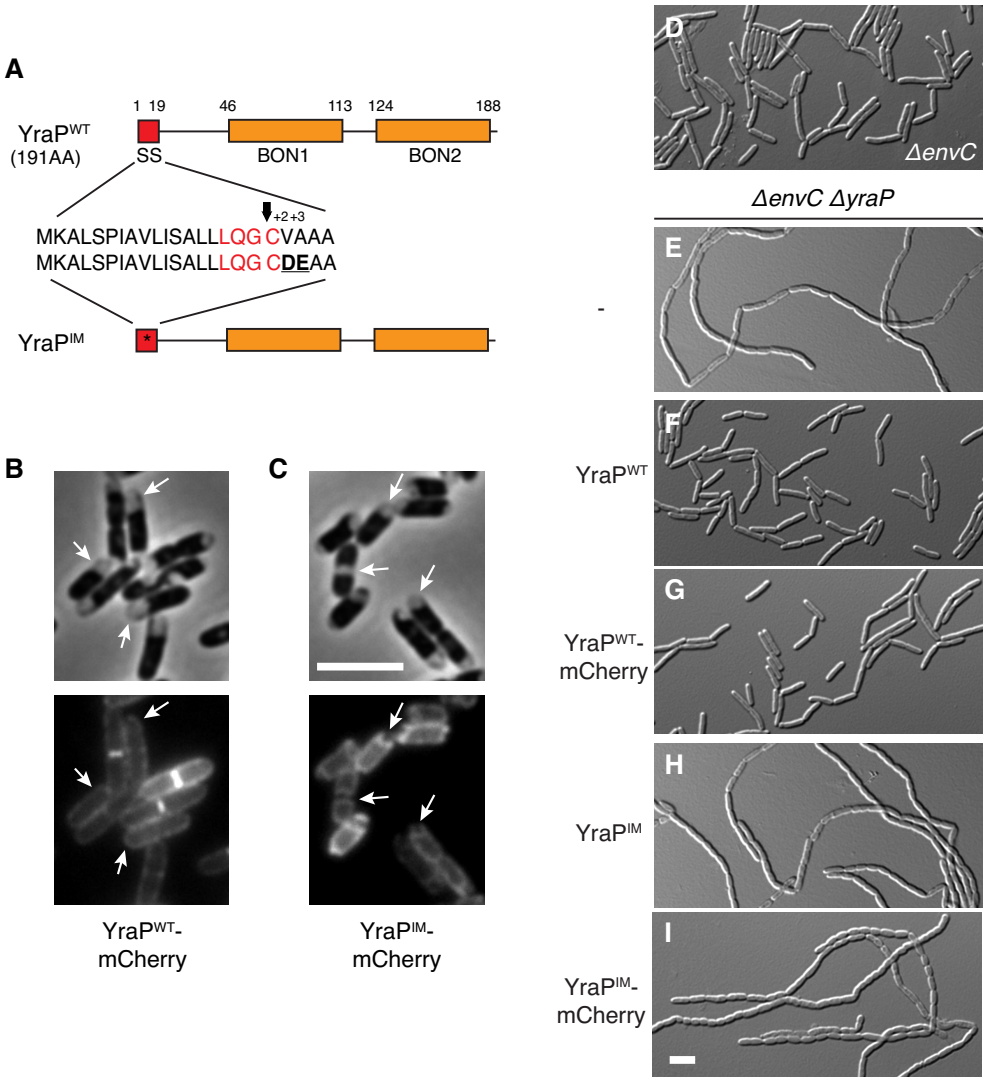

Figure 4.7. OM localization of YraP is required for cell separation in the absence of EnvC. (**A**) The domain structure of YraP is illustrated. Indicated are the signal sequence (SS; red) and the two **b**acterial **O**smY and **n**odulation domains (BON1/2; orange). Details of the signal sequence are presented with the lipobox in red and the arrow indicating the cleavage site just before the acylated cysteine. The IM-retained variant (YraP^{IM}) contains a mutated signal sequence (indicated by the asterisk) with an aspartate and glutamate at the +2 and +3 positions after the acylated cysteine (bold and underlined). (**B-C**) Cytological assay to assess the subcellular localization of the YraP variants. Overnight cultures of MT140 (*ΔyraP*) harboring the integrated expression

Figure 4.7 (Continued). constructs (**B**) attλMT197 (*P*$_{lac}$*::yraP*^{WT}*-mCherry*) or (**C**) attλMT199 (*P*$_{lac}$*::yraP*^{IM}*-mCherry*) were diluted in minimal M9-maltose medium supplemented with 250μM IPTG. Cells were grown at 30°C to an OD_{600} of 0.2, washed, osmotically shocked, and visualized with phase contrast and mCherry optics. Arrows indicate peripheral OM mCherry signals (**B**) or signals that track with the IM (**C**) in the plasmolyzed bays that are phase gray in the phase contrast images. (**D-I**) Overnight cultures of (**D**) TB140 (*ΔenvC*) or MT135 (*ΔenvC ΔyraP*) either (**E**) alone or harboring the integrated construct (**F**) attλMT196 (*P*$_{lac}$*::yraP*^{WT}), (**G**) attλMT197 (*P*$_{lac}$*::yraP*^{WT}*-mCherry*), (**H**) attλMT198 (*P*$_{lac}$*::yraP*^{IM}), or (**I**) attλMT199 (*P*$_{lac}$*::yraP*^{IM}*-mCherry*) were diluted in minimal M9-maltose medium only (**D-E**) or supplemented with 10μM (**F-G**) or 100μM (**H-I**) IPTG. Cells were grown at 30°C to an OD_{600} of 0.1 - 0.2 before they were visualized on 2% agarose pads with DIC optics. Bar = 4μm.

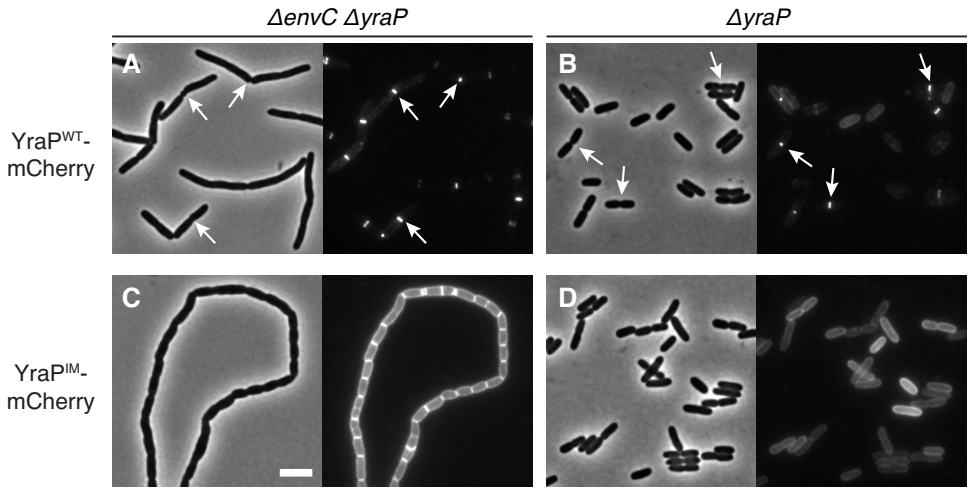

Figure 4.8. YraP localizes to the septal ring. Overnight cultures of (**A, C**) MT135 (*ΔenvC ΔyraP*) or (**B, D**) MT140 (*ΔyraP*) harboring the integrated expression constructs (**A-B**) attλMT197 (*P*$_{lac}$*::yraP*^{WT}*-mCherry*) or (**C-D**) attλMT199 (*P*$_{lac}$*::yraP*^{IM}*-mCherry*) were diluted in minimal M9-maltose medium supplemented with 10μM (**A-B**) or 100μM (**C-D**) IPTG. Cells were grown at 30°C to an OD_{600} of 0.1 - 0.2 before they were visualized on 2% agarose pads with phase contrast and mCherry optics. Arrows indicate localization of the protein fusion to division sites. Bar = 4μm.

Section 4.4: Discussion

This study investigated the regulatory mechanism(s) governing the ability of NlpD to activate its cognate amidase AmiC. Just as the activity of the other amidase activator EnvC is controlled by the FtsEX complex, we similarly hypothesized that NlpD may be regulated by other component(s) of the septal ring to coordinate its activity with additional functions of the division machine. In gram-negative bacteria, such as *E. coli*, cytokinesis requires the coordinated constriction of the three layers that make up the cell envelope. Such coupling requires the splitting of the septal peptidoglycan (PG) layer that is initially shared between the developing daughter cells in order to allow the OM to invaginate and follow the IM. To accomplish such a coordinated task, a potential regulatory connection may exist between OM constriction and amidase activation for septal PG processing. By virtue of its localization within the OM, the amidase activator NlpD is perfectly positioned to couple these two important processes.

NlpD is a lipoprotein with a serine after the acylated cysteine, which predicts that it is directed to the outer membrane by the Lol system [16]. We confirmed this localization using a cytological assay combining fluorescence microscopy and plasmolysis. By studying NlpD variants with altered subcellular localization, we inferred that OM localization is important for NlpD function and regulation. Accordingly, an IM-retained NlpD variant was non-functional whereas a soluble periplasmic variant resulted in increased cell lysis. In summary, the localization of NlpD within the OM is required for proper and efficient hydrolysis of septal PG during cell separation.

Next we attempted to identify potential regulators of NlpD using a flow cytometry-based cell sorting approach. We isolated transposon insertions that displayed a similar chaining phenotype as an *nlpD* null mutation when combined with *ΔenvC*. The inactivated genes may therefore be required for NlpD activity *in vivo*. We isolated multiple transposon insertions that mapped to the *yraP* gene and phenocopied the loss of functional NlpD. Accordingly, a *ΔyraP ΔenvC* double mutant displayed a severe chaining phenotype similar to that of a $^{\Delta SS}$*nlpD ΔenvC* mutant. YraP is a lipoprotein with two bacterial OsmY and nodulation (BON) domains and is predicted to localize to the OM [25, 28]. We confirmed this subcellular localization using a similar cytological assay as the one used for NlpD and found that the OM localization of YraP is necessary for proper NlpD activity. In addition, while wild-type YraP localized to the septal ring in dividing cells, the IM-retained variant was diffused around the cell periphery. This observation raises the possibility that YraP is recruited to the septal ring via a direct interaction with an OM protein.

Since the loss of YraP phenocopied the loss of NlpD in all growth media tested, we postulate that YraP stimulates NlpD activity, potentially through a direct protein-protein interaction (**Figure 4.9A-B**). The observation that IM-retained YraP failed to activate NlpD is consistent with this proposed regulatory mechanism as both proteins may need to be within the same membrane for proper activation. Interestingly, IM-retained YraP also failed to localize to the septal ring. Given that NlpD localizes to the division sites in the absence of YraP, one hypothesis is that YraP is recruited to the septal ring through its interaction with its target NlpD. The implications of this

hypothetical localization dependency is unclear at the moment, but the potential interaction between NlpD and YraP and whether or not YraP stimulates NlpD/AmiC activity *in vitro* need to be further investigated.

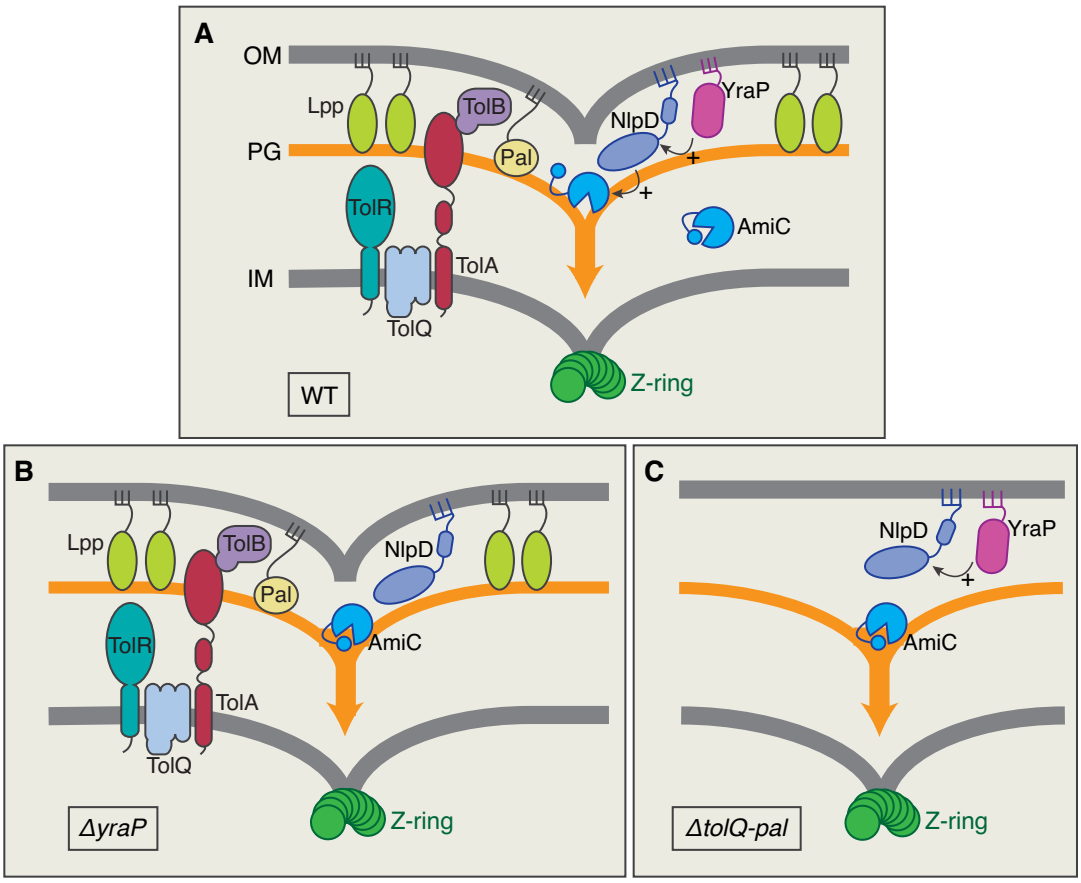

Figure 4.9. Potential mechanisms regulating NlpD activity. (**A-C**) Shown are diagrams of the division site highlighting the mechanisms present in (**A**) wild-type (WT), (**B**) *ΔyraP*, or (**C**) *ΔtolQ-pal* cells to regulate both NlpD and ultimately AmiC activities. The current model is that at the division site, the amidase activity of AmiC is controlled by a conformational switch involving the release of an autoregulatory helix from the amidase active site, which is stimulated by the LytM domain of NlpD. Our results support a model in which NlpD is further regulated *in vivo* by both the OM lipoprotein YraP and the Tol-Pal system, which has been implicated in OM constriction (**A**). We

Figure 4.9 (Continued). propose a potential direct activation of NlpD by YraP. Therefore, in the absence of YraP, NlpD remains in an inactive state that cannot promote septal PG splitting by AmiC (**B**). On the other hand, the Tol-Pal system indirectly "activates" NlpD by bringing it closer to the PG layer during OM constriction where it can promote AmiC-mediated septal PG splitting. In the absence of the Tol-Pal complex, NlpD remains out of reach of the PG layer and therefore AmiC cannot act on septal PG (**C**). Together, these two regulatory mechanisms may ensure proper coordination of OM constriction and septal PG remodeling by NlpD and AmiC.

Many of transposon insertions isolated in our screen for NlpD regulators also mapped to genes encoding for members of the Tol-Pal system. This highly conserved complex is important for OM integrity and has been implicated in OM constriction [14, 23, 24]. This finding was particularly interesting given our previous observation that the OM localization of NlpD was important for its proper function, thus suggesting a potential link between NlpD activity and OM constriction. Accordingly, a strain lacking EnvC and all members of the Tol-Pal system (*ΔtolQ-pal ΔenvC*) displayed a cell separation defect closely resembling that of cells lacking both EnvC and functional NlpD ($^{\Delta SS}$*nlpD ΔenvC*). However, the severity of the chaining phenotype was alleviated when the *ΔtolQ-pal ΔenvC* strain was grown in minimal M9-maltose medium. This behavior is consistent with previous reports that although cells lacking an intact Tol-Pal system display a delayed invagination of the OM, the severity of this defect is dependent on the osmolarity and/or ionic strength of the medium [14, 15]. Therefore, one possibility for the medium-dependent chaining phenotype is that the OM invagination defect upon loss of the Tol-Pal complex is somehow alleviated in minimal M9-maltose medium.

Based on the genetic results above, we propose that the Tol-Pal system may indirectly regulate NlpD function to link OM invagination and septal PG remodeling (**Figure 4.9A**). In this model, NlpD in the OM is physically separated from the PG layer at the division site, thus holding the protein and its cognate amidase AmiC inactive. However, upon cytokinesis and constriction of the OM by the Tol-Pal system, NlpD is indirectly brought closer to the PG layer where it is activated by YraP, thus triggering AmiC-mediated septal PG splitting to allow cell separation. Consequently, in Tol$^-$ cells lacking an intact Tol-Pal complex, NlpD remains out of reach of the PG layer and therefore AmiC cannot act on septal PG (**Figure 4.9C**). Since the OM defects of Tol$^-$ cells are dependent on the growth medium, we observed that the defect in NlpD activation upon loss of the Tol-Pal system is also alleviated under similar growth conditions. Although this growth medium dependency suggests a more indirect regulation, we cannot rule out the possibility that NlpD may require a direct interaction with one or more members of the Tol-Pal system to activate it. Further experiments are therefore needed to assess whether NlpD directly interacts with candidate proteins within the Tol-Pal complex, namely TolB, Pal, or TolA, which are either in the OM or can potentially bridge the gap to the OM.

Although the “indirect activation” model by the Tol-Pal system is compelling, the localization dependency of NlpD raises some interesting questions about its molecular mechanism. We have determined that the recruitment of NlpD to the septal ring is independent of the Tol-Pal complex. From the structure-function analysis of NlpD (see Chapter 3), we found that NlpD localizes to the division site via its lysin motif (LysM)

domain, which is reported to be a PG-binding module [29-31]. If the midcell localization of NlpD is mediated by an interaction between its LysM domain and the PG layer, the fact that NlpD still localizes in cells lacking an intact Tol-Pal system suggests that the LysM-PG interaction is still intact. This direct interaction would supposedly place the dLytM domain of NlpD within close proximity of the PG layer even in the absence of the Tol-Pal system, which is inconsistent with the “indirect activation” model. However, this interpretation stems from a simplistic analysis of the primary sequence of NlpD. Therefore, we cannot rule out the possibility that the subdomains of NlpD may adopt a more complex arrangement *in vivo* that ultimately restricts the ability of the dLytM domain to access the PG layer.

In summary, we propose that OM constriction by the Tol-Pal system brings NlpD in close proximity to the septal PG layer, where it is activated by YraP to promote AmiC-mediated septal PG splitting. Our results therefore suggest that OM constriction and septal PG splitting may be coupled at multiple levels in order to ensure the coordinated constriction of all three cell envelope layers in *E. coli*. Follow-up experiments are needed to shed light on the molecular details of these regulatory mechanisms.

Acknowledgements

The authors would like to thank all members of the Bernhardt and Rudner laboratories for helpful comments and suggestions, particularly Chris Sham for reading this chapter and providing useful edits.

Section 4.5: Experimental procedures

Media, bacterial strains and plasmids

Cells were grown in LB (1% tryptone, 0.5% yeast extract, 0.5% NaCl) or minimal M9 medium [32] supplemented with 0.2% casamino acids and 0.2% maltose. Unless otherwise indicated, antibiotics were used at 10 (chloramphenicol; Cm), 25 (kanamycin; Kan), 10 (tetracycline; Tet), 50 (ampicillin, Amp), or 50 (spectinomycin, Spec) μg/ml.

The bacterial strains used in this study are listed in **Table 4.1**. All *E. coli* strains used in the reported experiments are derivatives of MG1655 [33]. All deletion alleles were either sourced from the Keio knockout collection [34] or constructed to resemble those in the collection. Plasmids used in this study are listed in **Table 4.2**. All plasmids used for *in vivo* experiments are derivatives of CRIM plasmids [35] and were integrated into phage attachment sites (HK022 or λ) using the helper plasmids pTB102 [36] or pINT-ts [35] respectively as described [35]. PCR was performed using either KOD polymerase (Novagen) or Q5 polymerase (NEB) according to the manufacturer's instructions. Unless otherwise indicated, MG1655 chromosomal DNA was used as the template. Plasmid DNA and PCR fragments were purified using the Zyppy plasmid miniprep kit (Zymo Research) or the Qiaquick PCR purification kit (Qiagen) respectively. Sequencing reactions were carried out with an ABI3730xl DNA analyzer at the DNA Resource Core of Dana-Farber/Harvard Cancer Center (funded in part by NCI Cancer Center support grant 2P30CA006516-48).

Table 4.1. Strains used in this study

Strain	Genotype[a]	Source/Reference[b]
DH5α	*F– hsdR17 deoR recA1 endA1 phoA supE44 thi-1 gyrA96 relA1 Δ(lacZYA-argF)U169 ϕ80dlacZΔM15*	Gibco BRL
BW25113	*Δ(araD-araB)567 ΔlacZ4787(::rrnB-3) rph-1 Δ(rhaD-rhaB)568 hsdR514*	[34]
JW1667	BW25113 *Δlpp::kan^R*	[34]
MG1655	*rph-1 ilvG rfb-50*	[33]
TB10	MG1655 *λΔcro-bio nad::Tn10*	[37]
TB28	MG1655 *ΔlacIZYA*::*frt*	[38]
MT46	TB28 *$^{\Delta SS}$nlpD::kan^R*	P1(λRed) x TB28
MT47	TB28 *$^{\Delta SS}$nlpD::frt*	MT46/pCP20
MT50	TB28 *$^{\Delta SS}$nlpD::frt ΔenvC::kan^R*	P1(TB134) x MT47
MT51	TB28 *ΔtolQ-pal::kan^R*	P1(λRed) x TB28
MT53	TB28 *$^{\Delta SS}$nlpD::frt ΔtolQ-pal::kan^R*	P1(λRed) x MT47
MT55	TB28 *ΔenvC::frt ΔtolQ-pal::kan^R*	P1(λRed) x TB140
MT83	TB28 *ΔenvC::frt Δlpp::kan^R*	P1(JW1667) x TB140
MT121	MG1655 *$^{\Delta SS}$nlpD::kan^R*	P1(MT46) x MG1655
MT122	MG1655 *$^{\Delta SS}$nlpD::frt*	MT121/pCP20
MT123	MG1655 *$^{\Delta SS}$nlpD::frt ΔamiC::kan^R*	P1(TB137) x MT122
MT129	TB10 *ΔyraP::kan^R*	λRed
MT135	TB28 *ΔenvC::frt ΔyraP::kan^R*	P1(MT129) x TB140
MT140	TB28 *ΔyraP::kan^R*	P1(MT129) x TB28
MT141	TB28 *$^{\Delta SS}$nlpD::frt ΔyraP::kan^R*	P1(MT129) x MT47
MT144	TB28 *ΔamiA::frt ΔamiB::frt ΔyraP::kan^R*	P1(MT129) x TU207
TB134	TB28 *ΔenvC::kan^R*	[8]
TB137	TB28 *ΔamiC::kan^R*	[8]

Table 4.1 (Continued).

Strain	Genotype[a]	Source/Reference[b]
TB140	TB28 *ΔenvC::frt*	[8]
TU163	TB28 *Δlpp::kan^R*	[8]
TU207	TB28 *ΔamiA::frt ΔamiB::frt*	[9]

[a] The Kan^R cassette is flanked by *frt* sites for removal by FLP recombinase. An *frt* scar remains following removal of the cassette using FLP recombinase expressed from pCP20.

[b] Strain constructions by P1 transduction are described using the shorthand: P1(donor) x recipient. Transductants were selected on LB Kan, LB Cm, or LB Tet plates where appropriate. λRed indicates strains constructed by recombineering (see Experimental Procedures for details). Strains resulting from the removal of a drug resistance cassette using pCP20 are indicated as: Parental strain/pCP20.

Table 4.2. Plasmids used in this study

Plasmid	Genotype[a]	Origin	Source or Reference
pCP20	*bla cat cI857(ts) repA(ts)* P$_{\lambda R}$*::flp*	pSC101	[39]
pINT-ts	*bla repA(ts) cI857(ts)* P$_{\lambda R}$*::int(λ)*	R6K	[35]
pKD46	*bla repA101(ts) araC* P$_{ara}$*::γ-β-exo*	pSC101	[39]
pMT12	*att*HK022 *tetA tetR lacI* P$_{lac}$*::nlpD$^{(S27D)}$*	R6K	This study
pMT20	*att*HK022 *tetA tetR lacI* P$_{lac}$*::nlpD$^{(1-379)}$*	R6K	This study
pMT21	*att*HK022 *tetA tetR lacI* P$_{lac}$*::nlpD $^{(S27D)}$-mCherry*	R6K	This study
pMT94	*cat lacI* P$_{lac}$*::nativeRBS_ybgC_tolQRA*	pACYC/p15A	This study
pMT121	*att*HK022 *tetA tetR lacI* P$_{lac}$*::^{ss}dsbA-nlpD$^{(27-379)}$*	R6K	This study
pMT147	*att*HK022 *tetA tetR lacI* P$_{lac}$*::^{ss}dsbA-nlpD$^{(27-379)}$-mCherry*	R6K	This study

Table 4.2 (Continued).

Plasmid	Genotype[a]	Origin	Source or Reference
pMT149	*att*HK022 *tetA tetR lacI* P_{lac}*::nlpD*$^{(1-30)}$*-mCherry*	R6K	This study
pMT187	*aadA repA(ts)* P_{lac}*::envC-LE* SceI *cI857(ts)* $P_{\lambda R}$*::i-sceI*	pSC101	This study
pMT196	*attλ cat lacI* P_{lac}*::yraP*$^{(1-191)}$	R6K	This study
pMT197	*attλ cat lacI* P_{lac}*::yraP*$^{(1-191)}$*-mCherry*	R6K	This study
pMT198	*attλ cat lacI* P_{lac}*::yraP*$^{(VA-20,21-DE)}$	R6K	This study
pMT199	*attλ cat lacI* P_{lac}*::yraP*$^{(VA-20,21-DE)}$*-mCherry*	R6K	This study
pNP20	*att*HK022 *tetA tetR lacI*^{q} P_{lac}*::nlpD*$^{(1-379)}$*-mCherry*	R6K	[40]
pTB102	*cat repA(ts) cI857(ts)* $P_{\lambda R}$*::int(HK022)*	pSC101	[36]

[a] $P_{\lambda R}$, P_{ara}, and P_{lac} indicate the λR, arabinose, and lactose promoters respectively. *flp* encodes for FLP recombinase. ^{ss}*dsbA* corresponds to the first 24 codons of *dsbA* encoding its export signal to the periplasm. SceI indicates the presence of a substrate site for the I-SceI endonuclease.

Recombineering

The *ΔtolQ-pal::kan*^{R} allele was constructed by replacing the region between the 2nd codon of *tolQ* and the 7th codon from the stop codon of *pal* with the *kan*^{R} cassette by λ recombineering as described previously [34, 41]. The *kan*^{R} cassette was amplified from pKD13 [39] using the primers 5'-GTGCGCTTCCCAAGTCTATTGTCGCGGAGTTTAAGCAGTGATTCCGGGGATCCGTCGACC-3' and 5'-TACTGCTCATGCAATTCTCTTAGTAAACCAGTACCGCACGTGTAGGCTGGAGCTGCTTCG-3'. The resulting PCR product was purified and electroporated into strain TB28/

pKD46 as described previously [38] and the recombinants were selected at 30°C on LB Kan to generate the chromosomal deletion.

The *ΔyraP::kan*^{R} allele was constructed by replacing the region between the 2nd codon and the 7th codon from the stop codon of *yraP* with the *kan*^{R} cassette as described above. The *kan*^{R} cassette was amplified from pKD13 using the primers 5'-GTGCGCTTCCCAAGTCTATTGTCGCGGAGTTTAAGCAGTGATTCCGGGGATCCGTCGACC-3' and 5'-TACTGCTCATGCAATTCTCTTAGTAAACCAGTACCGCACGTGTAGGCTGGAGCTGCTTCG-3'. The resulting fragment was electroporated into strain TB10 and the recombinants were selected at 30°C on LB Kan to generate the chromosomal deletion as described previously [37].

The *ΔtolQ-pal::kan*^{R} and *ΔyraP::kan*^{R} alleles were transferred between strains by P1 transduction. The P1 lysate for *ΔtolQ-pal::kan*^{R} was made on a strain with *ΔtolQ-pal::kan*^{R} and carrying pMT94 (P_{lac}*::nativeRBS_ybgC_tolQRA)* to express the TolQRA genes. If necessary, the Kan^R cassette was removed using FLP recombinase expressed from pCP20 [39].

Plasmolysis

Overnight cultures were backdiluted in minimal M9 medium supplemented with 0.2% maltose and the appropriate concentration of IPTG and grown at 30°C (see figure legend for specific IPTG concentration and the final OD_{600} of the cultures). Cells were harvested by centrifugation, washed in M9-maltose once, resuspended in plasmolysis

buffer (15% sucrose, 25mM HEPES, pH 7.5, 20mM sodium azide), and imaged on 1% agarose pads containing 15% sucrose using phase contrast and mCherry optics as described below.

Microscopy

Cells were images on 2% agarose pads, unless stated otherwise, using a Nikon TE2000 inverted microscope outfitted with a Nikon Intensilight illuminator, a Coolsnap HQ2 CCD camera from Photometrics, a Nikon CFI Plan Apo VC 100x objective (1.4 NA) for differential interference contrast (DIC) imaging or a CFI Plan Apo DM 100x objective (1.4 NA) for phase contrast imaging. Please see figure legends for details about growth conditions used for specific experiments. Filter cubes for fluorescence image acquisition were from Chroma. mCherry fluorescence images were taken using the ET-mCherry filter set (Chroma 49008). Images were captured using Nikon Elements software, exported, and cropped for figure preparation in MetaMorph (Molecular Devices).

Immunoblotting

Strains were grown as described in the figure legends. At the designated times, cells were harvested and whole-cell extracts were prepared as described previously [42]. The protein concentration of each extract was determined using the non-interfering protein assay (Genotech) according to the manufacturer's instructions. Protein concentrations were normalized between extracts and the indicated amount of total protein from each extract was separated on a 4-20% Mini-PROTEAN® TGX™ precast protein gel (BioRad). Proteins were transferred to a PVDF membrane (Whatman) and

the membrane was blocked with 2% skim milk in TBS-T (10mM Tris HCl, pH 7.5, 100mM NaCl, 0.1% Tween 20) for 1 hour at room temperature. The membrane was incubated with affinity-purified anti-NlpD antibodies diluted 1:10,000 in TBS-T with 0.2% skim milk overnight at 4°C. The next day, the primary antibody solution was removed and the membrane was quickly rinsed with TBS-T and then thoroughly washed three times with TBS-T for 5-10 minutes each wash. Following the final wash, the membrane was incubated with the secondary goat anti-rabbit antibodies conjugated to horseradish peroxidase (Rockland) diluted 1:40,000 in TBS-T with 0.2% skim milk for 1 hour with gentle agitation at room temperature. After this incubation period, the secondary antibody solution was discarded and the membrane was again quickly rinsed with TBS-T and then thoroughly washed an additional four times with TBS-T for 5-10 minutes each. The blot was developed using the Super Signal West Pico system (Pierce) according to the manufacturer's protocol. Chemiluminescence was detected using a BioRad Chemidoc system.

Making transposon library in *ΔenvC*

It was difficult to make a good size transposon library using *ΔenvC* cells. Instead, a depletion strain, TB140/pMT187 [*ΔenvC/Plac::envC-LE*], was mutagenized with the Ez-Tn5 <Kan-2> transposome (Epicentre) as previous described [38]. Mutants were selected at 37°C on minimal M9 medium containing 50μg/ml kanamycin, yielding a library of ~ 50,000 independent transposon insertions. Growth at 37°C resulted in the loss of the pMT187 plasmid (through the combined effects of its temperature-sensitive

origin of replication and cleavage by I-Sce-I [22]), rendering the strain *ΔenvC.* The mutant library was pooled as a slurry and aliquots stored frozen at -80°C.

Flow cytometry and sorting

For the control strains (TB140 (*ΔenvC*) and MT50 ($^{\Delta SS}$*nlpD ΔenvC*)), overnight cultures were diluted in LB and grown at 30°C to an OD_{600} of 0.2 - 0.3. For the transposon mutagenized *ΔenvC* library, a frozen aliquot was thawed, back-diluted twice in LB and grown at 30°C to an OD_{600} of ~ 0.3. The cells were then harvested by a low spin centrifugation (1,000 x g for 1-2 min), resuspended in PBS (137 mM NaCl, 10 mM Na_2HPO_4, 1.8 mM KH_2PO_4, 2.7 mM KCl, pH 7.4) to an OD_{600} ~ 0.1 - 0.2 and filtered through a 70µm filter (Corning) before analysis and sorting. Flow cytometry analysis and sorting was carried out on the MoFlo Astrios EQ (Beckman Coulter) at the Division of Immunology's Flow Cytometry Facility at Harvard Medical School. Cell resuspensions were analyzed and sorted with a 100µm nozzle. Gates for sorting were defined on a side scatter pulse height (SSC-H; y-axis) versus side scatter pulse width (SSC-W; x-axis) dot plot.

Sorted cells were plated on minimal M9-maltose plates and incubated at 37°C overnight. Mucoid colonies were purified on LB, the chaining phenotype confirmed by phase contrast microscopy, and the sites of the transposon insertions were identified by arbitrarily primed PCR followed by sequencing [38].

Section 4.6: References

1. Höltje, J. V. (1998). Growth of the stress-bearing and shape-maintaining murein sacculus of Escherichia coli. Microbiol Mol Biol Rev *62*, 181–203.

2. de Boer, P. A. (2010). Advances in understanding E. coli cell fission. Current Opin Microbiol *13*, 730–737.

3. Höltje, J. V. (1995). From growth to autolysis: the murein hydrolases in Escherichia coli. Arch Microbiol *164*, 243–254.

4. Uehara, T., and Bernhardt, T. G. (2011). More than just lysins: peptidoglycan hydrolases tailor the cell wall. Curr Opin Microbiol *14*, 698–703.

5. Heidrich, C., Templin, M. F., Ursinus, A., Merdanovic, M., Berger, J., Schwarz, H., de Pedro, M. A., and Höltje, J. V. (2001). Involvement of N-acetylmuramyl-L-alanine amidases in cell separation and antibiotic-induced autolysis of Escherichia coli. Mol Microbiol *41*, 167–178.

6. Priyadarshini, R., de Pedro, M. A., and Young, K. D. (2007). Role of peptidoglycan amidases in the development and morphology of the division septum in Escherichia coli. J Bacteriol *189*, 5334–5347.

7. Yang, D. C., Tan, K., Joachimiak, A., and Bernhardt, T. G. (2012). A conformational switch controls cell wall-remodelling enzymes required for bacterial cell division. Mol Microbiol *85*, 768–781.

8. Uehara, T., Dinh, T., and Bernhardt, T. G. (2009). LytM-domain factors are required for daughter cell separation and rapid ampicillin-induced lysis in Escherichia coli. J Bacteriol *191*, 5094–5107.

9. Uehara, T., Parzych, K. R., Dinh, T., and Bernhardt, T. G. (2010). Daughter cell separation is controlled by cytokinetic ring-activated cell wall hydrolysis. EMBO J *29*, 1412–1422.

10. Peters, N. T., Morlot, C., Yang, D. C., Uehara, T., Vernet, T., and Bernhardt, T. G. (2013). Structure-function analysis of the LytM domain of EnvC, an activator of cell wall remodelling at the Escherichia coli division site. Mol Microbiol *89*, 690–701.

11. Yang, D. C., Peters, N. T., Parzych, K. R., Uehara, T., Markovski, M., and Bernhardt, T. G. (2011). An ATP-binding cassette transporter-like complex governs cell-wall hydrolysis at the bacterial cytokinetic ring. Proc Natl Acad Sci USA *108*, E1052–60.

12. Rothfield, L. I., and Justice, S. S. (1997). Bacterial cell division: the cycle of the ring. Cell *88*, 581–584.

13. Hiemstra, H., Nanninga, N., Woldringh, C. L., Inouye, M., and Witholt, B. (1987). Distribution of newly synthesized lipoprotein over the outer membrane and the peptidoglycan sacculus of an Escherichia coli lac-lpp strain. J Bacteriol *169*, 5434–5444.

14. Gerding, M. A., Ogata, Y., Pecora, N. D., Niki, H., and de Boer, P. A. J. (2007). The trans-envelope Tol-Pal complex is part of the cell division machinery and required for proper outer-membrane invagination during cell constriction in E. coli. Mol Microbiol *63*, 1008–1025.

15. Meury, J., and Devilliers, G. (1999). Impairment of cell division in tolA mutants of Escherichia coli at low and high medium osmolarities. Biol. Cell *91*, 67–75.

16. Seydel, A., Gounon, P., and Pugsley, A. P. (1999). Testing the “+2 rule” for lipoprotein sorting in the Escherichia coli cell envelope with a new genetic selection. Mol Microbiol *34*, 810–821.

17. Lewenza, S., Vidal-Ingigliardi, D., and Pugsley, A. P. (2006). Direct visualization of red fluorescent lipoproteins indicates conservation of the membrane sorting rules in the family Enterobacteriaceae. J Bacteriol *188*, 3516–3524.

18. Lange, R., and Hengge-Aronis, R. (1994). The nlpD gene is located in an operon with rpoS on the Escherichia coli chromosome and encodes a novel lipoprotein with a potential function in cell wall formation. Mol Microbiol *13*, 733–743.

19. Battesti, A., Majdalani, N., and Gottesman, S. (2011). The RpoS-Mediated General Stress Response in Escherichia coli. Annu Rev Microbiol *65*, 189–213.

20. Paradis-Bleau, C., Kritikos, G., Orlova, K., Typas, A., and Bernhardt, T. G. (2014). A Genome-Wide Screen for Bacterial Envelope Biogenesis Mutants Identifies a Novel Factor Involved in Cell Wall Precursor Metabolism. PLoS Genet *10*, e1004056.

21. Burke, C., Liu, M., Britton, W., Triccas, J. A., Thomas, T., Smith, A. L., Allen, S., Salomon, R., and Harry, E. (2013). Harnessing single cell sorting to identify cell division genes and regulators in bacteria. PLoS ONE *8*, e60964.

22. Liu, B., Persons, L., Lee, L., and de Boer, P. A. J. (2015). Roles for both FtsA and the FtsBLQ subcomplex in FtsN-stimulated cell constriction in Escherichia coli. Mol Microbiol *95*, 945–970.

23. Webster, R. E. (1991). The tol gene products and the import of macromolecules into Escherichia coli. Mol Microbiol *5*, 1005–1011.

24. Lazzaroni, J. C., Germon, P., Ray, M. C., and Vianney, A. (1999). The Tol proteins of Escherichia coli and their involvement in the uptake of biomolecules and outer membrane stability. FEMS Microbiol Lett *177*, 191–197.

25. Onufryk, C., Crouch, M. L., Fang, F. C., and Gross, C. A. (2005). Characterization of Six Lipoproteins in the sigmaE Regulon. J Bacteriol *187*, 4552–4561.

26. Suzuki, H., Nishimura, Y., Yasuda, S., Nishimura, A., Yamada, M., and Hirota, Y. (1978). Murein-lipoprotein of Escherichia coli: a protein involved in the stabilization of bacterial cell envelope. Mol Gen Genet *167*, 1–9.

27. Yem, D. W., and Wu, H. C. (1978). Physiological characterization of an Escherichia coli mutant altered in the structure of murein lipoprotein. J Bacteriol *133*, 1419–1426.

28. Yeats, C., and Bateman, A. (2003). The BON domain: a putative membrane-binding domain. Trends Biochem Sci *28*, 352–355.

29. Bateman, A., and Bycroft, M. (2000). The structure of a LysM domain from E. coli membrane-bound lytic murein transglycosylase D (MltD). J Mol Biol *299*, 1113–1119.

30. Buist, G., Steen, A., Kok, J., and Kuipers, O. P. (2008). LysM, a widely distributed protein motif for binding to (peptido)glycans. Mol Microbiol *68*, 838–847.

31. Mesnage, S., Dellarole, M., Baxter, N. J., Rouget, J.-B., Dimitrov, J. D., Wang, N., Fujimoto, Y., Hounslow, A. M., Lacroix-Desmazes, S., Fukase, K., et al. (2014). Molecular basis for bacterial peptidoglycan recognition by LysM domains. Nat Commun *5*, 4269.

32. Miller, J. H. (1972). Experiments in molecular genetics. (Cold Spring Harbor Laboratory Press).

33. Guyer, M. S., Reed, R. R., Steitz, J. A., and Low, K. B. (1981). Identification of a sex-factor-affinity site in E. coli as gamma delta. Cold Spring Harb Symp Quant Biol *45 Pt 1*, 135–140.

34. Baba, T., Ara, T., Hasegawa, M., Takai, Y., Okumura, Y., Baba, M., Datsenko, K. A., Tomita, M., Wanner, B. L., and Mori, H. (2006). Construction of Escherichia coli K-12 in-frame, single-gene knockout mutants: the Keio collection. Mol Syst Biol *2*, 2006.0008.

35. Haldimann, A., and Wanner, B. L. (2001). Conditional-replication, integration, excision, and retrieval plasmid-host systems for gene structure-function studies of bacteria. J Bacteriol *183*, 6384–6393.

36. Bernhardt, T. G., and de Boer, P. A. J. (2005). SlmA, a nucleoid-associated, FtsZ binding protein required for blocking septal ring assembly over Chromosomes in E. coli. Mol Cell *18*, 555–564.

37. Johnson, J. E., Lackner, L. L., Hale, C. A., and de Boer, P. A. J. (2004). ZipA is required for targeting of DMinC/DicB, but not DMinC/MinD, complexes to septal ring assemblies in Escherichia coli. J Bacteriol *186*, 2418–2429.

38. Bernhardt, T. G., and de Boer, P. A. J. (2004). Screening for synthetic lethal mutants in Escherichia coli and identification of EnvC (YibP) as a periplasmic septal ring factor with murein hydrolase activity. Mol Microbiol *52*, 1255–1269.

39. Datsenko, K. A., and Wanner, B. L. (2000). One-step inactivation of chromosomal genes in Escherichia coli K-12 using PCR products. Proc Natl Acad Sci USA *97*, 6640–6645.

40. Peters, N. T., Dinh, T., and Bernhardt, T. G. (2011). A fail-safe mechanism in the septal ring assembly pathway generated by the sequential recruitment of cell separation amidases and their activators. J Bacteriol *193*, 4973–4983.

41. Yu, D., Ellis, H. M., Lee, E. C., Jenkins, N. A., Copeland, N. G., and Court, D. L. (2000). An efficient recombination system for chromosome engineering in Escherichia coli. Proc Natl Acad Sci USA *97*, 5978–5983.

42. Hale, C. A., and de Boer, P. A. (1999). Recruitment of ZipA to the septal ring of Escherichia coli is dependent on FtsZ and independent of FtsA. J Bacteriol *181*, 167–176.

Chapter 5: Discussion

Chapter 5: Discussion

Sections of this chapter have been published [1]; adapted and reprinted with permission from Elsevier Publishing and the journal *Current Opinion in Microbiology*.

Section 5.1: Summary of results

Bacterial cell division is a complex process carried out by a ring-shaped, multi-protein complex known as the divisome or septal ring. This cytokinetic apparatus is initially formed by the polymerization of the tubulin-like FtsZ protein into the so-called Z-ring at midcell. In *E. coli*, the division machine ensures the coordinated constriction of both the inner and outer cell membranes as well as the synthesis and remodeling of the so-called septal peptidoglycan (PG) cell wall layer located between them, ultimately leading to the formation of the new daughter cell poles [2]. Over the years, dozens of proteins, both essential and non-essential, have been localized to this apparatus [3-5]. However, major questions remain about the molecular function of these factors and the mechanisms that ensure the coordination of the activities of this complex machine.

Once the divisome is assembled and in position, cell constriction can begin. However, the triggering event that initiates the constriction process remains largely unclear. I gained new insights into the controls governing constriction initiation through the study of a previously reported lytic allele of *ftsL* that has a phenotype indicative of defects occurring post-initiation of constriction. In fact, using both genetics and microscopy, I determined that this *ftsL** mutation induced a divisome malfunction that

accelerated the division process by prematurely initiating cell constriction. Further genetic analyses revealed a link between FtsL and two division proteins previously implicated in constriction initiation, the Z-ring associated protein FtsA and FtsN, the last essential protein recruited to the divisome in the dependency pathway. Therefore, I propose a role for these proteins as part of a signaling system that “senses” divisome assembly and initiates cell constriction upon its completion (**Figure 5.1**).

In this model, FtsA is the “sensor” and exists in an OFF or ON state, depending on the state of divisome assembly. The recruitment of downstream divisome components, such as FtsN, progressively converts FtsA to the ON state until a threshold level of this altered form of FtsA is achieved (**Figure 5.1**, step 1). This transition of FtsA may involve a change in its polymerization state via a direct interaction with the cytoplasmic N-terminal tail of FtsN (^{N}FtsN) [6-9]. The ON conformation of FtsA may then promote an altered, more stable, form of the Z-ring as well as directly or indirectly signal its altered status to the FtsQLB complex (**Figure 5.1**, step 2). Within the septal ring, the small, membrane-proximal, essential domain of FtsN (^{E}FtsN) is likely to communicate the status of divisome assembly directly to the FtsQLB complex (**Figure 5.1**, step 3) or stimulate the synthesis of septal PG by activating the septal PG biogenesis machinery directly in a manner that is redundant with FtsQLB activity. The input from upstream signals received by FtsQLB is likely to cause a conformational change in this complex that is, in turn, communicated to the PG synthetic apparatus to stimulate septal PG synthesis (**Figure 5.1**, step 4). This new cell wall material is subsequently remodeled by the amidases during cell constriction (**Figure 5.1**, step 5). The denuded glycan strands

produced by the amidases then serve as the recruitment signal for the C-terminal, PG-binding SPOR domain of FtsN (^{S}FtsN) [10] (**Figure 5.1**, step 6). This in turn brings more ^{E}FtsN to the division site to stimulate more cell wall synthesis and remodeling, thus reinforcing the entire process.

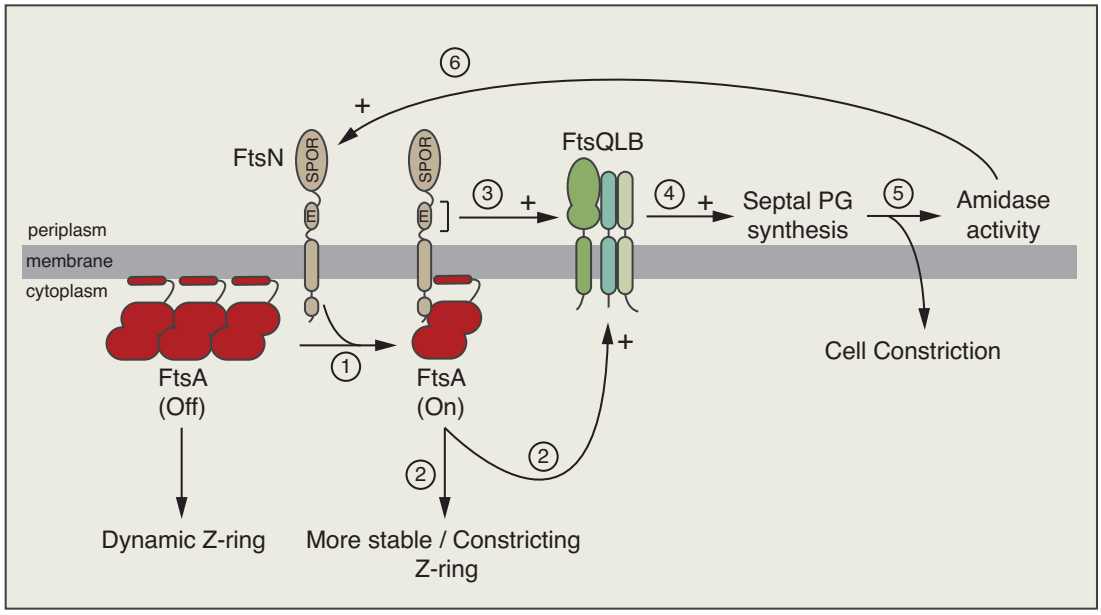

Figure 5.1. A potential signaling system controlling the conversion of the divisome from a state of assembly to one of active constriction. Shown is an illustration highlighting the major features of a sensing mechanism that governs constriction initiation. The recruitment of downstream divisome proteins such as FtsN converts FtsA to an ON state (step 1), which promotes a more stable form of the Z-ring as well as signal to the FtsQLB complex (step 2). In addition, the essential domain of FtsN may directly signal to the FtsQLB complex (step 3) to ultimately stimulate septal PG synthesis (step 4) and remodeling by the amidases to promote cell constriction (step 5). This signaling pathway may be reinforced by a positive feedback loop involving FtsN recruitment via its PG-binding SPOR domain (step 6). See text for more details.

During active cell constriction, an important role of the divisome is to synthesize and remodel the septal PG layer to shape the new cell poles and allow cell separation. Septal PG splitting involves two sets of periplasmic proteins, the amidases (AmiA, AmiB, and AmiC) that possess PG hydrolytic activity [11, 12], and the LytM factors (EnvC and NlpD) that activate them [13-15]. Although recent studies have uncovered details about the function and regulation of EnvC [15, 16], the OM lipoprotein NlpD has been poorly characterized. In order to gain molecular insight into its activity, I performed a structure-function analysis of NlpD. I determined that the LysM domain of NlpD is necessary and sufficient for its recruitment to the septal ring, potentially via a direct interaction with PG. On the other hand, the degenerate LytM (dLytM) domain required for NlpD function is not sufficient for proper cell separation. In fact, the expression of soluble truncated variants of NlpD containing only the dLytM domain led to increased cell lysis, possibly due to aberrant activation of the amidases throughout the cell. Interestingly, in cells lacking the other amidase activator EnvC, this mislocalized amidase activity likely led to the delocalization of FtsN, which binds the denuded glycan strands produced by the amidases. Ultimately, this resulted in Z-ring instability, division inhibition, and cell filamentation. Given these results, I hypothesize that septal PG processing by the amidases influences the stability and positioning of the Z-ring. I propose a model in which, through its interaction with FtsA, FtsN anchors the Z-ring to the denuded glycan strands present within the PG meshwork at the division site, thus marking and reinforcing the position where the Z-ring is first stabilized.

In gram-negative bacteria like *E. coli*, cytokinesis requires the efficient splitting of the septal PG layer to allow the outer membrane (OM) to invaginate in step with the inner membrane (IM). Such a coordinated task may involve coupling between OM constriction and septal PG remodeling by the amidases. By virtue of its localization within the OM, the amidase activator NlpD is perfectly positioned to couple these two important processes. In fact, by studying NlpD variants with altered subcellular localization, I determined that the OM localization of NlpD is required for proper and efficient activation of its cognate amidase AmiC. I also hypothesized that NlpD may be regulated by other component(s) of the divisome to coordinate its activity with additional functions of the division machine. In order to identify these potential regulators, I used flow cytometry-based cell sorting to isolate transposon insertions that displayed a similar chaining phenotype as an *nlpD* null mutation when combined with *ΔenvC*. Such chaining phenotype would be expected upon loss of a gene required for NlpD activity *in vivo*. From the screen, I identified the Tol-Pal system and YraP as potential regulators of NlpD. Based on these genetic results, I propose a model in which OM constriction by the Tol-Pal system at the division site indirectly "activates" NlpD by bringing it closer to the PG layer where it is activated by YraP to promote AmiC-mediated septal PG splitting.

Section 5.2: Future directions

We are just beginning to uncover new molecular details about the mechanisms that ensure proper coordination of the many activities of the division machine in *E. coli*.

My work has provided some insights in the process but has also raised additional questions, especially concerning the controls governing constriction initiation and the role and regulation of septal PG remodeling. This section will discuss these emerging questions as well as other unanswered questions in the field and propose potential ways to address them.

What is the ON state of FtsA and how does it affect the Z-ring dynamics?

One hypothesis regarding the event that triggers constriction is that FtsA serves as a "sensor" of divisome assembly, and therefore exists in an OFF or ON state. A recent study of hyperactive *ftsA* mutants that bypass the requirement for ZipA suggests that this conformational change may be related to the polymeric status of FtsA, with the polymeric form being inhibitory (OFF) and the monomeric or reduced polymeric form being stimulatory for division (ON) [8]. However, whether the ON state of FtsA merely relies on reduced polymerization or whether it involves other conformational changes is still unclear. Interestingly, an FtsA(E124A) derivative that bypasses the requirement for FtsN and may therefore exist in the ON state did not show any qualitative difference in self-interaction compared to the wild-type protein [8, 17]. This suggests that the mutation may instead induce a structural change or lead to increased affinity for another divisome component. Structural analysis of FtsA variants suspected to be preferentially in the ON conformation may shed light on the role of FtsA in the control of cell constriction.

Another interesting question concerns the effect of FtsA on Z-ring dynamics. A recent study of FtsZ polymer dynamics on supported lipid bilayers showed that polymers brought to the membrane by FtsA were highly dynamic, suggesting that FtsA destabilizes the FtsZ polymer network [18]. Therefore, an attractive possibility is that FtsA in the OFF state may, at least initially, promote the formation of a more dynamic, less stable Z-ring at midcell. Indeed, *in vivo* results indicate that the FtsA/FtsZ ratio is important for proper division and an excess of FtsA may inhibit Z-ring formation [19, 20]. As the divisome is assembled and the downstream divisome components, such as FtsN, are recruited, we postulate that FtsA is converted to a reduced polymeric ON state, which may change the effect of FtsA on FtsZ polymer dynamics such that it now stabilizes the Z-ring structure and promotes cell constriction. In support of this hypothesis, the self-interaction-defective FtsA(R286W) derivative has been shown to alter the Z-ring thus reducing its sensitivity to negative regulators [21]. However, this variant of FtsA did not alter FtsZ polymer dynamics in the supported lipid bilayer experiments [18], suggesting that other factors, in addition to changes in FtsA self-association status, may contribute to the effect of FtsA in the ON conformation. A possible candidate is FtsN since its N-terminal region is known to interact with FtsA [6]. It would, therefore, be interesting to determine how FtsZ polymer dynamics change in the presence of both FtsA and the N-terminal part of FtsN. If the polymers become more stable under those conditions, it would suggest that FtsA indeed stabilizes the Z-ring when in the ON state and that the ON state might involve more than a change in polymerization status.

How are the input signals communicated to FtsQLB to induce a possible conformational change?

In my proposed model of constriction initiation, FtsA acts as a sensor of divisome assembly, and the accumulation of a threshold level of its ON form directly or indirectly signals to the FtsQLB complex to ultimately trigger cytokinesis. How FtsA communicates with the FtsQLB complex is not well understood. One possibility involves a direct protein-protein interaction between FtsA and the cytoplasmic domain of one or more member(s) of the FtsQLB complex. FtsB has only a short 3-amino-acid cytoplasmic domain so it is not a likely candidate [22]. Of the other two proteins, the cytoplasmic N-terminal region of FtsQ is dispensable, but that of FtsL is required for function [23-25], suggesting that it may be important for an interaction with FtsA. However, positive interaction between FtsA and FtsL is not detected by bacterial two-hybrid assay [26]. If FtsA primarily exists in the OFF form in that system, it would not be expected to signal to or interact with FtsL, so it would be worth revisiting the bacterial two-hybrid assay using variants of FtsA that are suspected to be preferentially in the ON state. Alternatively, the ON form of FtsA may indirectly signal to FtsQLB via effects on the Z-ring.

According to the model, upon receiving input from upstream signals, the FtsQLB complex undergoes a conformational change (from OFF to ON) that stimulates cell wall synthesis and remodeling. However, the details of this proposed structural change, as well as the protein partners involved, are unclear. The FtsL* variant studied in Chapter 2

is thought to promote a spontaneous conversion to the ON conformation of the FtsQLB complex such that it prematurely stimulates cell constriction. This *ftsL** mutation replaces a negatively-charged glutamate with a positively-charged lysine. Other similar substitutions in FtsL and FtsB, from charged residues to ones with no or opposite charge, also appear to initiate cytokinesis prematurely [27], indicating that these electrostatic interactions may be critical either in the maintenance of the OFF conformation of the FtsQLB complex or in the transition to the ON conformation. Therefore, the FtsL* variant may aberrantly interact with its protein partner such that it stimulates septal PG biogenesis and cell constriction before the division machine is capable of safely initiating the process, thus rendering cells sensitive to low osmolarity and temperature extremes. If that is the case, compensatory mutations within the protein partner may restore the normal protein-protein interaction. These mutations would therefore suppress the division defect and lethality under non-permissive growth conditions. In addition, allele-specific suppression would indicate direct interaction between FtsL and the partner protein. Some interaction partners of FtsL that may be tested are individual members of the FtsQLB complex and of the septal PG biogenesis machinery (FtsI and FtsW) for which evidence of a possible interaction exists [25, 26, 28, 29].

Why is divisome assembly a two-step process in *E. coli*?

Studies of the temporal sequence of protein recruitment to the divisome have shown that the assembly is likely to be a two-step process. In *E. coli*, the components of

the Z-ring (FtsZ, FtsA, and ZipA) assemble early and persist for about 20% of the cell cycle prior to the near simultaneous localization of the remaining “late” divisome components at about the time when the first signs of cell constriction become apparent [30]. However, studies reporting a reduced frequency of Z-rings in mutants defective in some late divisome proteins suggest that these downstream proteins may be important within the nascent divisome at stages preceding detection of their localization at midcell [31-34]. My model for constriction initiation provides possible clues to resolve this discrepancy. I propose that the entire signaling system is likely to be self-enhancing and intimately connected with the recruitment of the relevant late divisome components. Following Z-ring formation, only a few molecules of each factor may be recruited to midcell to initiate the cycle, and the resulting low protein abundance may be below the detection limit of wide-field microscopy. However, the activity of these molecules is expected to be rapidly amplified via the positive feedback loop of FtsN recruitment [10], thus attracting additional components and stimulating a sustained and visible constriction of the cell envelope. Such a possibility may, therefore, explain the observed two-step divisome assembly process and the near simultaneous arrival of the late proteins coincident with the onset of constriction.

What role does amidase activity play in Z-ring stability and positioning during cytokinesis?

In Chapter 3, I implicate FtsN as the Z-ring anchor in a putative mechanism that marks the position where the Z-ring first forms such that constriction occurs at this

specific site via a single septal ring. I also present the attractive possibility that denuded glycan strands produced by amidase activity act as the positional signal since this form of PG is specifically enriched at the division site and is likely produced upon constriction initiation [10, 27, 35, 36]. This model predicts that the absence of either the positional signal or the protein anchor might lead to increased levels of misplaced Z-rings. Although this increase in Z-ring mislocalization may not be lethal, it could result in the formation of double or multiple Z-rings in close proximity to each other. One approach to assess the contribution of the putative positional signal is to determine the frequency of double Z-rings in cells either partially or completely devoid of amidase activity. Similarly, the potential role of FtsN in divisome positioning can be addressed by determining Z-ring localization in cells expressing FtsN variants that lack either the PG-binding module (^{S}FtsN) or the FtsA-interacting domain (^{N}FtsN). Such strains are reported to be viable [10], but may require the overexpression of the respective FtsN truncations. Together, these experiments would provide insights into the role of amidase activity and/or FtsN in Z-ring stability and positioning.

What signals or factors recruit NlpD, AmiC, and AmiB to the divisome?

The structure-function analysis of NlpD showed that it is recruited to the division site via its LysM domain, which is reported to be a PG-binding module [37, 38]. NlpD, AmiC, and AmiB require FtsN for septal localization, but the amidases localize independently of their cognate LytM activators [39]. If the localization of NlpD is indeed mediated by an interaction between its LysM domain and PG, this raises the question of

how the LysM domain distinguishes septal PG from the rest of the PG structure. This is especially puzzling given that NlpD still localizes to septal rings when septal PG synthesis is inhibited with the β-lactam cephalexin [39]. On the other hand, AmiC and AmiB fail to localize under these conditions [39], which indicates that their N-terminal targeting domains may directly bind to septal PG for localization to division sites. Since cephalexin only inhibits the transpeptidation reaction of the septal PG synthetic machine, one possibility is that the uncross-linked glycan strands that are still produced are somehow specifically recognized by the LysM domain of NlpD, thus allowing septal recruitment. Alternatively, the localization of NlpD may be mediated by a protein-protein interaction. If that is the case, the screen for NlpD regulators described in Chapter 4 might uncover this putative interacting protein.

How does the Tol-Pal system regulate NlpD function?

The findings presented in Chapter 4 provide support for a regulatory connection between amidase activation by NlpD and OM constriction by the Tol-Pal system [40]. I propose a model in which the localization of NlpD in the OM physically separates it from the PG layer at the division site, thus keeping the protein and its cognate amidase AmiC inactive. However, upon cytokinesis and constriction of the OM by the Tol-Pal system, NlpD is indirectly brought closer to the PG layer so that it can activate AmiC and promote septal PG splitting to allow cell separation. However, we cannot rule out the possibility that NlpD may require direct interaction with one or more members of the Tol-Pal system to activate it. Further experiments are, therefore, needed to assess whether

NlpD directly interacts with candidate proteins within the Tol-Pal complex, namely TolB, Pal, or TolA , which are either in the OM or can potentially bridge the gap to the OM.

Another intriguing model for NlpD regulation stems from recent studies showing that OM lipoproteins can be exposed to the surface on the outer leaflet of the OM [41-45]. Preliminary results for NlpD suggest that it may be surface-exposed (data not shown). However, more experiments are required to confirm this observation. That being said, if NlpD indeed adopts such an orientation, this raises the attractive possibility that NlpD may be physically separated from both AmiC and the PG layer by the OM, thus ensuring a complete absence of amidase activation. During cell division, NlpD may then be retained in the periplasm by the Tol-Pal system or other protein interactions, thus allowing it to activate AmiC for septal PG splitting. How the orientation of NlpD might be modulated is unclear, but it may involve interactions between its LysM domain and septal PG or other protein-protein interactions that prevent its transport to the outer leaflet of the OM. Alternatively, NlpD may be internalized at the division site by the Tol-Pal system, which is known for its ability to use the proton-motive force to facilitate the entry of external agents such as bacteriocins and filamentous phages across the outer membrane [46, 47]. Overall, although the model I am proposing is speculative, it leads to testable hypotheses. For example, the internalization of NlpD is predicted to be division-dependent, suggesting that the levels of surface-exposed NlpD should increase upon cell division inhibition.

What is the role of YraP in the activation of NlpD during cell division?

My screen for NlpD regulators led to the identification of YraP, an OM lipoprotein of unknown function, which is recruited to the septal ring. The OM localization of YraP is required for proper NlpD activity, suggesting that both proteins need to be in the same membrane for proper function. Given these results, I hypothesize that YraP may activate NlpD through a direct protein-protein interaction. Follow-up experiments will, therefore, investigate a direct interaction between NlpD and YraP. In addition, it would be interesting to test if an IM-retained NlpD variant, which is generally non-functional for AmiC activation, becomes active when YraP is also localized to the inner membrane. If that is the case, it would be support a direct activation of NlpD by YraP. Additionally, I can test whether YraP stimulates NlpD/AmiC activity *in vitro* using a dye-release assay [14].

Another interesting observation was that an IM-retained YraP variant failed to localize to the division site, which may indicate that YraP is recruited to the septal ring via a direct interaction with an OM protein. Given that NlpD localizes to the division site independently of YraP, one hypothesis is that the recruitment of YraP to the divisome is mediated by an interaction with its target NlpD. Consequently, wild-type YraP would fail to localize in an *nlpD* null strain. The implications of such a localization dependency are unclear at the moment, but the potential interaction between NlpD and YraP needs to be further investigated to shed more light on the regulation of NlpD, as well as to provide new information about the function of YraP.

Section 5.3: Concluding remarks

Although bacterial cytokinesis has been extensively studied over the years, we are only beginning to uncover the mechanisms involved in both the remodeling of the cell envelope by the division apparatus and the controls that exist to prevent any misstep in this complicated endeavor. Progress in these areas is being made thanks to multidisciplinary efforts, from genetics to cell biology to biochemical reconstitutions and structural biology. A detailed understanding of the mechanisms underlying the coordination between the many activities of the division machine might also reveal weak points in the regulation that could be exploited as attractive targets for new lytic antibiotics. Additionally, defects in septal PG remodeling leads to the formation of long chains of cells that fail to separate [11, 12, 48]. Interestingly, these cell chains display increased outer membrane permeability and hyper-susceptibility to antibiotics [48], thus raising the possibility that blocking cell separation may be a new avenue to sensitize gram-negative bacteria to antimicrobial agents. Ultimately, a better understanding of bacterial cell division will not only advance our knowledge of this fundamental process, but also inform us on the best ways to disrupt it for the development of new classes of antibacterial therapies.

Section 5.4: References

1. Tsang, M.-J., and Bernhardt, T. G. (2015). Guiding divisome assembly and controlling its activity. Curr Opin Microbiol *24*, 60–65.

2. de Boer, P. A. (2010). Advances in understanding E. coli cell fission. Current Opin Microbiol *13*, 730–737.

3. Goehring, N. W., and Beckwith, J. (2005). Diverse paths to midcell: assembly of the bacterial cell division machinery. Curr Biol *15*, R514–26.

4. Typas, A., Banzhaf, M., Gross, C. A., and Vollmer, W. (2012). From the regulation of peptidoglycan synthesis to bacterial growth and morphology. Nat Rev Microbiol *10*, 123–136.

5. Lutkenhaus, J., Pichoff, S., and Du, S. (2012). Bacterial cytokinesis: From Z ring to divisome. Cytoskeleton *69*, 778–790.

6. Busiek, K. K., Eraso, J. M., Wang, Y., and Margolin, W. (2012). The Early Divisome Protein FtsA Interacts Directly through Its 1c Subdomain with the Cytoplasmic Domain of the Late Divisome Protein FtsN. J Bacteriol *194*, 1989–2000.

7. Szwedziak, P., Wang, Q., Freund, S. M., and Löwe, J. (2012). FtsA forms actin-like protofilaments. EMBO J *31*, 2249–2260.

8. Pichoff, S., Shen, B., Sullivan, B., and Lutkenhaus, J. (2012). FtsA mutants impaired for self-interaction bypass ZipA suggesting a model in which FtsA's self-interaction competes with its ability to recruit downstream division proteins. Mol Microbiol *83*, 151–167.

9. Pichoff, S., Du, S., and Lutkenhaus, J. (2015). The bypass of ZipA by overexpression of FtsN requires a previously unknown conserved FtsN motif essential for FtsA-FtsN interaction supporting a model in which FtsA monomers recruit late cell division proteins to the Z ring. Mol Microbiol *95*, 971–987.

10. Gerding, M. A., Liu, B., Bendezú, F. O., Hale, C. A., Bernhardt, T. G., and de Boer, P. A. J. (2009). Self-enhanced accumulation of FtsN at Division Sites and Roles for Other Proteins with a SPOR domain (DamX, DedD, and RlpA) in Escherichia coli cell constriction. J Bacteriol *191*, 7383–7401.

11. Heidrich, C., Templin, M. F., Ursinus, A., Merdanovic, M., Berger, J., Schwarz, H., de Pedro, M. A., and Höltje, J. V. (2001). Involvement of N-acetylmuramyl-L-alanine amidases in cell separation and antibiotic-induced autolysis of Escherichia coli. Mol Microbiol *41*, 167–178.

12. Priyadarshini, R., de Pedro, M. A., and Young, K. D. (2007). Role of peptidoglycan amidases in the development and morphology of the division septum in Escherichia coli. J Bacteriol *189*, 5334–5347.

13. Uehara, T., Dinh, T., and Bernhardt, T. G. (2009). LytM-domain factors are required for daughter cell separation and rapid ampicillin-induced lysis in Escherichia coli. J Bacteriol *191*, 5094–5107.

14. Uehara, T., Parzych, K. R., Dinh, T., and Bernhardt, T. G. (2010). Daughter cell separation is controlled by cytokinetic ring-activated cell wall hydrolysis. EMBO J *29*, 1412–1422.

15. Peters, N. T., Morlot, C., Yang, D. C., Uehara, T., Vernet, T., and Bernhardt, T. G. (2013). Structure-function analysis of the LytM domain of EnvC, an activator of cell wall remodelling at the Escherichia coli division site. Mol Microbiol *89*, 690–701.

16. Yang, D. C., Peters, N. T., Parzych, K. R., Uehara, T., Markovski, M., and Bernhardt, T. G. (2011). An ATP-binding cassette transporter-like complex governs cell-wall hydrolysis at the bacterial cytokinetic ring. Proc Natl Acad Sci USA *108*, E1052–60.

17. Bernard, C. S., Sadasivam, M., Shiomi, D., and Margolin, W. (2007). An altered FtsA can compensate for the loss of essential cell division protein FtsN in Escherichia coli. Mol Microbiol *64*, 1289–1305.

18. Loose, M., and Mitchison, T. J. (2013). The bacterial cell division proteins FtsA and FtsZ self-organize into dynamic cytoskeletal patterns. Nat Cell Biol *16*, 38–46.

19. Wang, H. C., and Gayda, R. C. (1990). High-level expression of the FtsA protein inhibits cell septation in Escherichia coli K-12. J Bacteriol *172*, 4736–4740.

20. Dai, K., and Lutkenhaus, J. (1992). The proper ratio of FtsZ to FtsA is required for cell division to occur in Escherichia coli. J Bacteriol *174*, 6145–6151.

21. Geissler, B., Elraheb, D., and Margolin, W. (2003). A gain-of-function mutation in ftsA bypasses the requirement for the essential cell division gene zipA in Escherichia coli. Proc Natl Acad Sci USA *100*, 4197–4202.

22. Gonzalez, M. D., and Beckwith, J. (2009). Divisome under construction: distinct domains of the small membrane protein FtsB are necessary for interaction with multiple cell division proteins. J Bacteriol *191*, 2815–2825.

23. Guzman, L. M., Weiss, D. S., and Beckwith, J. (1997). Domain-swapping analysis of FtsI, FtsL, and FtsQ, bitopic membrane proteins essential for cell division in Escherichia coli. J Bacteriol *179*, 5094–5103.

24. Ghigo, J. M., and Beckwith, J. (2000). Cell division in Escherichia coli: role of FtsL domains in septal localization, function, and oligomerization. J Bacteriol *182*, 116–129.

25. Gonzalez, M. D., Akbay, E. A., Boyd, D., and Beckwith, J. (2010). Multiple interaction domains in FtsL, a protein component of the widely conserved bacterial FtsLBQ cell division complex. J Bacteriol *192*, 2757–2768.

26. Karimova, G., Dautin, N., and Ladant, D. (2005). Interaction network among Escherichia coli membrane proteins involved in cell division as revealed by bacterial two-hybrid analysis. J Bacteriol *187*, 2233–2243.

27. Liu, B., Persons, L., Lee, L., and de Boer, P. A. J. (2015). Roles for both FtsA and the FtsBLQ subcomplex in FtsN-stimulated cell constriction in Escherichia coli. Mol Microbiol *95*, 945–970.

28. Goehring, N. W., Gonzalez, M. D., and Beckwith, J. (2006). Premature targeting of cell division proteins to midcell reveals hierarchies of protein interactions involved in divisome assembly. Mol Microbiol *61*, 33–45.

29. D'Ulisse, V., Fagioli, M., Ghelardini, P., and Paolozzi, L. (2007). Three functional subdomains of the Escherichia coli FtsQ protein are involved in its interaction with the other division proteins. Microbiology (Reading, Engl) *153*, 124–138.

30. Aarsman, M. E. G., Piette, A., Fraipont, C., Vinkenvleugel, T. M. F., Nguyen-Distèche, M., and Blaauwen, den, T. (2005). Maturation of the Escherichia coli divisome occurs in two steps. Mol Microbiol *55*, 1631–1645.

31. Boyle, D. S., Khattar, M. M., Addinall, S. G., Lutkenhaus, J., and Donachie, W. D. (1997). ftsW is an essential cell-division gene in Escherichia coli. Mol Microbiol *24*, 1263–1273.

32. Pogliano, J., Pogliano, K., Weiss, D. S., Losick, R., and Beckwith, J. (1997). Inactivation of FtsI inhibits constriction of the FtsZ cytokinetic ring and delays the assembly of FtsZ rings at potential division sites. Proc Natl Acad Sci USA *94*, 559–564.

33. Chen, J. C., and Beckwith, J. (2001). FtsQ, FtsL and FtsI require FtsK, but not FtsN, for co-localization with FtsZ during Escherichia coli cell division. Mol Microbiol *42*, 395–413.

34. Rico, A. I., García-Ovalle, M., Palacios, P., Casanova, M., and Vicente, M. (2010). Role of Escherichia coli FtsN protein in the assembly and stability of the cell division ring. Mol Microbiol *76*, 760–771.

35. Tsang, M.-J., and Bernhardt, T. G. (2015). A role for the FtsQLB complex in cytokinetic ring activation revealed by an ftsL allele that accelerates division. Mol Microbiol *95*, 925–944.

36. Yahashiri, A., Jorgenson, M. A., and Weiss, D. S. (2015). Bacterial SPOR domains are recruited to septal peptidoglycan by binding to glycan strands that lack stem peptides. Proc Natl Acad Sci USA *112*, 11347–11352.

37. Buist, G., Steen, A., Kok, J., and Kuipers, O. P. (2008). LysM, a widely distributed protein motif for binding to (peptido)glycans. Mol Microbiol *68*, 838–847.

38. Mesnage, S., Dellarole, M., Baxter, N. J., Rouget, J.-B., Dimitrov, J. D., Wang, N., Fujimoto, Y., Hounslow, A. M., Lacroix-Desmazes, S., Fukase, K., et al. (2014). Molecular basis for bacterial peptidoglycan recognition by LysM domains. Nat Commun *5*, 4269.

39. Peters, N. T., Dinh, T., and Bernhardt, T. G. (2011). A fail-safe mechanism in the septal ring assembly pathway generated by the sequential recruitment of cell separation amidases and their activators. J Bacteriol *193*, 4973–4983.

40. Gerding, M. A., Ogata, Y., Pecora, N. D., Niki, H., and de Boer, P. A. J. (2007). The trans-envelope Tol-Pal complex is part of the cell division machinery and required for proper outer-membrane invagination during cell constriction in E. coli. Mol Microbiol *63*, 1008–1025.

41. Cowles, C. E., Li, Y., Semmelhack, M. F., Cristea, I. M., and Silhavy, T. J. (2011). The free and bound forms of Lpp occupy distinct subcellular locations in Escherichia coli. Mol Microbiol *79*, 1168–1181.

42. Webb, C. T., Selkrig, J., Perry, A. J., Noinaj, N., Buchanan, S. K., and Lithgow, T. (2012). Dynamic association of BAM complex modules includes surface exposure of the lipoprotein BamC. J Mol Biol *422*, 545–555.

43. Cho, S.-H., Szewczyk, J., Pesavento, C., Zietek, M., Banzhaf, M., Roszczenko, P., Asmar, A., Laloux, G., Hov, A.-K., Leverrier, P., et al. (2014). Detecting envelope stress by monitoring β-barrel assembly. Cell *159*, 1652–1664.

44. Konovalova, A., Perlman, D. H., Cowles, C. E., and Silhavy, T. J. (2014). Transmembrane domain of surface-exposed outer membrane lipoprotein RcsF is threaded through the lumen of β-barrel proteins. Proc Natl Acad Sci USA *111*, E4350–8.

45. Michel, L. V., Shaw, J., MacPherson, V., Barnard, D., Bettinger, J., D'Arcy, B., Surendran, N., Hellman, J., and Pichichero, M. E. (2015). Dual orientation of the outer membrane lipoprotein Pal in Escherichia coli. Microbiology (Reading, Engl) *161*, 1251–1259.

46. Webster, R. E. (1991). The tol gene products and the import of macromolecules into Escherichia coli. Mol Microbiol *5*, 1005–1011.

47. Lazzaroni, J. C., Germon, P., Ray, M. C., and Vianney, A. (1999). The Tol proteins of Escherichia coli and their involvement in the uptake of biomolecules and outer membrane stability. FEMS Microbiol Lett *177*, 191–197.

48. Heidrich, C., Ursinus, A., Berger, J., Schwarz, H., and Höltje, J.-V. (2002). Effects of multiple deletions of murein hydrolases on viability, septum cleavage, and sensitivity to large toxic molecules in Escherichia coli. J Bacteriol *184*, 6093–6099.